Class II phosphatidylinositol 3-kinase β in nutrient signaling, endocytosis and centronuclear myopathy

Inaugural-Dissertation

to obtain the academic degree

Doctor rerum naturalium (Dr. rer. nat.)

submitted to the Department of Biology, Chemistry, Pharmacy

of Freie Universität Berlin

by

Philipp Alexander Koch

2022

This dissertation was completed between February 2018 and October 2022 under the supervision of Prof. Dr. Volker Haucke at the Leibniz-Forschungsinstitut für Molekulare Pharmakologie in Berlin Buch.

1st reviewer: Prof. Dr. Volker Haucke

2nd reviewer: Prof. Dr. Markus Wahl

Date of defense: 09.12.2022

Affidavit

I declare that this dissertation has been written independently and with no other sources and aids than quoted.

Berlin, October 10, 2022

_____

Philipp Alexander Koch

I. Acknowledgements

I would like to express my gratitude to my supervisor, **Prof. Dr. Volker Haucke**, for giving me the opportunity to work on these exiting projects, for the excellent and inspiring scientific discussions and for the guidance throughout the time of my PhD studies.

I would particularly like to thank **Dr. Alexander Wallroth** for getting me started in the lab, introducing me to time efficient experimental design and for his excellent input to both projects I worked on during my studies.

I am grateful for the support from **Dr. Wen-Ting Lo** who always helped to perform biochemical assays and gave me a lot of information on structural biology.

I would like to thank **Dr. Martin Lehmann** for being part of my thesis advisory committee, great scientific discussions and introducing me to microscopy.

I owe special thanks to **Paula Samsó** and **Dr. York Posor** for their contributions to the second project and for the fruitful discussions we had during our subgroup meetings.

I want to thank **Heike Stephanowitz** and the FMP Mass Spectrometry Core Facility for processing my samples.

I would like to express my gratitude to **Silke Zillmann** and **Delia Löwe** for their excellent technical help.

Further, I would like to thank all past and present members of the 'AG Haucke' for creating an excellent atmosphere:
Kerem Akkaya, Weronika Albrecht, Dr. Domenico Azarnia Tehran, Svenja Bolz, Dr. Michael Ebner, Uwe Fink, Dr. Hannes Gonschior, Dr. Wonyul Jang, Dr. Maria Jäpel, Dr. Mudassar Khan, Dr. Natalie Kaempf, Dr. Gaga Kochlamazashvili, Kinga Konkel, Prof. Dr. Michael Krauß, Dr. Marijn Kuijpers, Dr. Tanja López Hernández, Max Lucht, Dr. Albert Mackintosh, Prof. Dr.

Tanja Maritzen, Phuong Nguyen, Kristine Oevel, Dr. Dmytro Puchkov, Dr. Sila Rizalar, Julia Riedlberger, Giulia Russo, Dr. Linda Sawade, Yanwei Su, Claudia Schmidt, Dr. Tolga Soykan, Dr. Miaomiao Tian, Rozemarijn van der Veen, Dr. Dennis Vollweiter, Dr. Haibin Wang, Dr. Agata Witkowska and Dr. Klaas Yperman.

Most importantly, I want to thank **my parents**, **my brother** and **Ramonique Lim** for their unlimited support.

អរគុណសម្រាប់ការគាំទ្រមិនចេះចប់របស់អ្នក។ខ្ញុំមិនអាចធ្វើវាដោយគ្មានអ្នកបានទេ។ ខ្ញុំស្រលាញ់អ្នក

II. Contents

Table of Contents

III. Zusammenfassung

Um sich an die Verfügbarkeit von Nährstoffen und Wachstumsfaktoren anzupassen, müssen Zellen deren Verfügbarkeit wahrnehmen und ihren Stoffwechsel und ihre Proliferation entsprechend anpassen. Defekte in diesen Prozessen werden mit vielen Krankheiten wie z.B. Krebs und Diabetes in Verbindung gebracht. Die Nährstoffsignalwege werden vom mTOR-Komplex 1 (mTORC1) reguliert. Wenn Nährstoffe und Wachstumsfaktoren verfügbar sind, lokalisiert mTORC1 an Lysosomen und phosphoryliert Zielproteine, die anabole Prozesse wie Proteintranslation und Lipidsynthese initiieren und katabole Prozesse wie Autophagie hemmen. Aminosäuren induzieren die Translokation von mTORC1 zur lysosomalen Oberfläche über die Aktivität von Rag-GTPasen. Wachstumsfaktoren führen zur Aktivierung der kleinen GTPase Rheb am Lysosom, die mit mTORC1 interagiert, und dadurch aktiviert. Wenn die Wachstumsfaktoren niedrig sind, wird die mTORC1-Aktivität durch lysosomales PI(3,4)P_2 durch bisher unbekannte Mechanismen gehemmt. PI(3,4)P_2 wird aus PI(4)P durch die PI-3-Kinase β der Klasse II (PI3KC2β) synthetisiert. PI3KC2β selbst wird durch Wachstumsfaktor-Signalwege gehemmt. Aktive Wachstumsfaktorrezeptoren fördern die Aktivität des mTORC2-Komplexes, der dann die Proteinkinase N2 (PKN2) durch Phosphorylierung aktiviert. PKN2 wiederum phosphoryliert PI3KC2β in seiner unstrukturierten N-terminalen Domäne und löst die Assoziation von inhibitorischen 14-3-3-Proteinen aus, die PI3KC2β im Zytoplasma sequestrieren. Wie PI3KC2β aktiv an die lysosomale Oberfläche rekrutiert wird, wenn Wachstumsfaktoren fehlen, war bisher unbekannt. In dieser Studie zeige ich, dass aktives, GTP-gebundenes Rab7A mit PI3KC2β interagiert und es bei Wachstumsfaktormangel an die lysosomale Oberfläche rekrutiert. Rab7A war für die Interaktion von PI3KC2β mit der mTORC1-Untereinheit Raptor und die Translokation von PI3KC2β zum Lysosom erforderlich. Darüber hinaus hing die Hemmung von lysosomalem PI(3,4)P_2 und mTORC1 von der Rab7A-Aktivität ab.

Um den Einfluss von PI3KC2β auf die mTORC1-Zusammensetzung weiter zu untersuchen, habe ich eine mittels CRISPR/Cas9 eine HEK293T-Zelllinie generiert, die eGFP-Raptor endogen exprimiert. Diese Zelllinie ermöglichte die Isolierung von mTORC1 durch Immunpräzipitation. Eine Depletion von PI3KC2β veränderte die mTORC1-Zusammensetzung,

da die Interaktion der inhibitorischen Untereinheit PRAS40 mit mTORC1 reduziert wurde. Die genauen Mechanismen dieser Beobachtung bleiben Gegenstand weiterer Studien.

Neben seiner Rolle bei der mTORC1-Signalübertragung ist PI3KC2β auch als wichtiger Regulator bei der x-chromosomalen zentronukleären Myopathie (XLCNM) bekannt. XLCNM ist eine schwere Muskelerkrankung, die durch Funktionsverlustmutationen in der PI(3)P-Phosphatase MTM1 verursacht wird. Die Depletion von PI3KC2β in MTM1-Knockout-Mäusen verhindert den Krankheitsausbruch durch bisher unbekannte Mechanismen. MTM1 ist für die Dephosphorylierung von PI(3)P auf Recycling-Endosomen erforderlich, um die Synthese von PI(4)P durch PI4KIIα zu ermöglichen, was wiederum für die Rekrutierung des Exozyst-komplexes und die Exozytose von Recycling-Cargo erforderlich ist. Dies führt zur endosomalen Akkumulation von β1-Integrinen und löst Defekte in der Muskelfasererzeugung durch Myoblastenfusion aus, ein Prozess, der von der richtigen Lokalisierung und Aktivierung von β1-Integrin abhängt. Unter Verwendung von C2C12-Myoblastenzelllinien, die Knockouts (KO) von MTM1, PI3KC2β oder sowohl MTM1 als auch PI3KC2β enthielten, konnte ich den durch MTM1-Verlust induzierten Myoblastenfusionsdefekt in einem Zellmodell reproduzieren. Außerdem konnte ich bestätigen, dass MTM1 KO C2C12-Zellen weniger aktives β1-Integrin an der Zelloberfläche hatten. Im Gegensatz dazu hatten HeLa-Zellen, die von PI3KC2β depletiert wurden, erhöhte aktive β1-Integrin-Oberflächenlevel und verringerte Endozytose von aktivem β1-Integrin. Beide Befunde konnten durch Re-expression von Wildtyp PI3KC2β gerettet werden, nicht aber mit Kinase-inaktivem PI3KC2β oder einer Mutante, die nur PI(3)P, aber nicht PI(3,4)P_2 synthetisiert. Somit wird PI3KC2β für die aktive β1-Integrin-Endozytose durch die Synthese von PI(3,4)P_2 benötigt. In Übereinstimmung damit lokalisierte PI3KC2β in Clathrin-Pits (CCPs) und co-immunopräzipitierte mit dem Integrin-Endozytose-Adapter Dab2 und den endozytischen Proteinen Clathrin und Intersectin-1. Daraus ergibt sich ein Modell, bei dem MTM1 für das Recycling von aktivem β1-Integrin und PI3KC2β für die Endozytose von aktivem β1-Integrin erforderlich ist. Wenn der Recyclingprozess aufgrund von MTM1-Verlust fehlschlägt, können die aktiven β1-Integrinlevel der Zelloberfläche wiederhergestellt werden, indem PI3KC2β deletiert wird und somit die Rate der β1-Integrin-Endozytose reduziert wird.

IV. Summary

To adapt to the availability of nutrients and growth factors, cells must sense these cues and adapt their metabolism and proliferation accordingly. Defects in these processes have been associated with many diseases ranging from diabetes to cancer. Nutrient signaling is controlled by the master regulator mTOR complex 1 (mTORC1). When nutrients and growth factors are readily available, mTORC1 localizes to lysosomes and phosphorylates target proteins initiating anabolic processes like protein translation and lipid synthesis and inhibiting catabolic processes like autophagy. Amino acids induce the translocation of mTORC1 to the lysosomal surface via the activity of Rag GTPases whereas growth factors lead to the activation of the small GTPase Rheb at the lysosome that interacts with mTORC1 to activate it. When growth factor levels are low, mTORC1 activity is inhibited by lysosomal $PI(3,4)P_2$ through so far unknown mechanisms. $PI(3,4)P_2$ is synthesized from PI(4)P by the class II PI 3-kinase β (PI3KC2β). PI3KC2β itself is inhibited by growth factor signaling. Active growth factor receptors promote the activity of the mTORC2 complex which then activates protein kinase N2 (PKN2) by phosphorylation. PKN2 in turn phosphorylates PI3KC2β in its unstructured N-terminal domain, triggering the association of inhibitory 14-3-3 proteins that sequester PI3KC2β in the cytoplasm. How PI3KC2β is actively recruited to the lysosomal surface upon growth factor starvation was previously unknow. In this study I demonstrate that active, GTP bound Rab7A interacts with PI3KC2β and recruits it to the lysosomal surface upon growth factor starvation. Rab7A was required for the interaction of PI3KC2β with the mTORC1 subunit Raptor and PI3KC2β translocation to lysosome. Furthermore, lysosomal $PI(3,4)P_2$ and mTORC1 inhibition depended on Rab7A activity.

To further investigate the influence of PI3KC2β on mTORC1 composition, I generated a HEK293T cell line that endogenously expresses eGFP-Raptor using CRISPR/Cas9 mediated genome editing. This cell line allowed for the isolation of mTORC1 by immunoprecipitation. PI3KC2β depletion indeed altered the mTORC1 composition, as the interaction of the inhibitory subunit PRAS40 was reduced by 40 %. The exact mechanisms of this observation remain the subject of further studies.

Beyond its role in mTORC1 signaling, PI3KC2β is known as an important regulator in x-linked centronuclear myopathy (XLCNM). XLCNM is a severe muscular disorder caused by loss

of function mutations in the PI(3)P phosphatase MTM1. The depletion of PI3KC2β in MTM1 knock out mice prevents disease onset by hereto unknown mechanisms. MTM1 is required for the depletion of PI(3)P from recycling endosomes to enable the synthesis of PI(4)P by PI4KIIα which is in turn required for the recruitment of the exocyst complex and exocytosis of cargo destined for recycling. This leads to the endosomal accumulation of β1 integrins and triggers defects in muscle fiber generation through myoblast fusion, a process that depends on proper β1 integrin localization and activation. Using C2C12 myoblast cell lines harboring knockouts (KO) of MTM1, PI3KC2β or both MTM1 and PI3KC2β I could reproduce the myoblast fusion defect induced by MTM1 loss in a cellular model. Furthermore, I could confirm that MTM1 KO C2C12 cells had less active β1 integrin at the cell surface. Contrarily, HeLa cells depleted of PI3KC2β had elevated active β1 integrin surface levels and decreased rates of active β1 integrin endocytosis. Both findings could be rescued with the re-expression wild type PI3KC2β but not with kinase inactive PI3KC2β or a mutant that only synthesizes PI(3)P but not PI(3,4)P_2. Thus PI3KC2β is required for active β1 integrin endocytosis trough the synthesis of PI(3,4)P_2. In line with that, PI3KC2β localized to clathrin coated pits (CCPs) and co-immunoprecipitated with the integrin endocytosis adaptor Dab2 and the endocytic proteins clathrin heavy chain and intersectin-1. I therefore propose a model where MTM1 is required for active β1 integrin recycling and PI3KC2β is required for active β1 integrin endocytosis. If the recycling process fails due to MTM1 loss, active surface β1 integrin levels can be restored by depleting PI3KC2β and thus reducing the rate of β1 integrin endocytosis.

1 Introduction

1.1 Transport processes in mammalian cells

Transport across and between cellular membranes is essential for homeostasis. For example, it enables the uptake of nutrients and ions required for energy production and cell signaling. Transport can be achieved by various means. It can be driven by passive diffusion of a solute along a concentration gradient either straight through the lipid bilayer or facilitated by transmembrane transporters such as ion channels. Transport against concentration gradients however does require energy usually provided by ATP. This so-called active transport is enabled by carrier proteins. Larger structures such as transmembrane receptors cannot diffuse into the cell by any means. They must be taken up by endocytosis, a process where a portion of the plasma membrane invaginates into the cell and is subsequently cleaved from the plasma membrane to form an intracellular vesicle called endosome. Endosomes in turn can take various routes within the cell: they can mature to late endosomes to eventually fuse with lysosomes leading to the degradation of their content or they can develop into recycling endosomes, integrating their content (usually receptors) into the plasma membrane at a different location. This process is especially important in cell migration (Paul, Jacquemet, & Caswell, 2015). The fate of endosomes is controlled by various factors such as the nature of their cargo, the Rab GTPases they acquire and their lipid composition.

1.2 Clathrin mediated endocytosis

Clathrin mediated endocytosis (CME) is required for the uptake of a large range of cargoes from the cell surface to the interior (Kaksonen & Roux, 2018). It results in the formation of clathrin coated cargo vesicles that transport mainly transmembrane receptors and their respective ligands. Thereby, it also regulates the surface abundance of these receptors. Thus, CME is essential for a wide range of cellular processes ranging from nutrient uptake to cell signaling and migration (McMahon & Boucrot, 2011). CME can be divided into four stages: initiation, stabilization, maturation, and membrane fission (Mettlen, Chen,

Srinivasan, Danuser, & Schmid, 2018). During initiation, the adaptor protein AP-2 binds to local pools of PI(4,5)P_2 at the plasma membrane and to sorting motifs in cargo receptors (Kadlecova et al., 2017). PI(4,5)P_2 is generated by the constitutive phosphorylation of PI to PI(4)P by PI 4-kinase IIIα and further phosphorylation to PI(4,5)P_2 by type I PI 4-phosphate 5-kinases (PIPKIs) (Wallroth & Haucke, 2018). AP-2 in turn recruits clathrin, initiates clathrin coat assembly and triggers further clustering of cargo and the recruitment of endocytic accessory proteins (EAPs) (Kaksonen & Roux, 2018; Mettlen et al., 2018). These EAPs such as the F-BAR protein FCHo1/2, and the scaffolding proteins Eps15 and intersectin stabilize AP-2 clusters at the plasma membrane and induce membrane curvature, generating a clathrin coated pit (CCP) (Kaksonen & Roux, 2018). Further maturation requires the turnover of PI(4,5)P_2 to PI(3,4)P_2 (Posor et al., 2013; Wallroth & Haucke, 2018). Therefore, the 5-phosphatases synaptojanin, OCRL and SHIP2 are recruited to maturing CCPs to generate PI(4)P (Erdmann et al., 2007; Nakatsu et al., 2010; Schuske et al., 2003). This is accompanied by the recruitment of PI3KC2α via clathrin itself and the subsequent generation of PI(3,4)P_2. This facilitates the recruitment of SNX9, which is required for the constriction of the neck and subsequent membrane cleavage by dynamin 2 (Posor et al., 2013), and FCHDS2, a protein that facilitates actin assembly and, thereby, force generation (Almeida-Souza et al., 2018). After scission by dynamin 2, clathrin coated vesicles are uncoated and fuse with early endosomes (Kaksonen & Roux, 2018)(Figure 1). Of note, there are also several clathrin independent uptake pathways that are beyond the focus of this introduction (Sandvig, Kavaliauskiene, & Skotland, 2018).

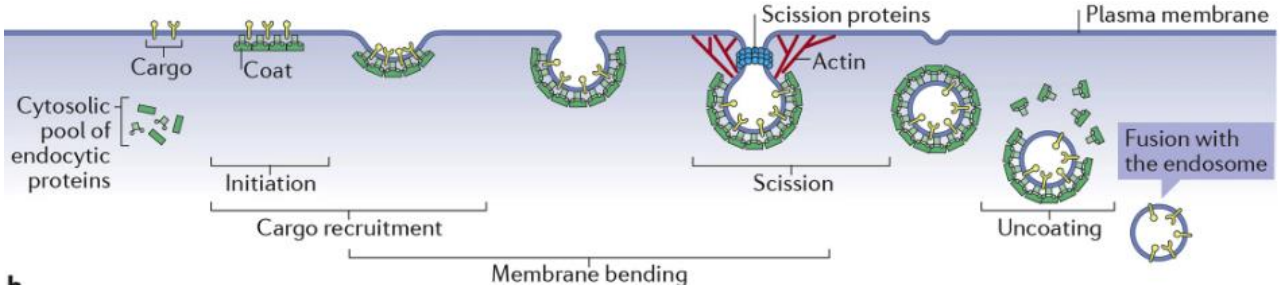

Figure 1: Time course of clathrin mediated endocytosis. Adapted from (Kaksonen & Roux, 2018). AP-2 binds to plasma membrane PI(4,5)P_2 to recruit cargo, clathrin and EAPs. This is followed by membrane bending, the acquisition of actin and membrane scission by dynamin 2. Subsequently, CCVs are uncoated and fuse with endosomes.

1.3 Endosomal sorting

After endocytosis, nascent endosomal vesicles rapidly acquire PI(3)P as the hallmark phosphoinositide of endosomes to enable fusion with pre-existing endosomes (Elkin, Lakoduk, & Schmid, 2016; Wallroth & Haucke, 2018). PI(3)P synthesis is mainly mediated by the class III PI3 kinase Vps34 (Devereaux et al., 2013) which is recruited to early endosomes via Rab5 (Christoforidis et al., 1999). At early endosomes, cargo is sorted for degradation, recycling, or retrograde trafficking to the trans-Golgi network (TGN).

Retrograde trafficking to the TGN is initiated by the Retromer complex, comprising Vps26, Vps29, Vps35 and a SNX dimer, which recognizes transport signals in cargo proteins. It furthermore recruits SNX3 to initiate membrane tubulation, fission and transport to the TGN (Tu, Zhao, Billadeau, & Jia, 2020).

Recycling can occur directly from endosomes via a fast recycling pathway that requires Rab4 and Rab35, activity (Grant & Donaldson, 2009) or through recycling endosomes in a slow recycling pathway (Cullen & Steinberg, 2018). Recycling endosomes are formed through the SNX4 or SNX11 dependent tubulation and budding of Rab11 positive subdomains from early endosomes (Cullen, 2008). This is accompanied by a loss of active Rab5 (Sonnichsen, De Renzis, Nielsen, Rietdorf, & Zerial, 2000). Rab11 recruits the PI(3)P phosphatase MTM1 (Campa et al., 2018) which removes the 3’ phosphate generating PI. Through the action of PI4KIIα, PI(4)P is acquired and enables the recruitment of exocyst components to enable exocytic fusion with the plasma membrane by SNARE proteins (Ketel et al., 2016).

Endosomal cargo primed for degradation transitions from Rab5 positive early endosomes to Rab7 positive multivesicular bodies (MVB). Through the action of the ESCRT protein machinery, cargo is sorted into intraluminal vesicles and degraded by the fusion of MVBs with lysosomes (Hurley, 2015). This is dependent on endosomal PI(3)P as it recruits the ESCRT subunit Hrs (Raiborg & Stenmark, 2009) and also promotes the activation of the Rab7 GEF Mon1-Ccz1 and thus Rab5 to Rab7 conversion (Cabrera et al., 2014). *En route* to fusion with lysosomes, endosomes acquire PI(3,5)P_2 identity by action of the 5-kinase PIKfyve (Wallroth & Haucke, 2018) (Figure 2).

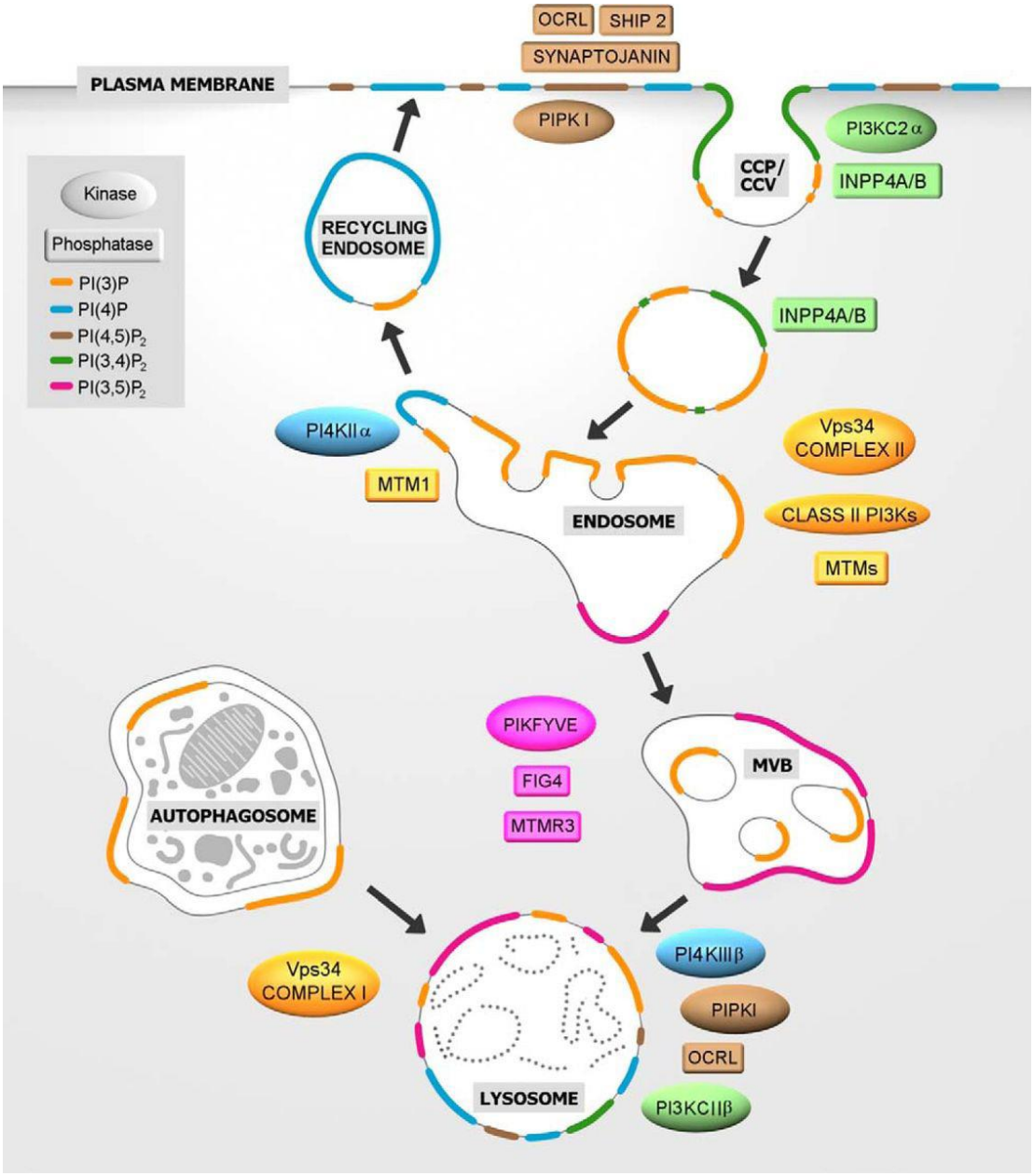

Figure 2: PIP conversion in endocytosis and in endolysosomal sorting. Adapted from (Wallroth & Haucke, 2018). The plasma membrane is enriched in PI(4)P and PI(4,5)P2, required for the initiation of clathrin mediated endocytosis. Furthermore, clathrin coated pits aquire PI(3,4)P_2 through PI3KC2α to recruit SNX9. On endosomes, INPP4A/B dephosphorylate PI(3,4)P2 to generate PI(3)P. Furthermore, PI(3)P on endosomes is generated by Vps34 complex II and through class II PI3Ks.

1.4 Lysosomes degrade endosomal cargo and regulate cellular nutrient signaling

Lysosomes are the terminal target compartment for endocytic cargo that is primed for degradation. They acquire an acidic pH through the action of vATPase and thus enable activity of luminal acid hydrolases leading to the degradation of endocytic cargos. Beyond that, lysosomes are essential for sensing the cellular nutrient status and regulating nutrient signaling via the master regulator mechanistic target of Rapamycin (mTOR) complex 1 (mTORC1). When nutrient abundance is low, catabolic processes like autophagy, glycolysis and lipolysis must be readily activated to provide sufficient energy for the maintenance of homeostasis. On the other hand, when nutrient abundance is high, anabolic processes like gluconeogenesis, protein synthesis and lipid biogenesis are initiated to enable cell proliferation. This is crucial for organisms to initiate processes like muscle and fat cell growth. A deregulation of these processes has been linked to a multitude of diseases ranging from obesity and diabetes to neurodegeneration and cancer (G. Y. Liu & Sabatini, 2020; Saxton & Sabatini, 2017).

1.4.1 Mechanistic target of rapamycin (mTOR)

mTOR is a serine/threonine kinase of the PI3K-related kinase family (Saxton & Sabatini, 2017). It is the key component of two distinct complexes, mTORC1 and mTORC2. mTORC1 consists of mTOR, Raptor and mLST8, a subunit shared with mTORC2. Raptor is an essential scaffolding protein that binds the TOR signaling motif (TOS) present in many mTORC1 targets (Nojima et al., 2003) whereas mLST8 associates with the catalytic domain of mTORC1. However, mLST8 may be dispensable for mTORC1, but not for mTORC2 activity (Hwang et al., 2019; Yip, Murata, Walz, Sabatini, & Kang, 2010). Additionally, PRAS40 and DEPTOR can associate with mTOCR1 to inhibit its activity (Peterson et al., 2009; Sancak et al., 2007).

1.4.2 Pathways regulating mTORC1 activity

As the master regulator of cellular nutrient signaling, mTORC1 controls all major pathways of anabolism and catabolism (G. Y. Liu & Sabatini, 2020; Saxton & Sabatini, 2017). Thus, mTORC1 activity needs to be tightly regulated. mTORC1 is activated by two major signaling pathways: amino acids and growth factor signaling. Amino acids are required for the Rag dependent recruitment of mTORC1 to the lysosome. Rags are small GTPases that function as heterodimers of RagA/B together with RagC/D. They are active when RagA/B is GTP bound, and RagC/D is GDP bound and inactive when GTP loading is reverse. Rag complex activity is regulated by the GATOR1 complex. When amino acid levels are low, GATOR1 acts on RagA/B to hydrolyse GTP. Rags are anchored to the lysosomal membrane by the Ragulator complex and when active directly interact with the mTORC1 subunit Raptor to recruit mTORC1 (Bar-Peled et al., 2013; Kim, Goraksha-Hicks, Li, Neufeld, & Guan, 2008; Sancak et al., 2010; Sancak et al., 2008).

For mTORC1 to be fully active, GTP bound Rheb, another small GTPase is required. GTP bound Rheb interacts with mTORC1 at the lysosomal surface and promotes mTORC1 activity (Long, Lin, Ortiz-Vega, Yonezawa, & Avruch, 2005). Rheb activity is controlled by growth factor availability. When growth factors are scarce, the Rheb GAP TSC complex is active and promotes Rheb GTP hydrolysis and, thereby, Rheb inactivation (Inoki, Li, Xu, & Guan, 2003). This is counteracted by active growth factor signaling. Growth factors activate the MAP kinase pathway leading to inhibitory phosphorylations on the TSC complex. Furthermore, insulin triggers class I PI3 kinase activity at the plasma membrane generating a pool of $PI(3,4,5)P_3$ (PIP_3). PIP_3 in turn promotes mTORC2 and PDK1 activity. Both kinases phosphorylate and activate the Akt kinase. Akt then phosphorylates and thereby inactivates the TSC complex (Garami et al., 2003; Ma, Chen, Erdjument-Bromage, Tempst, & Pandolfi, 2005; Manning, Tee, Logsdon, Blenis, & Cantley, 2002). Other pathways regulating mTORC1 activity such as hypoxia, energetic stress or DNA damage all converge on the TSC complex (G. Y. Liu & Sabatini, 2020) (Figure 3). Their detailed regulation is beyond the focus of this introduction.

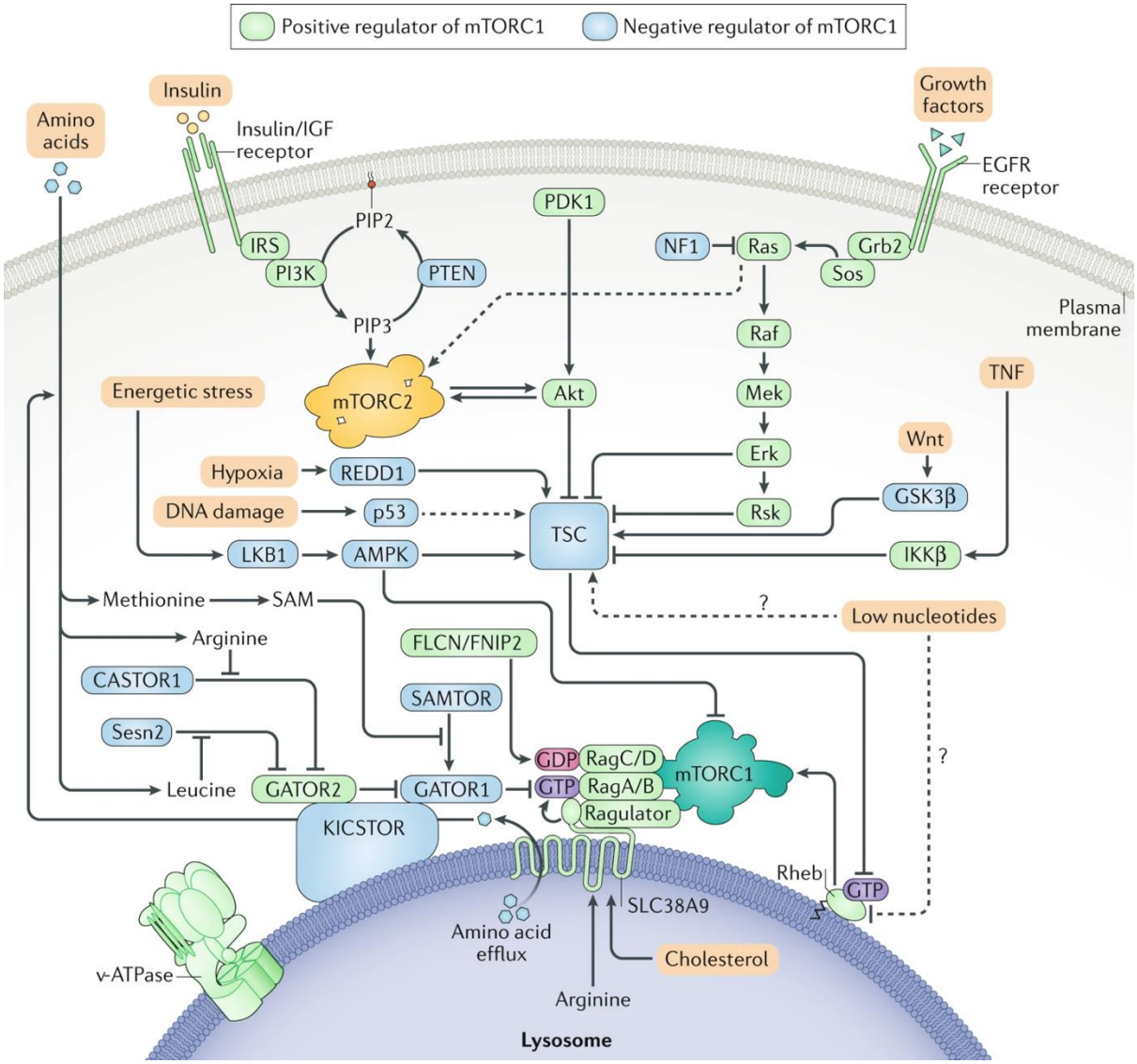

Figure 3: Signaling pathways regulating mTORC1 activity. Adapted from (G. Y. Liu & Sabatini, 2020). mTORC1 activity is regulated by two major signaling pathways: amino acid availability and growth factor signaling. Amino acids are sensed by multiple protein complexes at the lysosome. Amino acid availability enables the recruitment of mTORC1 to the lysosomal surface via the interaction with the Rag-Ragulator complex. To be fully active, mTORC1 requires stimulation by the activated small GTPase Rheb. Under low growth factor availability, Rheb is inactivated by its GAP the TSC complex. Growth factors trigger several pathways leading to TSC inactivation and thus Rheb and mTORC1 activity: Firstly, the MAP kinase pathway leads to an inhibitory phosphorylation on the TSC complex, secondly, insulin signaling activates Class I PI3Ks that produce $PI(3,4,5)P_3$ at the plasma membrane to stimulate mTORC2 and PDK1 activity. This leads to the phosphorylation and activation of Akt. Akt in turn inactivates the TSC complex by phosphorylation, too.

1.4.3 Pathways regulated by mTORC1

Active mTORC1 phosphorylates a large number of target proteins (Figure 4). Thereby, anabolic pathways are promoted, and catalytic pathways are repressed: The phosphorylation of 4E-BPs and S6 kinase promotes protein synthesis and the phosphorylation of ATF4, S6 kinase, SREBP transcription factors and HIF1α promote nucleotide and lipid synthesis as well as aerobic glycolysis. Through the phosphorylation of UVRAG and ULK1, mTORC1 inhibits autophagy and through the phosphorylation of the TFEB transcription factor, it inhibits lysosome biogenesis (G. Y. Liu & Sabatini, 2020).

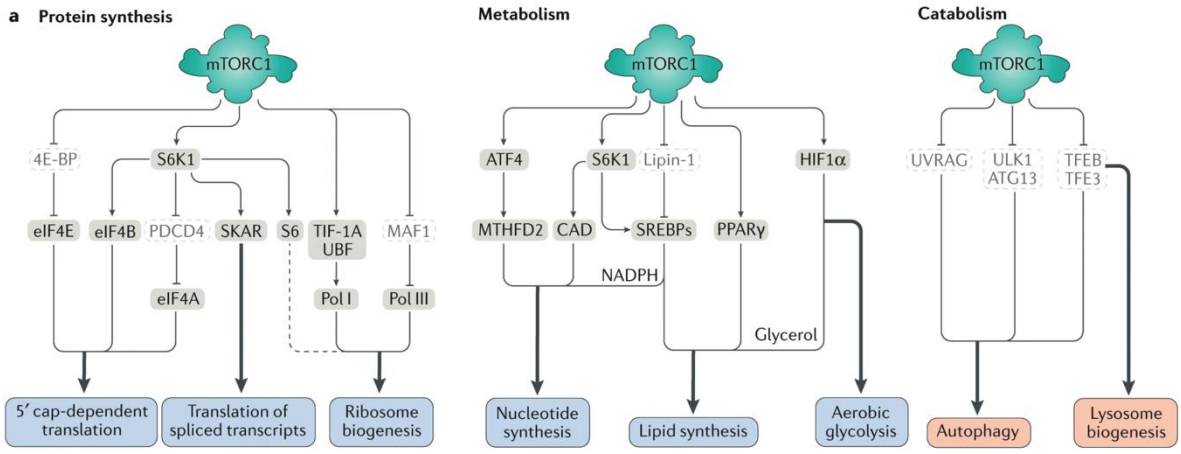

Figure 4: Signaling pathways regulated by mTORC1. Adapted from (G. Y. Liu & Sabatini, 2020). mTORC1 phosphorylates many target proteins leading to the activation of translation and protein synthesis and to synthesis of metabolites like nucleotides and lipids. Furthermore, catabolic processes like autophagy and lysosome biogenesis are inhibited.

1.5 Regulation of endosomal membrane trafficking

As highlighted in previous sections, endosomal membrane traffic and cell signaling are intimately linked to one another. Therefore, the regulation of endosomal membrane trafficking plays a major role in the cellular response to cues like nutrients and growth factors. Endosomal membrane trafficking requires the action of Rab GTPases and the conversion of phosphoinositides along the pathway. Rab GTPases recruit many effector proteins required

for membrane transport and fusion. Phosphoinositides serve as key components mediating membrane identity and thus regulating proper membrane transport. Both components are to be discussed in greater detail in the following sections.

1.5.1 Rab GTPases

Rab GTPases are key regulators of membrane trafficking in eukaryotic cells (Homma, Hiragi, & Fukuda, 2021). They form a family of more than 60 small GTPases that can cycle between two states: the active, GTP-bound state and the inactive GDP-bound state (Park, 2013; Stenmark, 2009). The active form is closely associated with membranes through their prenylated c-terminus and facilitates the recruitment of effector proteins to these membranes (Goody, Rak, & Alexandrov, 2005; Stenmark, 2009). These effectors then trigger processes associated with vesicle transport, tethering, fusion, or fission (Homma et al., 2021; Pfeffer, 2005; Stenmark, 2009). Rab GTPases are catalytically almost inactive and require co-factors, so called GTPase activating proteins (GAPs) to hydrolyze GTP to GDP and thus switch to their inactive form (Cherfils & Zeghouf, 2013). Similarly, their activation requires other co-factors, so called guanine nucleotide exchange factors (GEFs) that facilitate the exchange of GDP to GTP and thus trigger Rab activation (Cherfils & Zeghouf, 2013). Newly translated Rab proteins need to be prenylated to be able to interact with membranes. Therefore, they are bound by the Rab escort protein (REP) which enables geranylgeranyl transferase to prenylate them at their c-terminus (Alexandrov, Horiuchi, Steele-Mortimer, Seabra, & Zerial, 1994; Alexandrov et al., 1999). Inactive Rabs can be shuttled between membranes and the cytosol by a protein called GDP dissociation inhibitor (GDI). GDI masks the prenylated C-terminus and thus extracts inactive Rabs from membranes and solubilizes them (Y. W. Wu, Tan, Waldmann, Goody, & Alexandrov, 2007). At the membrane, inactive, GDP-bound Rabs can either be extracted by GDI or activated by GEFs. Rab activity is thus largely controlled by GEFs and reversely by GAPs. Higher GEF activity leads to more GTP bound Rab associated with membranes and higher GAP activity reversely leads to more GDP bound Rab that can be extracted by GDI (M. P. Muller & Goody, 2018).

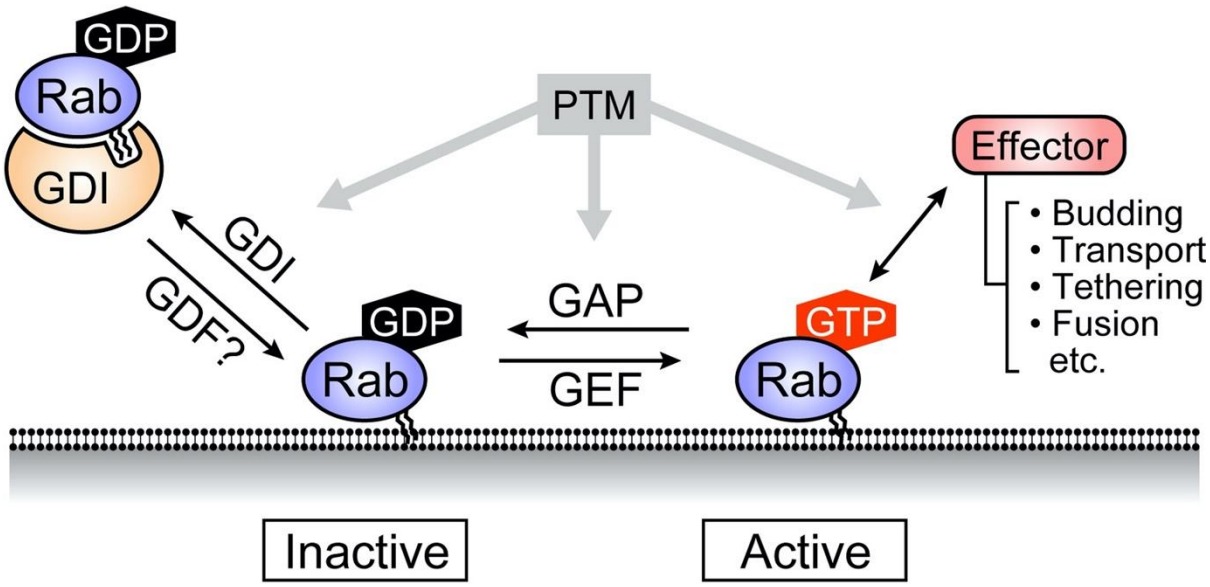

Figure 5: Rab GTPase cycle. Adapted from (Homma et al., 2021). Prenylated, GDP bound Rabs can be shuttled between the cytosol and membranes by GDI. Membrane bound, inactive Rabs can be activated by GEFs. Active, GTP-bound Rabs the facilitate the recruitment effector proteins that enable vesicel transport, tethering, fusion or fission. They can be inactivated by GTP hydrolysis which is facilitated by GAPs.

Rab GTPases are closely related to the Ras GTPase and resemble it in their overall structure. They contain a six-stranded β sheet, five with parallel strands and one with an anti-parallel strand. The β sheet is surrounded by 5 α helices (Park, 2013; Pfeffer, 2005). Their overall sequence is quite conserved over all different Rab proteins except for two highly divers regions termed switch I and switch II. Switch regions undergo conformational changes upon GTP binding to expose hydrophobic elements that in turn mediate binding to ras binding domains (RBDs) of effector proteins (Pfeffer, 2005).

1.5.2 Phosphoinositides

Rab GTPases often act together with signalling lipids, in particular phosphoinositides, to converge specificity to membrane traffic and signalling pathways. Phosphatidyl inositol is composed of myo-inositol phosphorylated at the D1 position linked to diacylglycerol via a phosphodiester bond (Falkenburger, Jensen, Dickson, Suh, & Hille, 2010). The remaining hydroxyl groups at positions D2-D6 can be phosphorylated by phosphatidyl inositol kinases

giving rise to seven distinct phosphoinositides (PIPs) (Balla, 2013). An overview of PIP conversion is given in Figure 6.

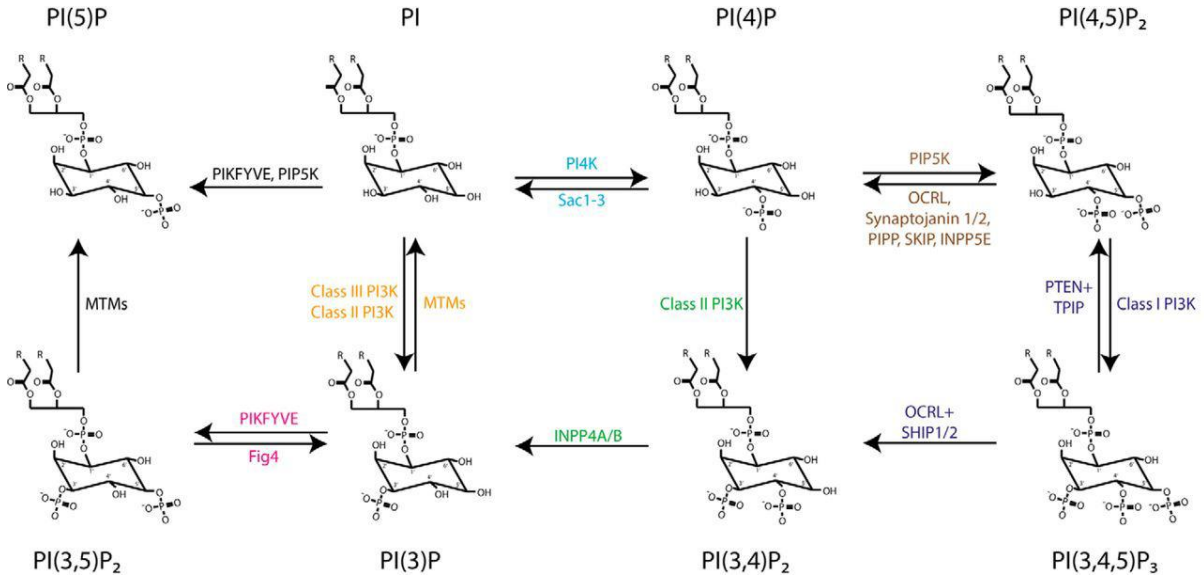

Figure 6: PIP conversion by PIP kinases and phosphatases. Adapted from (Wallroth & Haucke, 2018). Phosphatidylinositiol (PI) can be phosphorylated to PI(3)P by Class III PI3K or class II PI3Ks. This reaction can be reversed by MTM phosphatases. PI can be phosphorylated to PI(4)P by PI4Ks. This reaction can be reversed by the phosphatases Sac1-3. PI can be phosphorylated to PI(5)P by PIKFYVE and PIP5K. PI(3)P can be phosphorylated to PI(3,5)P2 by PIKFYVE. This reaction can be reversed by the Fig4 phosphatase. PI(4)P can be phosphorylated to PI(4,5)P2 by PIP5K. This reaction can be reversed by the phosphatases OCRL, Synaptojanin 1/2, PIPP, SKIP and INPP5E. PI(4)P can be phosphorylated to PI(3,4)P2 by class II PI3Ks. PI(4,5)P2 can be phosphorylated to PI(3,4,5)P3 by class I PI3Ks. This reaction can be reversed by PTEN and TPIP phosphatases. PI(3,4,5)P3 can also be dephosphorylated to yield PI(3,4)P2 by OCRL and SHIP1/2. PI(3,4)P2 can be dephosphorylated to PI(3)P by INPP4A/B. PI(3,5)P2 can be dephosphorylated to yield PI(5)P by MTMs.

PIPs are metabolized by kinases phosphorylating the D2-D6 positions of the myo-inositol ring and phosphatases removing these phosphorylations. The human PIP metabolizing enzymes are summarized in Table 1.

Table 1: Main human PIP metabolizing enzymes (Balla, 2013).

Enzyme	Isoform	Substrates	Localization
Kinases			
3-kinases	Class I: IA: p110α / β / δ IB: p110γ	$PI(4,5)P_2$	PM
	Class II: PI3KC2α / β / γ	PI, PI(4)P	PM, EE, RE, LeLys
	Class III: VPS34	PI	EE, AP
4-kinases	Class II: PI4KIIα / β	PI	PM, TGN, EE, LeLys
	Class III: PI4KIIIα / β	PI	PM, TGN
	PIP4Kα / β / γ	PI(5)P	PM
5-kinases	PIKfyve	PI, PI(3)P	LeLys
	PIP5Kα / β / γ	PI(4)P	PM
Phosphatases			
3-phosphatases	Myotubularins: MTM1, MTMR1-4, 6-8	PI(3)P, $PI(3,5)P_2$	PM, EE, LeLys
	PTEN	$PI(3,4,5)P_3$, $PI(3,4)P_2$	PM
	TPTE2	$PI(3,4,5)P_3$	PM
4-phosphatases	Sac1 / 2 / 3	PI(4)P	ER, Golgi
	Synaptojanin1 / 2	$PI(4,5)P_2$	PM
	INPP4A / B	$PI(3,4)P_2$	EE, LeLys
	TMEM55A / B	$PI(4,5)P_2$	LeLys
5-phosphatases	SHIP1 / 2	$PI(3,4,5)P_3$	PM
	Synaptojanin1 / 2	$PI(4,5)P_2$	PM
	OCRL	$PI(4,5)P_2$	PM, EE, LeLys
	INPP5A / E / J / K	$PI(4,5)P_2$	PM, ER

1.5.3 PIP phosphatases

PIP phosphatases can be classified into multiple classes depending on the position they mainly dephosphorylate. Here I will focus on the largest group of 3-phosphatases, the myotubularins (MTMs). They are essential for homeostasis and mutations in several MTMs have been linked to diseases ranging from myopathies to neurodegenerative disorders (Amoasii, Hnia, & Laporte, 2012; Hnia, Vaccari, Bolino, & Laporte, 2012). They contain 9 active and 5 inactive phosphatases. Active isoforms are MTM1, MTMR1-4, MTMR6-8 and MTMR14 whereas MTMR5, MTMR9, MTMR10, MTMR12 and MTMR13 are phosphatase dead as they do not contain the $C(X)5_R$ motif required for catalytic activity (Figure 7). MTMs share multiple domains: a PH-GRAM domain enabling phosphoinositide binding at membranes, a RID domain required for membrane binding, a phosphatase domain (active or inactive), SID and ODZ domains facilitating protein-protein interactions and a coiled-coil domain required for homo- and heterodimerization. Heterodimerization is mainly observed between active and phosphatase dead isoforms. These interactions seem to serve several purposes: firstly, the enzymatic activity can be increased in vitro, secondly phosphatase dead isoforms can recruit active isoforms to specific membranes and thirdly phosphatase dead isoforms seem to influence and modify the substrate specificity of active isoforms (Hnia et al., 2012).

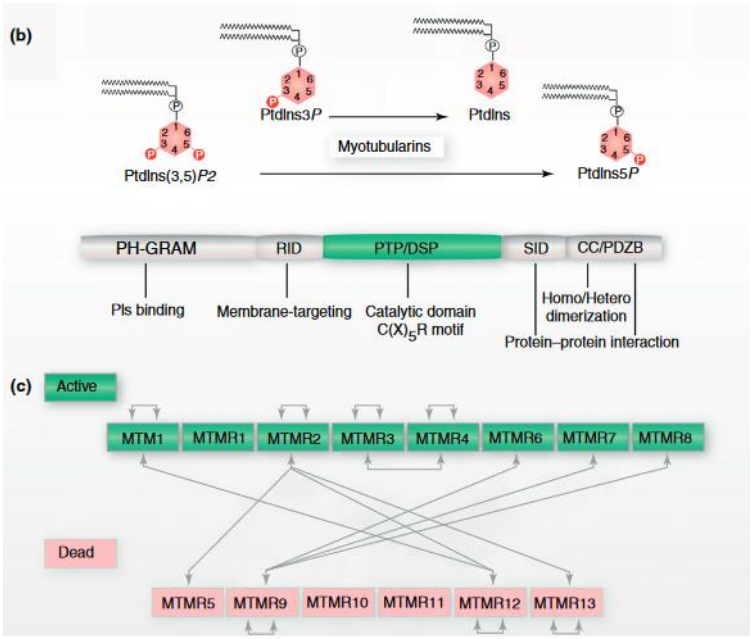

Figure 7: Myotubularin domain architecture and dimerization. Adapted from (Hnia et al., 2012). Myotubularins dephosphorylate PI(3)P or $PI(3,5)P_2$ to generate PI and PI(5)P, respectively. Their

domain architecture from n- to c-terminus is composed of a phosphoinositide binding PH-GRAM, a membrane-targeting RID, a catalytic, a protein-protein interaction promoting SID and a homo/hetero dimerization enabling CC/PDZB domain. There are active (MTM1, MTMR1-4, MTMR6-8, MTMR14) and inactive (MTMR5, MTMR9-13) isoforms. Inactive heterodimerize with active isoforms to influence their membrane localization, catalytic activity, and specificity.

1.5.4 PIP kinases

PIP kinases can be classified into multiple classes depending on the position they mainly phosphorylate.

PI3 kinases phosphorylate the D3 position of the myo inositol ring generating PI(3)P, PI(3,4)P_2 and PI(3,4,5)P_3 and thereby regulate a vast number of cellular processes ranging from cell signaling to endocytosis and membrane trafficking. They consist of three distinct classes that will be discussed in detail in the following sections.

PI4 kinases phosphorylate the D4 position of the myo inositol ring generating PI(4)P from PI. There are two classes of PI4 kinases, class II and class III (Boura & Nencka, 2015). Class I PI4 kinases do not exist as what was previously identified to be the first PI4 kinase turned out to actually be a PI3 kinase (Stephens, Hawkins, & Downes, 1989).

There are two isoforms of class II PI4 kinases: PI4KIIα and PI4KIIβ (Boura & Nencka, 2015). With around 50 kDa, they are relatively small kinases consisting of only a kinases domain and an extended unstructured n-terminus (Boura & Nencka, 2015). They tightly associate with membranes through the palmitoylation of a CCPCC motive in their catalytic domain and palmitoylation is essential for localization and catalytic activity (Barylko et al., 2009).

There are also two isoforms of class III PI4Ks: PI4KIIIα and PI4KIIIβ. They are completely unrelated to class II PI4Ks and harbor a vastly different domain architecture. They contain an extended unstructured n-terminus, a helical domain and a kinase domain, resembling the structural organization of PI3 kinases (Boura & Nencka, 2015). They lack the CCPCC motif of the class II PI4Ks and therefore are much more cytoplasmatic and require scaffold proteins for membrane recruitment (Klima et al., 2016; Sasaki, Ishikawa, Arita, & Taniguchi, 2012). Interestingly, PI4KIIIβ also fulfills scaffolding functions and facilitates Rab11 membrane

recruitment through an atypical interaction between the helical domain of PI4KIIIβ and a sequence just outside the switch I region of Rab11 (Burke et al., 2014).

Furthermore, the D4 position of PI(5)P is phosphorylated by type II PIP kinases (PIP4Kα, -β, -γ) to generate PI(4,5)P_2 (Balla, 2013). Because PI(5)P is of very low abundance and thus most PI(4,5)P_2 is generated by the PIPKI mediated phosphorylation of PI(4)P , the cellular role of PIP4Ks is still debated and it was suggested that the main function is to regulate PI(5)P levels rather than contribute to PI(4,5)P_2 synthesis (D. G. Wang et al., 2019).

The D5 position is phosphorylated by phosphatidylinositol phosphate kinases (PIP kinases). Type I PIP kinases generate PI(4,5)P_2 from PI(4)P and contain three enzymes: PIPKIα, -β, -γ (Balla, 2013). They regulate PI(4,5)P_2 levels at the plasma membrane and are crucial for the initiation of endocytosis and the regulation of actin dynamics (Mandal, 2020).

Mammalian type III PIP kinases only consist of PIKfyve, which generates PI(3,5)P_2 from PI(3)P (Balla, 2013). PI(3,5)P2 is thought to be most abundant on late endosomes and lysosomes and is crucial for their proper function. It activates ion channels such as TRPML1 and TPC1,2 a loss of PIKfyve leads to swelling of lysosomes and impairs lysosome function (Hasegawa, Strunk, & Weisman, 2017).

1.5.5 PI 3-kinases

PI3 kinases phosphorylate the D3 position of the myo inositol ring generating PI(3)P (class II + III), PI(3,4)P_2 (class II) and PI(3,4,5)P_3 (class I). They can be divided into three subgroups, class I, class II, and class III (Figure 8). Whereas class I PI3Ks primarily localize to the plasma membrane to regulate cellular signaling downstream of activated plasma membrane receptors (Auger, Serunian, Soltoff, Libby, & Cantley, 1989), class II and class III PI3Ks localize to a broader spectrum of membranes, including the plasma membrane, endosomes, lysosomes, and autophagosomes (Braccini et al., 2015; Brown & Auger, 2011; Franco et al., 2016; Marat et al., 2017; Posor et al., 2013; Russell et al., 2013). All classes of PI3Ks are evolutionarily related as they are all sensitive to inhibition by Wortmannin and contain a conserved PI3K core (Brown & Auger, 2011) (Figure 2). The PI3K core consists of a C2 domain, a helical domain and a bilobal kinase domain. The N-lobe and C-lobe form the ATP and lipid substrate binding cleft containing the activation loop, catalytic loop, and P-loop. The activation loop is essential for lipid substrate binding and specificity and for its coordination

towards the catalytic center. It contains a DFG motif that is conserved across all PI3Ks and variable polybasic stretches that bind to the phosphate groups of phosphoinositides (Burke, 2018; Miller et al., 2014; Walker, Perisic, Ried, Stephens, & Williams, 1999).

1.5.5.1 Class I

Class I PI3Ks can be further divided into two classes, class IA containing p110α, p110β and p110δ and class IB containing p110γ. Upon their activation by plasma membrane receptors, class I PI3Ks promote cell growth, proliferation, migration and anabolic signaling (Bilanges, Posor, & Vanhaesebroeck, 2019). Class I PI3Ks contain an n-terminal Ras binding domain (RBD) and Ras binding facilitates the association of class IA with the plasma membrane (Buckles, Ziemba, Masson, Williams, & Falke, 2017; Siempelkamp, Rathinaswamy, Jenkins, & Burke, 2017). The class I activation loop consists of two basic boxes: an N-terminal KKKK motif (in p110α) binds the 5' phosphate, and a C-terminal KRER motif (in p110α) binds the 4' phosphate of $PI(4,5)P_2$ (Pirola et al., 2001). Furthermore, class I activity is controlled by the association with regulatory subunits. Class IA associates with p85α, p85β, p55α, p50α and p55γ, whereas class IB associates with p101 and p84 (Rathinaswamy & Burke, 2020).

1.5.5.2 Class II

The Class II PI3Ks consists of three isoforms: PI3KC2α, PI3KC2β and PI3KC2γ. All of them contain a PI3K core, an RBD and C-terminal PX and C2 domains (Koch, Dornan, Hessenberger, & Haucke, 2021). PI3KC2α and PI3KC2β also contain an extended, unstructured N-terminal domain that mediates protein-protein interactions required for their recruitment to membranes. PI3KC2α and PI3KC2β both contain a clathrin binding motif and PI3KC2β additionally contains stretches that mediate binding to the mTORC1 subunit Raptor and a phosphorylation site at Thr279 that facilitates the phosphorylation dependent association of inhibitory 14-3-3 proteins (Gaidarov, Smith, Domin, & Keen, 2001; Marat et al., 2017; Wallroth, Koch, Marat, Krause, & Haucke, 2019; Wheeler & Domin, 2006). Furthermore, PI3KC2β can bind to the endocytic scaffolding protein intersectin-1 presumably through interactions between SH3 domains of intersectin-1 and proline stretches in the n-terminus of PI3KC2β (Das et al., 2007).

So far, only PI3KC2γ has been shown to bind to a small GTPase through the RBD. Rab5 recruits PI3KC2γ to early endosomes and is required for its regulation of AKT2 at endosomes (Braccini et al., 2015). It is very likely however, that PI3KC2α and PI3KC2β can also be activated and recruited to membranes by small GTPases (Koch et al., 2021).

The C-terminal PX and C2 domain of PI3KC2α have been studied in detail. They both enable binding to PI(4,5)P_2 independently of Ca^{2+} ions (Chen, Tillu, Chandra, & Collins, 2018; L. Liu et al., 2006; Stahelin et al., 2006). So far it is not known if the PX and C2 domains of PI3KC2β and PI3KC2γ also mediate binding to PI(4,5)P_2 but given the high conservation of these domains it at least seems plausible.

The activation loop of class II PI3Ks lacks the N-terminal basic box found in class I, and thus class II PI3Ks show very low activity towards PI(4,5)P_2. However, they contain the C-terminal basic box as a KRDR/KRER motif and thus can bind and phosphorylate PI(4)P to generate PI(3,4)P_2. Interestingly, when the class II activation loop is integrated into class I PI3Ks, the substrate specificity changes from PI(4,5)P_2 to PI(4)P and PI (Bondeva et al., 1998; Pirola et al., 2001).

HDX proteomic studies with PI3KC2α gave insights into the activation of class II PI3Ks. It was found that PI3KC2α can occur in an auto-inhibited, closed conformation in which the PX and C2 domains fold back onto the kinase domain to form contacts with the kα7-kα8 loop. This greatly reduces catalytic activity. In cells, this closed conformation is opened by the association of the PX and C2 domains with PI(4,5)P_2 at the plasma membrane and the interaction of the n-terminus with clathrin, drastically increasing catalytic activity (H. Wang et al., 2018).

Furthermore, structural studies identified a unique, stalk-forming helical bundle domain (HBD) in between the RBD and N-C2 domain of PI3KC2α. This domain was dispensable for catalytic activity but was required for the interaction of PI3KC2α with the microtubule-binding protein TACC3, suggesting that it plays a role as a scaffold in mitosis (Gulluni et al., 2017; Lo, Zhang, et al., 2022). Since this region is conserved in all class II PI3Ks, it is very likely that PI3KC2β and PI3KC2γ also contain an HDB.

1.5.5.3 Class III

The class III of PI3Ks contains VPS34 as its only member. The VPS34 activation loop does not contain basic boxes and thus cannot bind the 4'- or 5'- phosphate explaining why VPS34 only synthesizes PI(3)P from PI. Furthermore, the activation loop of VPS34 is completely ordered, unlike in class I and class II PI3Ks (Ohashi, 2021). VPS34 is the smallest of all PI3Ks only containing PI3K core (Koch et al., 2021). VPS34 is present in two distinct complexes that both contain VPS34, VPS15 and Beclin 1. ATG14L is specific for complex I and UVRAG is specific for complex II (Baskaran et al., 2014; Ohashi, 2021). Complex I is essential for the initiation of autophagy (Jaber et al., 2012). It localizes to ER membranes where the enrichment of PI(3)P leads to the recruitment of WIPI proteins and phagophore formation (Axe et al., 2008; Grimmel, Backhaus, & Proikas-Cezanne, 2015).

Complex II is required for the endocytic pathway. It is recruited to early endosomes by active Rab5 and leads to the accumulation of PI(3)P on endosomes (Christoforidis et al., 1999; Murray, Panaretou, Stenmark, Miaczynska, & Backer, 2002). This enables the recruitment of PI(3)P effector proteins like Hrs which are crucial for receptor sorting and the formation of multivesicular bodies (Bache, Brech, Mehlum, & Stenmark, 2003).

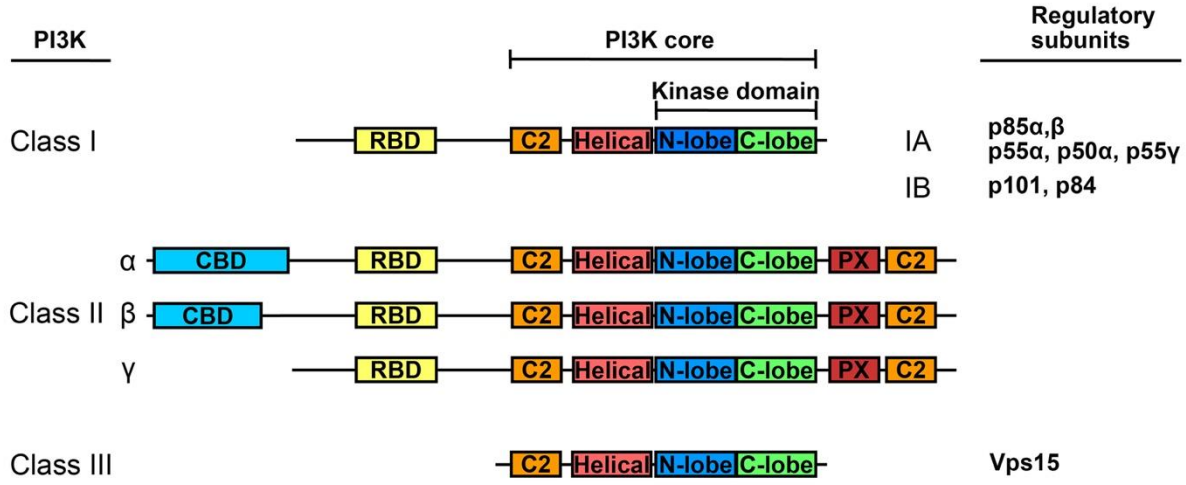

Figure 8: Domain architecture of PI 3-kinases. Adapted from (Koch et al., 2021). PI 3-kinases share (from n to c terminus) a ras binding domain (RBD; yellow), a C2 domain (orange), a helical domain (light red), and a kinase domain consisting of an N-lobe and a C-lobe (blue and green). They can be

divided into three classes: Class I contains two subclasses, IA and IB and requires several regulatory subunits; Class II contains PI3KC2α, PI3KC2β and PI3KC2γ harboring an extended unstructured n-terminus mediating regulatory protein interactions; Class III contains Vps34 requiring the regulatory subunit Vps15.

1.6 Cellular functions of Class II PI 3-kinase β

Class II PI 3-kinases have been linked to the regulation of many cellular processed ranging from endocytosis to endosomal membrane sorting and cellular signaling (Koch et al., 2021). This introduction will focus on the cellular functions of PI3KC2β.

1.6.1 PI3KC2β regulates membrane trafficking

Like PI3KC2α, PI3KC2β was initially identified as a plasma membrane localized lipid kinase. Both enzymes bind clathrin and PI3KC2β further binds to the endocytic adaptor protein intersectin as well as to Grb2 (Das et al., 2007; Wheeler & Domin, 2001, 2006). The functions of PI3KC2β at the plasma membrane are not fully understood. It was speculated that PI3KC2β acts downstream of the EGF receptor, as EGF triggers the recruitment of PI3KC2β to Grb2. However, a function of PI3KC2β in EGF signaling remains unknown (Arcaro et al., 2000; Wheeler & Domin, 2001). Furthermore, PI3KC2β has been linked to clathrin-mediated pinocytosis as it is required for actin filament assembly at clathrin coated structures (Aung et al., 2019). The exact mechanism of this process is unknown.

In metabolic tissues PI(3)P on APPL1 positive very early endosomes produced by PI3KC2β was required for trafficking of the insulin receptor to conventional, EEA1 positive early endosomes. A loss of PI3KC2β lead to the expansion of the APPL1 compartment and an increase in insulin induced Akt signaling (Alliouachene et al., 2015).

1.6.2 PI3KC2β regulates nutrient signaling

PI3KC2β was shown to be recruited to late endosomes and lysosomes upon growth factor deprivation in HEK293T and HeLa cells. There, it produces a local pool of PI(3,4)P_2

inhibiting mTORC1 activity (Marat et al., 2017). PI(3,4)P_2 produced by PI3KC2β has also been shown to be required for cholesterol transport between late endosomes and the ER via the cholesterol transporter ORP1L (Dong et al., 2019). The regulation of PI3KC2β recruitment to late endosomes and lysosomes is not fully understood. In growth factor abundant conditions, PI3KC2β is mainly cytoplasmatic. This is achieved via an inhibiting phosphorylation by PKN2 at threonine 279 in the unstructured N-terminal domain. The phosphosite is then bound by inhibitory 14-3-3 proteins that induce PI3KC2β dimerization and sequestration into the cytoplasm (Wallroth et al., 2019). PKN2 itself is activated by the small GTPase RhoA and through phosphorylation by mTORC2 (Flynn, Mellor, Casamassima, & Parker, 2000; Schmidt, Durgan, Magalhaes, & Hall, 2007).

1.6.3 PI3KC2β regulates cell migration and is implicated in various cancers

PI3KC2β has been implicated in cancer and metastasis as it is overexpressed in several tumors (Boller et al., 2012; Chikh et al., 2016). Furthermore, it was shown to be required for cell migration and thus metastasis formation (Domin et al., 2005; Katso et al., 2006; Kitatani et al., 2016; Mavrommati, Cisse, Falasca, & Maffucci, 2016). In line with that, the overexpression of PI3KC2β in HEK293T cells was shown to inhibit cell migration (Domin et al., 2005). Mechanistically, PI3KC2β is recruited to focal adhesions upon growth factor starvation. PI3KC2β induced PI(3,4)P_2 synthesis in turn activates the RhoA GAP ARAP3 leading to RhoA inactivation and stress fiber destabilization (Posor et al., 2022). This destabilizes focal adhesions and facilitates their turnover. Focal adhesion turnover is a key requirement for cell migration (Ezratty, Bertaux, Marcantonio, & Gundersen, 2009; Moreno-Layseca, Icha, Hamidi, & Ivaska, 2019).

1.6.4 PI3KC2β depletion rescues x-linked centronuclear myopathy

Centronuclear myopathy (CNM) is a rare congenital muscular disorder caused by loss of function (LoF) mutations in MTM1 (x-linked) (Laporte et al., 1996), LoF mutations in BIN1 (autosomal recessive) (Nicot et al., 2007) and gain of function (GoF) mutations in DNM2 (autosomal dominant) (Bitoun et al., 2005; Gomez-Oca, Cowling, & Laporte, 2021). It is

characterized by a generalized muscle weakness with severe histological alterations like the presence of very small, rounded muscle fibers with enlarged, centrally located nuclei (Lawlor & Dowling, 2021) and disorganized T-tubules (Dowling et al., 2009). Boys carrying mutations in MTM1 rarely live to adulthood with up to 60% dying within the first two years of life (Biancalana et al., 2003). To date there are three treatments in clinical trials, but none are approved so far. Treatment options explored are either based on gene replacement therapy (Lawlor & Dowling, 2021; Tasfaout, Cowling, & Laporte, 2018) (NCT03199469, NCT03368742, NCT03375164) or on RNA based knockdown of DNM2 (Tasfaout et al., 2018; Trochet et al., 2018). Of note, these approaches come with high risks of adverse events and are extremely expensive. This underlines the need for a safe and simple therapy for XLCNM ideally based on small molecule inhibitors.

Strikingly, muscle specific depletion of PI3KC2β was shown to rescue the onset of XLCNM in a MTM1 knock out mouse model. Even postnatal depletion of PI3KC2β after symptoms had already occurred, largely reversed the symptoms observed (Sabha et al., 2016). There is speculation that this rescue is mediated by the restoration of endosomal PI(3)P levels (Koch et al., 2021; Ribeiro, Yuan, Tanentzapf, Dowling, & Kiger, 2011; Velichkova et al., 2010), although the exact mechanism of this rescue remains unclear.

1.7 Pathophysiology of CNM

The mechanisms underlying CNM remain unclear but there is a plethora of cellular pathways that are affected in similar manners by LoF mutations in MTM1 and BIN1 respectively or GoF mutations in DNM2. Most prominently, trafficking of the β1 integrin adhesion receptor seems to be impaired in CNM (Ketel et al., 2016). All disease associated genes are involved in endocytic trafficking: MTM1 is required for the removal of PI(3)P on recycling endosomes to enable the PI4KIIα mediated generation of PI(4)P. This leads to the recruitment of exocyst components and facilitates exocytosis (Ketel et al., 2016; Mizuno-Yamasaki, Medkova, Coleman, & Novick, 2010). In line with these findings, β1 integrin was observed to accumulate in recycling endosomes upon MTM1 depletion in HeLa cells and in primary fibroblast obtained from CNM patients (Ketel et al., 2016). This likely leads to reduced surface levels of β1 integrin or to miss localized surface β1 integrin clusters and this might be

problematic due to their importance in muscle development (Ketel et al., 2016; Koch et al., 2021; Schwander et al., 2003). DNM2 is a large GTPase involved in membrane scission in endocytosis and recycling (Antonny et al., 2016; Ferguson & De Camilli, 2012). Strikingly, DNM2 is known to be involved in the clathrin mediated endocytosis of β1 integrin (Lee et al., 2014; Y. Wang, Cao, Chen, & McNiven, 2011).

1.7.1 Integrin dynamics

Integrins are the core receptors required for the adhesion of cells to the extracellular matrix. They are a family of 24 heterodimeric type I transmembrane glycoproteins and are formed by the non-covalent association of one of 18 α and one of 8 β subunits (Mishra & Manavathi, 2021). Integrins occur in three different conformations: a bend, inactive conformation, a primed, extended-closed conformation that is formed by the association of the scaffolding proteins Talin and Kindlin with the cytoplasmatic tail of the β subunit, and an active, ligand bound, extended-open conformation. The binding of Talin to the β subunit is crucial for integrin activation and ligand binding, as it forces a conformational change that strongly increases the affinity of the integrin receptor for its ECM ligands. This process is termed inside-out signaling (Askari, Buckley, Mould, & Humphries, 2009; Chinthalapudi, Rangarajan, & Izard, 2018; Mishra & Manavathi, 2021; Schumacher, Vazquez Nunez, Biertumpfel, & Mizuno, 2022). Talin itself is regulated by $PI(4,5)P_2$ at the plasma membrane as $PI(4,5)P_2$ binding to Talin is required for a conformational change that enables its association with the β1 integrin tail (Ye, McLean, & Sligar, 2016). Furthermore, Talin directly links integrins to the actin cytoskeleton thereby enabling force generation and transmission (Calderwood, Campbell, & Critchley, 2013). To form a new adhesion, activated integrins form clusters regulated by scaffolding proteins and lipids (Mishra & Manavathi, 2021; C. Wu, 2007). These initial adhesions acquire several other proteins like Paxillin, Vinculin and Zyxin as they mature to become focal adhesions (Schumacher et al., 2022). Active integrin receptors initiate a number of signaling pathways (outside-in signaling).

To enable cell migration, focal adhesions serve as anchorage points for actomyosin dependent forces that pull the cell forward (D'Souza et al., 2020). Focal adhesions at the rear end of a migrating cell need to disassemble to allow cell-body translocation (Huttenlocher &

Horwitz, 2011). Disassembly is initiated by actin destabilization at the focal adhesion and subsequent internalization of integrins (Chao & Kunz, 2009; Posor et al., 2022).

After internalization, integrins are largely recycled to the leading edge of the cell where they are required for the formation of new adhesions. A small portion of internalized integrins is also targeted for lysosomal degradation (Moreno-Layseca et al., 2019). Integrins are internalized by clathrin dependent and independent pathways (Moreno-Layseca et al., 2019). This seems to depend on their localization and activation status: endocytosis from disassembling focal adhesions in migrating cells is thought to occur in a clathrin dependent manner (Chao & Kunz, 2009; Ezratty et al., 2009). There is increasing evidence that the active conformation of integrins is internalized from disassembling adhesions (Arjonen, Alanko, Veltel, & Ivaska, 2012). Integrins remain in the ligand bound active conformation and are endocytosed together with the ligand (mostly fibronectin). CME of active β1 integrins requires the Dab2 adaptor protein but occurs independently of AP-2 function (Teckchandani, Mulkearns, Randolph, Toida, & Cooper, 2012). After internalization, the ligand dissociates from the integrin dimer, but Talin and FAK stay bound to the integrin tail to keep the integrin dimer in the active conformation (Nader, Ezratty, & Gundersen, 2016). Internalized active integrins are then sorted into Rab5 positive early endosomes and then further directed to recycling, predominantly through the Rab11 and SNX17 dependent long recycling pathway (Arjonen et al., 2012; Powelka et al., 2004). A small portion of internalized integrins is also targeted to late endosomes for subsequent lysosomal degradation (Bottcher et al., 2012) (Figure 9). This occurs at relatively low rates and results in an integrin half life time of around 12-24 hours depending on cell type (Moreno-Layseca et al., 2019).

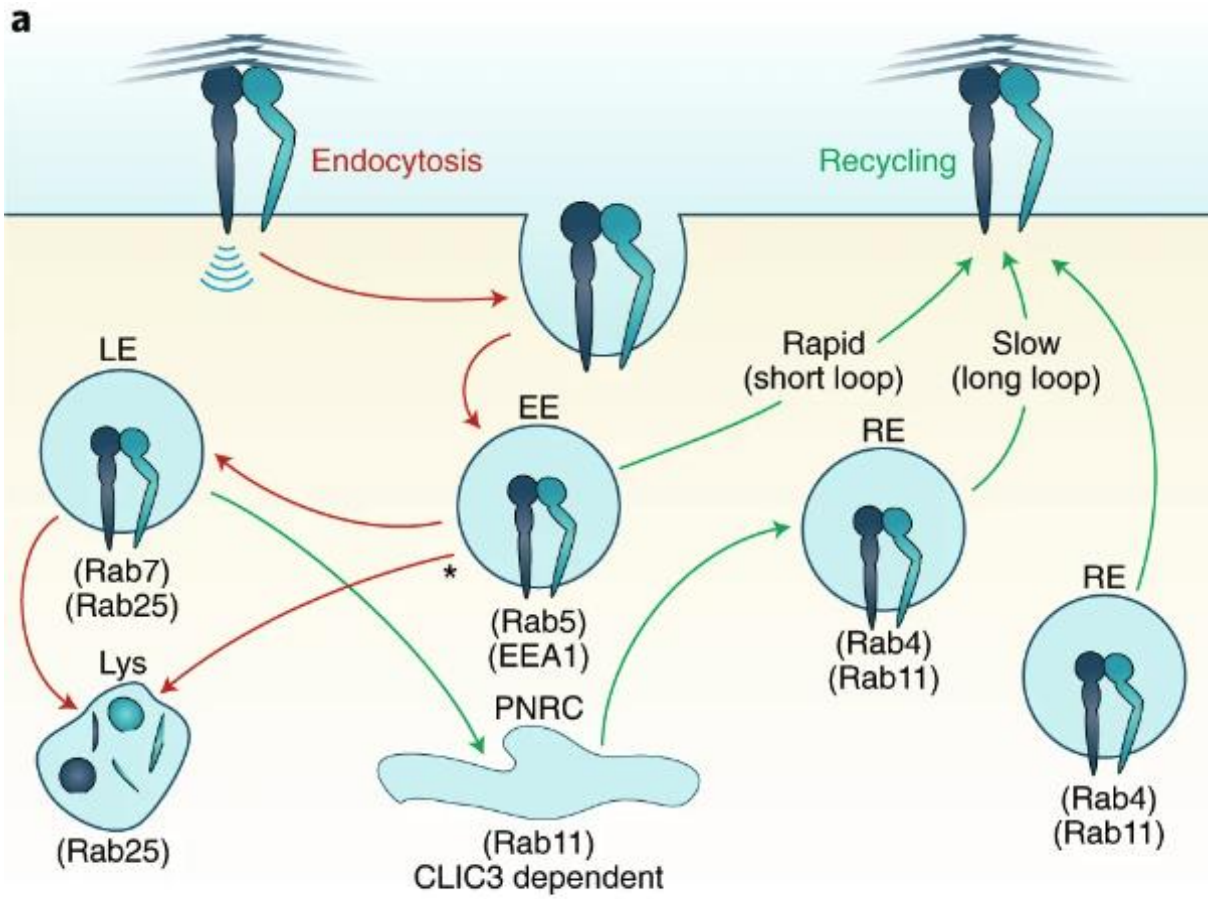

Figure 9: Integrin surface levels are controlled by endocytosis and recycling. Adapted from (Moreno-Layseca et al., 2019). After the destabilization of integrin mediated adhesions, integrins detach from the ECM while still binding the fibronectin ligand. They are in turn internalized by CME and sorted into early endosomes (EE). From there, they can either directly recycle back to the plasma membrane or take the longer route via Rab11 containing recycling endosomes (RE). A small portion of internalized integrins is targeted for lysosomal degradation.

1.7.2 Healthy muscle structure and physiology

Skeletal muscle is composed of bundles of fasciles which consist of bundles of myofibers (Figure 10). Myofibres, also called myotubes, are single, multinucleated muscle cells that form through the fusion of precursor cells called myoblasts. Myotubes contain multiple myofibrils, wrapped by the sarcoplasmic reticulum, that are essential for muscle function. Myofibrils are formed by series of sarcomers, the smallest functional units of striated muscle. Sarcomers consist of actin and myosin filaments that enable muscle

contraction: myosin heads attach to the actin filaments and pull them along the myosin chains towards the center of the sarcomere thus leading to muscle contraction. A sarcomere is composed of a Z line required to anchor actin filaments, an I band containing thin actin filaments and an A band containing the entire thick filaments. Within the A band, there is the H zone which only contains thick myosin filaments but no actin (Mukund & Subramaniam, 2020).

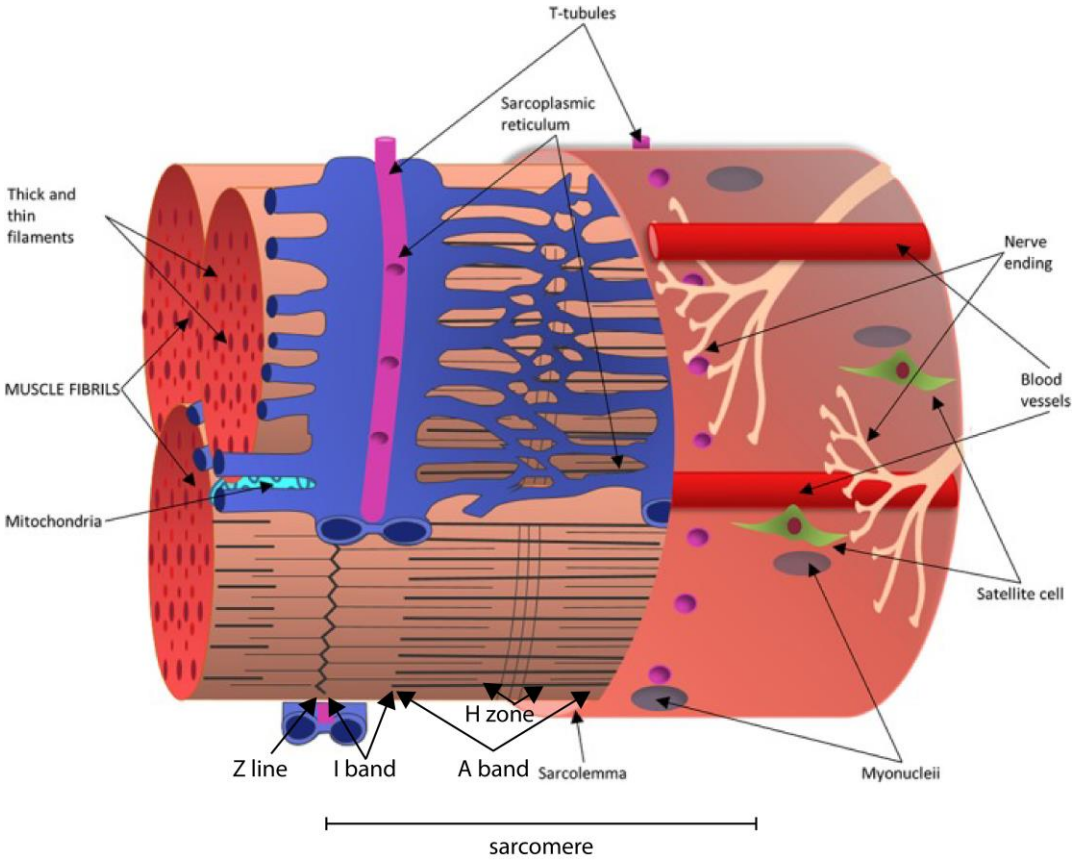

Figure 10: Organization of a myotube. Modified from (Mukund & Subramaniam, 2020). Skeletal muscle is composed of bundles of fasciles which consist of bundles of myofibers. Myofibers contain multiple myofibrils, wrapped by the sarcoplasmic reticulum. They are formed by a series of sacomeres required for muscle contraction. Myofibers are traversed by T-tubels which are crucial for ion homeostasis and contraction.

Myotubes are traversed by so called T-tubules at the overlap between A and I bands. They are extensions of the plasma membrane that extend into the center of muscle cells and contain large numbers of ion channels required for muscle contraction.

1.7.3 Myotubes form by myoblast fusion

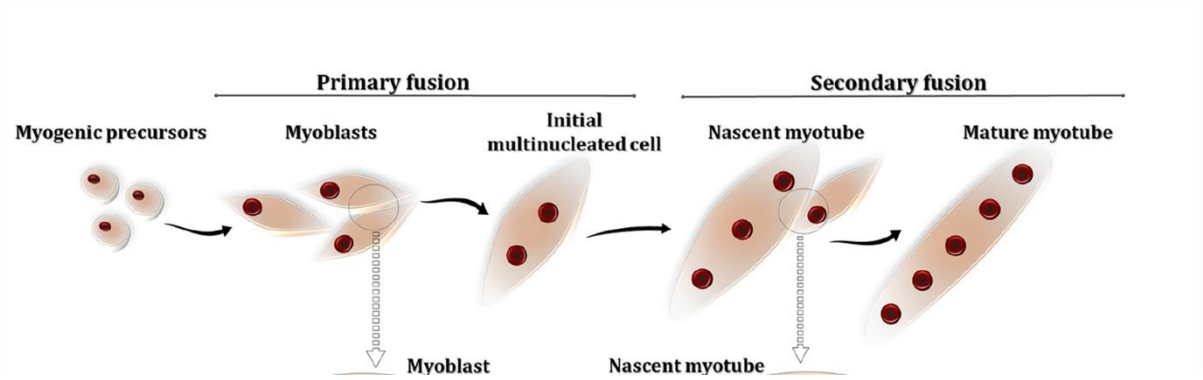

Figure 11: Myoblast fusion. Adapted from (Lehka & Redowicz, 2020). Myotube generation is initiated by the differentiation of myogenic precursor cells into myoblasts. These myoblasts further differentiate and fuse with one another generating an initial multinucleated cell (primary fusion). Subsequently, additional myoblasts fuse to the nascent myotube, eventually generating a mature and fully functional myotube.

Myoblast fusion is integral to embryonic muscular development, muscle regeneration and muscle growth (Figure 11). The fusion process is initiated by the expression of myogenic regulatory factors (MRFs), a class of transcription factors composed of MyF5, MyoD, myogenin and MRF4. Myoblast then exit the cell cycle to terminally differentiate (Girardi et al., 2021). Subsequently, they elongate, migrate and align to one another (Griffin, Kafadar, & Pavlath, 2009). This enables the formation of cell-cell contacts required for fusion (Lehka & Redowicz, 2020). These cell-cell contacts require the proper localization of adhesion receptors such as β1 intergin (Schwander et al., 2003) and cadherin (Kaufmann, Kirsch, Irintchev, Wernig, & Starzinski-Powitz, 1999). Once myoblast successfully adhere to each other, fusion can occur. Therefore, the outer membrane leaflets fuse generating an unstable membrane stalk intermediate state that eventually expands into a fusion pore completing the process (Lehka & Redowicz, 2020). This process requires the action of multiple proteins to overcome the large energy barrier, most notably Myomaker (Millay et al., 2013) and Myomerger (Bi et al., 2017). After an initial fusion step (primary fusion), multinucleated myotubes can further expand by the secondary fusion of additional myoblasts. This process is especially important in muscle regeneration after injury and hypertrophy (Lehka & Redowicz, 2020).

2 Objective

The first objective of this thesis has been to investigate how PI3KC2β is recruited to late endosomal and lysosomal membranes upon growth factor starvation. Given the Ras binding domain contained in PI3KC2β, I have aimed to identify potentially interacting Rab GTPases and to investigate whether these GTPases are required for the recruitment of PI3KC2β.

Furthermore, I have investigated whether potentially interacting Rab GTPases are required for PI3KC2β function with regard to $PI(3,4)P_2$ production at late endosomes and lysosomes and the suppression of mTORC1 activity.

The second part of this thesis has been dedicated to the role of PI3KC2β in the pathogenesis of x-linked centronuclear myopathy (XLCNM). To this aim I have investigated if and how PI3KC2β regulates β1 integrin trafficking as miss localized β1 integrins are key features of centronuclear myopathies. Given the known interaction of PI3KC2β with clathrin and the endocytic adaptor protein Intersectin-1, I hypothesized that PI3KC2β plays a role in clathrin mediated endocytosis (CME) of β1 integrins. I therefore wanted to elucidate if PI3KC2β localizes to clathrin coated pits and interacts with other proteins involved in CME of β1 integrins. Finally, I aimed to investigate if C2C12 myoblasts harboring knock outs of either MTM1, PI3KC2β or both, can differentiate into myotubes and wanted to study whether results obtained in the previous part translate to C2C12 cells.

3 Material & Methods

3.1 Materials

3.1.1 Chemicals

Chemicals used in this study are listed in Table 2.

Table 2: Chemicals used in this study.

Chemical	Supplier
Agarose	Roth
Ampicillin sodium salt	Applichem
Ammoniumperoxydisulfat (APS)	Roth
Coomassie Brillant Blue G250	Roth
Acetic acid 99-100 %	Roth
β-mercaptoethanol	Sigma-Aldrich
BSA, fatty acid free	Sigma-Aldrich
CHAPS	
Ethanol 96 %	Roth
Ethidiumbromide 10 mg/ml	Roth
Glutathione	Roth
Glycine	Roth
Hydrochloric acid, 37%	Roth
Kanamycinsulfate	Applichem
Matrigel	Corning
Methanol	Merck
MOPS 20x SDS PAGE running buffer	Thermo Fischer Scientific
PBS	Life Technologies
Ponceau S	Roth

Saponin	Roth
Sodium chloride	Roth
N,N,N',N'-Tetramethylethylendiamin, 1,2-Bis(dimethylamino)-ethan (TEMED)	Roth
Tris-(hydroxymethyl)-aminomethan (Tris)	Roth
Triton X-100	Sigma-Aldrich
Trypsin/EDTA	Life Technologies
Tween-20	Merck

3.1.2 Buffers & Media

All buffers and media used in this study are listed in Table 3.

Table 3: Buffers & Media used in this study.

Buffer	Composition
10X TBE	890 mM Tris 20 mM EDTA 890 mM Boric acid
LB medium	1.0 % (w/v) yeast extract 0.5% (w/v) Trypton 0.5% (w/v) NaCl pH 7.4
LB plates	LB medium 15 g/l Agar-agar
1000X Ampicillin	100 mg/ml in milliQ water, sterile filtered

1000X Kanamycin	50 mg/ml in milliQ water, sterile filtered
2X YT medium	1.0 % (w/v) yeast extract 1.6% (w/v) Trypton 0.5% (w/v) NaCl pH 7.4
10X TBS	200 mM Tris 1.4 M NaCl pH 7.6
TBS-T	TBS + 0.05 % Tween 20
Coomassie Blue staining solution	1 g/l Coomassie G250 10 % Acetic acid 25 % Methanol
Coomassie destain	10 % Acetic acid 25 % Methanol
Immunoblot transfer buffer	24.6 mM Tris 0.192 M Glycine 20 % Methanol
Immunoblot blocking solution	Licor Blocking Buffer (TBS)
Integrin blocking buffer	1x PBS 10 % NGS
2X Bradford reagent	140 g/l Coomassie G250 200 ml 85% H_3PO_4 0.02% NaN_3
IPTG	0.5 M in milliQ water, filtered
Lysis buffer IP	50 mM HEPES, pH 7.4 150 mM NaCl 0.3 % CHAPS Protease inhibitor cocktail Phosphatase inhibitor cocktail 2 + 3
Lysis buffer PD	20 mM HEPES, pH 7.4 150 mM NaCl

	0.5 % CHAPS Protease inhibitor cocktail Phosphatase inhibitor cocktail 2 + 3
Lysis buffer integrins	75 mM Tris-HCl, pH 7.5 200 mM NaCl 7.5 mM EDTA 7.5 mM EGTA 1.5 % Triton X-100 0.75 % IGEPAL® CA-630 Protease inhibitor cocktail Phosphatase inhibitor cocktail 2 + 3
Lysis buffer RIPA	50 mM Tris-HCl, pH 7.5 150 mM NaCl 1 % IGEPAL® CA-630 0.5 % Sodium deoxycholate 0.1 % SDS Protease inhibitor cocktail Phosphatase inhibitor cocktail 2 + 3
Lysis buffer E.coli	50 mM Tris-HCl, pH 7.5 200 mM NaCl 1 mM EDTA 1 mM DTT 1 mg/ml lysozyme 1 mM PMSF 0.5 % Triton X-100 Protease inhibitor cocktail
PAGE sample buffer (5x)	0.25 M Tris-HCl, pH 6.8 10 % SDS 0.5 M DTT 50 % Glycerol 0.5 % bromphenol blue

Ponceau solution	0.1 % Ponceau S 5 % acetic acid
10X PBS (autoclaved)	1.37 M NaCl 27 mM KCl 43 mM Na_2HPO_4 14mM NaH_2PO_4 pH 7.4
DMEM incl. Glutamax (HeLa, and Hek293 cells)	Dulbecco's modified eagles medium 4.5g/l glucose 10% heat- inactived fetal calf serum 100 U/ml Penicillin 0.1 mg/ml Streptomycin
Trypsin/EDTA	200 mg/ml Versene (EDTA) 170,000 U trypsin/ml
PFA fixation	4 % PFA 4 % Sucrose 1x PBS, pH 7.4
Saponin blocking buffer	1x PBS 10 % NGS 0.05 % saponin
Triton blocking buffer	1x PBS 10 % NGS

3.1.3 Enzymes & purification kits

All restriction enzymes used were high fidelity enzymes from New England Biolabs (NEB). Other enzymes and purification kits are listed in Table 4.

Table 4: Enzymes & purification kits used in this study.

Enzyme or kit name	Supplier
Phusion® high fidelity DNA Polymerase	ThermoFisher
T4 DNA Ligase	ThermoFisher
T4 PNK	NEB
DNA miniprep kit	Machery-Nagel
DNA midiprep kit	Machery-Nagel
Genomic DNA extraction kit	Machery-Nagel

3.1.4 Antibodies

All antibodies used in this study are listed in Table 5.

Table 5: Antibodies used in this study.

Antigen	Species	Source	WB	IF	FACS
AP2µ	Mouse	BD transduction, 611351	1:1000	1:100	
Clathrin heavy chain	Rabbit	Abcam, ab21679	1:1000	1:100	
Dab2	Mouse	BD transduction, 610465	1:500		
GAPDH	Mouse	Sigma-Aldrich, G8795	1:20,000		
GFP	Mouse	Clonetech	1:2000	1:250	
Intersectin-1	Rabbit	In house	1:500		
Lamp2a	Rabbit	Abcam, ab18528		1:200	
LBPA	Mouse	Echelon, Z-PLBPA		1:200	

mCherry	Rabbit	Clonetech, 632496	1:1000		
Myogenin	Mouse	Abcam, ab1835			
Myosin heavy chain	Mouse	R&D, MAB4470	1:1000	1:100	
NUMB	Goat	Abcam, ab4147	1:500		
$PI(3,4)P_2$	Mouse	Echelon, Z-P034b		1:150	
PKN2	Rabbit	Abcam, ab138514	1:500		
Raptor	Rabbit	Millipore, 09-217	1:500		
Rab5	Rabbit	Abcam, 18211	1:500		
Rab7	Rabbit	Cell Signaling, 9367	1:500	1:50	
Rab14	Rabbit	Abcam, 28639	1:500		
Rab35	Rabbit	Proteintech, 11329-2-AP	1:500		
S6 kinase *(*P-T389*)*	Rabbit	Cell Signaling, 9234	1:500		
S6 kinase	Rabbit	Cell Signaling, 2708	1:500		
β3-tubulin	Rabbit	Synaptic System, 302302	1:1000		
β1 integrin (active, 9EG7; for C2C12)	Rat	BD Bioscience, 550531		1:250	1:200
β1 integrin (active, 12G19; for HeLa) – Alexa 647	Mouse	Abcam, ab202643		1:200	
β1 integrin (total; for HeLa)	Mouse	BD transduction, 610467	1:500		

β1 integrin (total; for C2C12)	Rat	Merck Millipore, MAB1997			1:200
β-actin	Mouse	Sigma, A5441	1:1000		

3.1.5 Oligonucleotides

All oligonucleotides used in this study are listed in Table 6.

Table 6: Oligonucleotides used in this study.

Name	Function	Sequence 5' – 3'
PI3KC2β_D1168K_f	Mutagenesis	CAGCCTTCTCATACTCCTTCTCCCCAGGGTTGTGT
PI3KC2β_D1168K_r	Mutagenesis	ACACAACCCTGGGGAGAAGGAGTATGAGAAGGCTG
PX458_Raptor_f	Cloning	CACCGAGCATTTCGGACTCCATCAG
PX458_Raptor_r	Cloning	AAACCTGATGGAGTCCGAAATGCTC
Upstream_Raptor_f	Gibson	AAATTTAAGCTACAACAAGGCAAGGCTTGACCGACGGATTGACTTTAATAACACGCCTCTACTG
Upstream_Raptor_r	Gibson	TTGCTCACCATACCGGTCATCAGTGGGGGAGGGGG
GFP_Raptor_f	Gibson	CCCCCTCCCCCACTGATGACCGGTATGGTGAGCAAGGGCGAG
GFP_Raptor_r	Gibson	TTGCAGCATTTCGGACTCGAATTCCGGGCCCTGAAACAGCACTTCCAGCTTGTACAGCTCGTCCATGC
Downstream_Raptor_f	Gibson	CTGGAAGTGCTGTTTCAGGGCCCGGAATTCGAGTCCGAAATGCTGCAATC
Downstream_Raptor_r	Gibson	CACAGTCGAGGCTGATCAGCGGGTTTAAACGGGCCTAAAAGCAGCCTGGAGGG

3.1.6 siRNAs

All siRNAs used in this study are listed in Table 7. If not stated otherwise, all siRNAs were ordered from Sigma. Smartpool siRNA mixes were acquired from Dharmacon. They were 21-mers including 3' dTdT overhangs.

Table 7: siRNAs used in this study.

Target	Sequence (5' – 3')
PI3KC2β	GCUACCAGCUAUGAAGAUU
MTM1	GATGCAAGACCCAGCGTAA
Exo70	GGUUAAAGGUGACUGAUUA
Sec3	CCUGUUGGAUAUGGGAAACAU
Dab2	UAGAGCAUGAACAUCCAGUAA
Rab7A	Dharmacon Smartpool
ITSN1	Dharmacon Smartpool
PKN2	Dharmacon Smartpool
msCHC	AAUGGAUCUCUUUGAAUACGG
msDNM2	ACCUACAUCAGGGAGCGAGAA

3.1.7 Plasmids

All plasmids used in this study are listed in Table 8.

Table 8: Plasmids used in this study.

Insert	Backbone	Source
GFP	pcDNA3.1	In house
mCherry	pcDNA3.1	In house
GFP-PI3KC2α	pcDNA3.1	(Posor et al., 2013)
GFP-PI3KC2β	pcDNA3.1	(Marat et al., 2017)

GFP-PI3KC2β D1168K	pcDNA3.1	This study
GFP-PI3KC2β kinase inactive	pcDNA3.1	(Marat et al., 2017)
GFP-PI3KC2β ΔN	pcDNA3.1	(Marat et al., 2017)
GFP-PI3KC2β class III like	pcDNA3.1	(Gozzelino et al., 2022)
GST-PI3KC2β 27-106	pGEX-6P1	(Marat et al., 2017)
GST-PI3KC2β 27-126	pGEX-6P1	(Marat et al., 2017)
GST-PI3KC2β 27-156	pGEX-6P1	(Marat et al., 2017)
GST-PI3KC2β 27-184	pGEX-6P1	(Marat et al., 2017)
GST-PI3KC2β 27-226	pGEX-6P1	(Marat et al., 2017)
GFP-Rab7A Q67L	pcDNA3.1	Addgene #28049
GFP-Rab7A T22N	pcDNA3.1	Addgene #28048
mCherry-Rab7 Q67L	pcDNA3.1	This study
mCherry-Rab7 T22N	pcDNA3.1	This study
gRNA Raptor	PX458	This study
Donor GFP-Raptor	pcDNA3.1	This study
Empty vector	PX458	Addgene #48138

3.1.8 Chemically competent *E.coli* cells

All chemically competent E.coli cells used in this study are listed in Table 9.

Table 9: Chemically competent *E.coli* cells used in this study.

Cell type	Function	Supplier
Top10	Cloning	Thermo Fischer
BL21 DE3	Protein expression	Thermo Fischer
D5-alpha	Gibson Assembly	NEB

3.1.9 Mammalian cell lines

All mammalian cell lines used in this study are listed in Table 10.

Table 10: Mammalian cell lines used in this study.

Cell line	Source
C2C12	ATCC
C2C12 MTM1 KO#1	Paula Samsó, (Samsó et al., 2022)
C2C12 MTM1 KO#2	Paula Samsó, (Samsó et al., 2022)
C2C12 MTM1 KO#3	Paula Samsó, (Samsó et al., 2022)
C2C12 PI3KC2β KO	Paula Samsó, (Samsó et al., 2022)
C2C12 double KO	Paula Samsó, (Samsó et al., 2022)
C2C12 MTM1^{hypo} / PI3KC2β KO	Paula Samsó, (Samsó et al., 2022)
COS7	ATCC
CLC-GFP COS7	(Posor et al., 2013)
HEK293T	ATCC
GFP-PI3KC2β HEK293T	(Marat et al., 2017)
GFP-Raptor HEK293T	This study
HeLa	ATCC

GFP-PI3KC2β HeLa	(Wallroth et al., 2019)

3.1.10 Consumables

All consumables used in this study are listed in Table 11.

Table 11: Consumables

Name	Supplier
Cell culture dishes (15 cm, 10 cm, 6 cm, 6 well, 12 well)	Sarstedt
Coverslips (18 mm)	Carl Roth
Eppendorf tubes (1.5 ml, 2 ml)	Sarstedt
Falcon tubes (15 ml, 50 ml)	Sarstedt
Glass bottles (250 ml, 500 ml, 1000 ml)	Shield Scientific
Latex gloves	Shield Scientivic
Nitrocellulose membrane 0.2 NC	Cytiva
Parafilm®	Pechiney Plastic Packaging
Pasteur pipettes (5 ml, 10 ml, 25 ml)	Thermo Fischer
Pipette tips (20 µl, 300 µl, 1000 µl)	Sarstedt

Pipettes (0.1-2 µl, 0.5-10 µl, 2-20 µl, 20-200 µl, 100-1000 µl)	Sarstedt
SDS PAGE Gels (NuPAGE™ 4-12 % Bis-Tris	Thermo Fischer
Superfrost microscopy slides	Thermo Fischer
Whatman Paper, ROTILABO®	Carl Roth

3.1.11 Equipment

All equipment used in this study is listed in Table 12.

Table 12: Equipment used in this study.

Name	Model	Supplier
Analytical balance	MSA 125P-100-D	Sartorius
Centrifuges	Beckman J2-21; Rotors: JA-10, JA-17	Beckman Coulter
	Beckman Avanti J-26XP; Rotors: JS-5.3, JA25.50	Beckman Coulter
	Eppendorf 5417-R	Eppendorf
	Eppendorf 5702R	Eppendorf
	Optima TLX; Rotors: TLA100.2, TLA110	Beckman Coulter
Gel documentation	Biorad ChemiDoc XRS+ system	Biorad
Heating block		
Incubator, cell culture		ThermoElectron

Incubator, bacteria		Memmert
Laser-scanning microscope	LSM710, LSM780	Carl Zeiss
Magnetic stirrer	VMS-C7	VWR International
Microvolume spectrophotometer	NanoDrop 1000	Thermo Fischer
pH meter	SevenEasy	Mettler-Toledo
Power supply	Standard Power Pack P25	Whatman Biometra
FACS		BD Biosciences
SDS PAGE tank	Mini Gel Tank	Thermo Fischer
Shaker	3005	GFL
Shaking incubator	Innova 44	New Brunswick Scientific
Vortex	RS-VA 10	VWR International
Water bath	TW12	JULABO
Water purifier	Arium® advance	Sartorius
Western blot tank	Protean Mini	Bio-Rad
Western blot imager	LI-COR Odyssey Fc	LI-COR

3.1.12 Software

All software used in this study is listed in Table 13.

Table 13: Software used in this study.

Software	Function	Link / Supplier
Adobe Illustrator	Figure design	Adobe
CCTop	Guide RNA design	https://cctop.cos.uni-heidelberg.de/
Fiji (ImageJ)	Image analysis	https://fiji.sc/

Jalview	Design of alignment figures	http://www.jalview.org/
NEBuilder	Gibson Assembly design	https://nebuilder.neb.com/#!/
Netprimer	Primer design	http://www.premierbiosoft.com/netprimer/
GraphPad Prism 9	Statistical analysis	GraphStats
Blastp	Protein blast	https://blast.ncbi.nlm.nih.gov/Blast.cgi?PAGE=Proteins
Clustal omega	Multiple sequence alignment	https://www.ebi.ac.uk/Tools/msa/clustalo/
ProtParam	Determine biochemical properties of proteins	https://web.expasy.org/protparam/
UCSC genome browser	Analyze genomes	https://genome.ucsc.edu/index.html
Uniprot	Protein database	http://www.uniprot.org/

3.2 Methods

3.2.1 Molecular biological methods

3.2.1.1 Purification of plasmid DNA

Plasmids were expressed in *E.coli* Top10 cells and purified using the NucleoSpin Plasmid Miniprep kit (Macherey-Nagel) for small culture volumes (up to 10 ml) and the

Plasmid Midi kit (Machery-Nagel) for larger cuture volumes (up to 200 ml) according to the manufacturer's instructions.

3.2.1.2 Purification of PCR products

PCR products were analyzed for purity on an agarose gel and subsequently purified using the NucleoSpin Gel and PCR clean up kit (Macherey-Nagel) according to the manufacturer's protocol.

3.2.1.3 Extraction of genomic DNA from cultured mammalian cells

Extractions were performed using the NucleoSpin Tissue Mini kit (Machery-Nagel) according to the manufacturer's instructions. Briefly, 10^7 HEK293T cells were collected and washed in PBS, resuspended in Proteinase K containing lysis buffer, lysed, and bound to silica columns. After several washing steps, genomic DNA was eluted in H_2O.

3.2.1.4 Polymerase chain reaction (PCR)

Primers for the amplification of cDNA or genomic DNA were designed to contain between 20 and 25 gene-specific nucleotides, have a guanine/cytosine content of 40-60% and melting temperatures (Tm) between 60 °C and 68 °C. The Tm difference for primer pairs was kept to a minimum, not exceeding 2 °C and a GC clamp was used at 3' ends. For subsequent cloning into a vector, restriction sites were added to the 5' ends of the primers and 4 random nucleotides were added 5' of the restriction site to allow efficient cleavage. The software NetPrimer was used to design the primers accordingly.

PCRs were performed in 50 µl reactions using 1x GC polymerase buffer, template DNA (1-10 ng for plasmid DNA and up to 1 µg for genomic DNA), 10 pmol of each primer, 200 µM dNTPs and 1 U phusion DNA polymerase. A touchdown protocol consisting of 10 cycles denaturation at 98 °C for 10 s, annealing at 68 °C -1 °C/cycle for 30s and elongation at 72 °C for 20 s/kb followed by 25 cycles of denaturation at 98 °C for 10 s, annealing at 58 °C for 30s

and elongation at 72 °C for 20 s/kb and a final elongation for 10 min at 72 °C was used. For genomic DNA an initial denaturation step of 2 min at 98 °C was performed.

3.2.1.5 Site directed mutagenesis

To introduce point mutations, short insertions (up to 15 bp) and deletions, primer pairs containing the desired mutations were designed. Primers were chosen to amplify the entire plasmid. Insertions were split up between forward and reverse primers, all other mutations were introduced into the forward primer. Annealing temperatures of around 65 °C were chosen and the difference in annealing temperatures between forward and revers primers was kept below 1 °C. The PCR was performed as described in the previous section and amplification was confirmed by agarose gel electrophoresis. Subsequently, 0.5 µl DpnI were added to the PCR product and incubated o.n. at 37 °C to degrade methylated template DNA. Next, PCR products were phosphorylated to allow for subsequent ligation: 2 µl of PCR product were added to 1 µl T4 ligation buffer, 0.5 µl PNK and 6.5 µl H_2O. The phosphorylation was performed at 37 °C for 30 min. For ligation, 5 µl PCR product were added to 1 µl T4 ligase buffer, 1 µl 50 % (w/v) PEG4000, 0.5 µl T4 ligase and 1.5 µl H_2O. The ligation was performed at 22 °C for 1h. Subsequently, 5 µl ligation product were transformed into *E.coli* Top 10 cells.

3.2.1.6 Gibson Assembly

Gibson assembly reactions were performed using the NEBuilder HiFi DNA Assembly kit. It was used to join multiple (up to 5) DNA fragments obtained by PCR into a linearized plasmid. Primers were designed to introduce overlaps with the upstream and downstream fragments respectively. This was done using the NEBuilder software with a minimum overlap of 25 nucleotides. PCR reactions were performed as described above and the vector (pcDNA3.1) was linearized using ApaI and MfeI. For the assembly reaction, 0.5 pmol total DNA fragments were mixed in a molar ratio of 1:1 and diluted with H_2O to yield a total volume of 10 µl. Subsequently, they were mixed with 10 µl HiFi DNA Assembly Master Mix and incubated at 50 °C for 60 min. Finally, 5 µl were transformed into NEB 5-alpha *E.coli* cells.

3.2.1.7 Cloning

All restriction enzyme digestions were performed using high fidelity enzymes (NEB) in 50 µl reactions containing 1x cutsmart buffer, 1 µg DNA and 10 U of each enzyme. Reactions were incubated at 37 °C for 2 h.

Dephosphorylation reactions were performed in 20 µl reactions using 1x antarctic phosphatase buffer, up to 500 ng of digested vector DNA and 5 U antarctic phosphatase. Reactions wer performed at 37 °C for 30 min followed by heat inactivation at 80 °C for 2 min. Dephosphorylated vector DNA was used in ligation reactions without further purification.
To ligate overlapping DNA ends, 10 µl reactions containing 100 ng vector DNA, a 3 time molar excess of insert DNA, 1x T4 Ligase buffer and 400 U T4 DNA ligase were incubated o.n. at 4 °C. Subsequently, 5 µl of the reaction was transformed into *E.coli* Top10 cells. As a negative control, one reaction was performed without insert DNA.

3.2.1.7.1 mCherry-Rab7A Q67L + mCherry-Rab7A T22N

GFP-Rab7A Q67L and GFP-Rab7A T22N were obtained from addgene. GFP was removed by restriction digest with HindIII and BamHI and mCherry was obtained by the restriction digest of mCherry in pcDNA3.1 using the same enzymes. Both constructs were gel purified and ligated as described above.

3.2.1.7.2 GFP-PI3KC2β D1168K

GFP-PI3KC2β D1168K was generated by site directed mutagenesis using GFP-PI3KC2β as a template. The following primers were used:

Forward:	5’	CAGCCTTCTCATACTCCTTCTCCCCAGGGTTGTGT	3‘
Reverse:	5‘	ACACAACCCTGGGGAGAAGGAGTATGAGAAGGCTG	3‘

The PCR reaction was performed as described above.

3.2.1.7.3 PX458 Raptor

To clone the guide RNA sequences into PX458, oligonucleotides containing BbsI overlap sites were synthesized. The following oligonucleotides were used:

Forward: 5’ CACCGAGCATTTCGGACTCCATCAG

Reverse: 5’ AAACCTGATGGAGTCCGAAATGCTC

Oligonucleotides were adjusted to 50 µM and 10 µl of each oligonucleotide were mixed. To anneal them, they were heated to 95 °C and cooled down to RT at -1 °C / min. The PX458 vector was digested with BbsI and gel purified. Subsequently, the annealed oligonucleotides were diluted 1:100 and 2 µl were ligated into 100 ng of digested vector as described above.

3.2.1.7.4 Donor for GFP-Raptor CRISPR

Upstream and downstream homology regions were chosen as described in the CRISPR/Cas9 section. Primers were designed using NEBuilder software: The sequences of the vector (pcDNA3.1) digested with ApaI and MfeI, the sequence of the upstream homology region, GFP and the downstream homology region were used to calculated primer sequences. A minimum overlap of 25 nucleotides was chosen. The vector was digested using ApaI and MfeI and gel purified subsequently. Homology regions were amplified by touchdown PCR as described above with the difference the initial denaturation step was prolonged to 2 min at 98 °C and that 1 µg of genomic DNA obtained from HEK293T cells was used as template. GFP was amplified from pcDNA3.1 containing GFP. All PCR products were gel purified and assembled with the vector DNA as described above. The following primers were used:

Upstream_forward:

5’ AAATTTAAGCTACAACAAGGCAAGGCTTGACCGACGGATTGACTTTAATAACACGCCTCTACTG 3‘

Upstream_reverse:

5’ TTGCTCACCATACCGGTCATCAGTGGGGGAGGGGG 3‘

GFP_forward:

5’ CCCCCTCCCCCACTGATGACCGGTATGGTGAGCAAGGGCGAG 3‘

GFP_reverse:

5’
TTGCAGCATTTCGGACTCGAATTCCGGGCCCTGAAACAGCACTTCCAGCTTGTACAGCTCGTCCATGC
3‘
Downstream_forward:
5’ CTGGAAGTGCTGTTTCAGGGCCCGGAATTCGAGTCCGAAATGCTGCAATC
Downstream_reverse:
5’ CACAGTCGAGGCTGATCAGCGGGTTTAAACGGGCCTAAAAGCAGCCTGGAGGG 3‘

3.2.1.6 Quantitative and qualitative analysis of nucleic acids

The concentration of DNA in solution can be determined using the OD at 260 nm. An OD_{260} of 1 thereby equals a concentration of 50 µg/ml. The purity of the DNA sample can be judged by the ratio of OD_{260} to OD_{280} which gives an indication on a potential contamination with proteins. For pure aqueous DNA solutions, the ratio equals 1.8.

For the analysis of PCR products or vector DNA, agarose gels were prepared using 0.7-1.5 % (w/v) agarose in 1x TAE buffer containing 1 µg/ml ethidium bromide. The gel was run at 8 V/cm for up to 45 min. DNA bands were detected using UV light.

3.2.1.7 Plasmid amplification in E. coli

To amplify plasmid DNA in *E. coli,* chemically competent cells were thawed on ice. To 50 µl cells, 1 ng of purified plasmid DNA or up to 5 µl of ligation reactions were added. After 20 min of incubation on ice, the samples were subjected to a heat shocked in a water bath at 42 °C for 45 s and immediately transferred to ice for 2 min. Subsequently, 1 ml of pre-warmed LB media (37 °C) was added and the samples were incubated at 37 °C and 600 rpm for 1 h. Subsequently, the cells were pelleted by centrifugation (1000 xg, 3 min), resuspended in 100 µl LB media and plated onto LB-Agar plates containing antibiotics for selection. The plates were incubated o.n. at 37 °C. The next day, single colonies were picked for further amplification and purification.

To store transformed *E. coli* cells, a culture of 5 ml was inoculated with one colony and incubated at 37 °C o.n. The next day, 250 µl *E. coli* suspension was mixed with 750 µl of 90% glycerol, snap frozen in liquid nitrogen and kept at -80 °C.

3.2.2 Biochemical methods

3.2.2.1 Cell lysates

For immunoprecipitations, cells were washed twice in ice-cold PBS and collected in lysis buffer (25 mM HEPES, pH 7.5, 0.3% CHAPS, 0.3% protease inhibitor cocktail and phosphatase inhibitors (cocktails 2 and 3). Lysates were cleared by centrifugation at 17,000 xg, 4 °C.

To analyze integrins, a lysis buffer containing 75 mM Tris-HCl pH 7.5, 200 mM NaCl, 7.5 mM EDTA, 7.5 mM EGTA, 1.5% Triton X-100, 0.75% IGEPAL® CA-630, protease inhibitor cocktail and phosphatase inhibitors (cocktails 2 and 3) was used.

For analysis of myosin heavy chain and myogenin by immunoblotting, differentiated C2C12 cells were lysed in RIPA buffer (50 mM TRIS-HCl, pH 7.5, 150 mM NaCl, 1% IGEPAL® CA-630, 0.5% sodium deoxycholate, 0.1% SDS, protease and phosphatase inhibitor cocktails) and subjected to brief sonification. Lysates were cleared by centrifugation at 17,000 xg, 4 °C.

For pulldown experiments, HEK293T cells were lysed in PD buffer (20 mM HEPES, pH 7.4, 150 mM NaCl, 0.3% protease inhibitor cocktail, phosphatase inhibitor cocktails 2 and 3 and 0.5% CHAPS). Lysates were cleared by centrifugation at 17,000 xg, 4 °C.

3.2.2.2 Bradford protein assay

1 ml Bradford solution was mixed with different concentrations of BSA (1-10 µg) to determine a standard curve. Subsequently, 1 µl of the protein solution was added to 1 ml Bradford solution and measured against a blank sample. The absorbance was measured at 595 nm and concentrations were determined by linearly fitting the standard values.

3.2.2.3 SDS-PAGE

To separate proteins according to their molecular mass, a denaturating, discontinous polyacrylamide gelelectrophoresis (PAGE) was performed. For denaturation, samples were added to 2x PAGE sample buffer and boiled at 95 °C for 5 min. Subsequently, samples were loaded onto NuPAGE 4-12 % Bis-Tris gels and run for approx. 90 min at 100 V in MOPS buffer. Subsequently, gels were either subjected to immunoblotting or stained for 2 h in coomassise solution followed by destaining in destaining solution or H_2O o.n.

3.2.2.4 Immunoblotting

After SDS-PAGE, gels were transferred onto nitrocellulose membranes by wet blotting. Blots were performed in blotting buffer for 90 min at 110 V. Subsequently, the membranes were stained in ponceau solution for 5 min, destained using blotting buffer, rinsed with TBS and blocked for 30 min in TBS blocking buffer. Subsequently, the primary antibody was diluted in TBS blocking buffer + 0.1 % (v/v) Tween20 and added to the membrane. After incubation for 2 h at RT or o.n. at 4 °C, membranes were washed three times for 5 min in TBS-T and incubated for 1 h using the secondary licor antibodies diluted 1:10,000 in TBS blocking solution + 0.1 % (v/v) Tween20. After three washing steps (TBS-T, 5 min), membranes were rinsed with TBS and analyzed using the LicorOdyssey system. For analysis, bands were marked with boxes of equal size, background was substracted and the mean intensity was determined.

3.2.2.5 Protein expression and purification from E.coli

A 50 ml LB-ampicillin overnight culture of BL21 cells transformed with the pGEX3 expression vector containing the target protein was prepared and incubated at 37 °C o.n. The next day, the culture was diluted into 500 ml LB-ampicillin and cells were grown at 37 °C to an OD_{600} of 0.6 before 1 mM IPTG was added to start the protein expression. The cells were further grown at 15 °C for approx. 12 h, pelleted by centrifugation and resuspended in 15 ml ice cold PBS containing 1 mM PMSF. Pellets were stored at -80 °C until further processing.

For purification, resuspended pellets were thawed and 1 mM PMSF and lysozyme (tip of spatula) were added to the resuspended pellet. The cells were lysed at 4 °C on an end-over-end rotor for 60 min, followed by sonification. Subsequently, the lysates were centrifuged (20.000 xg, 4 °C, 30 min) and the supernatants were collected. 500 µl Glutathione Agarose beads were washed once in ice cold PBS and then added to the supernatants and incubated for 2 h at 4 °C on an end over end rotor. Subsequently, the beads were washed 3 times in PBS containing 0.5 % Triton X-100 and either used for pulldown experiments or eluted using 500 µl of glutathione elution buffer.

3.2.2.6 GST pulldowns

For pulldown assays using GST-tagged proteins were expressed in *E. coli* BL21. As a negative control, the empty pGEX4T3 vector was used. LB medium was inoculated with an overnight pre culture and grown to an OD_{600} of 0.6-0.8. Induction of expression was performed with 1 mM IPTG at 16 °C for 14 h. Bacteria were lysed on ice by sonication in lysis buffer (50 mM Tris HCl pH7, 200 mM NaCl, 1 mM EDTA, 1 mM DTT, complete protease inhibitor cocktail) supplemented with 1 mg ml−1 lysozyme, 1 mM PMSF, 0.5% Triton X-100, and then centrifuged at 20,000 g for 30 min. GST-tagged proteins were purified from filtered bacterial lysates by incubation with Glutathione Sepharose 4B beads (GE Healthcare) for 2 h followed by extensive washing with lysis buffer. Beads were equilibrated in PD buffer (20 mM HEPES, pH 7.4, 150 mM NaCl, 0.3% protease inhibitor cocktail, phosphatase inhibitor cocktails 2 and 3 and 0.5% CHAPS) incubated with HEK cell lysates generated in PD buffer for 2 h at 4 °C. Beads were washed four times with PD buffer, and bound proteins were eluted in SDS–PAGE sample buffer, resolved by SDS–PAGE and analyzed via immunoblot.

3.2.2.7 Co-Immunoprecipitation using GFP-trap

HEK293T or HeLa cells expressing eGFP tagged proteins were cultured on 10 cm dishes and processed at 75 % confluency. Cells were washed twice in PBS and lysed in IP buffer (20 mM HEPES pH 7.4, 150 mM NaCl, 0.3 % CHAPS, protease and phosphatase inhibitors). Samples were centrifuged at 17,000g for 10 min at 4 °C, protein concentrations were

determined and adjusted, and the supernatant was then incubated with 15 µl GFP-Trap magnetic microparticles for 1 h at 4 °C. Beads were washed four times with IP buffer, and bound proteins were eluted in SDS–PAGE sample buffer, resolved by SDS–PAGE and analyzed via immunoblot.

3.2.2.8 Integrin surface turnover

To determine the turnover of total β1-integrins at the plasma membrane, I made use of a surface biotinylation assay. It is based on Sulfo-NHS-SS-Biotin that is cell impermeable due to its negative charge and readily reacts with and covalently links to primary amines that are found in lysine side chains. Thus, the entire surface proteome can be labelled. The labelling reaction can be performed under very mild conditions on living cells that can be further cultivated afterwards. After endocytosis, biotin labelled, internalized β1-integrins are either recycled back to the plasma membrane or targeted for degradation. Thus, differences in turnover can be detected through the quantification of remaining biotinylated β1-integrins. After an incubation step of 24 h in normal culture medium at 37 °C, remaining β1-integrins can be isolated using streptavidin beads and their levels can be determined by immunoblotting. Experiments were carried out using the following protocol:

HeLa cells in 6 well plates were either treated with control (siSCR) or PI3KC2β (siPI3KC2β) targeting siRNA. Subsequently, cells were washed 3x in ice cold PBS and biotinylated with 0.5 mg/ ml EZ-Link™ Sulfo-NHS-SS-Biotin for 30 min at 4 °C on a shaker. The biotinylation reaction was quenched by washing 4x with ice-cold TBS (Tris saturates the biotinylation reaction). Subsequently, cells were incubated in full medium at 37 °C for 0 h or 24 h respectively. Cells were lysed as described above and subjected to streptavidin pulldown using 100 µl magnetic streptavidin agarose beads per reaction. After 2h incubation at 4 °C on an end over end rotor, beads were washed 4 times in lysis buffer, bound proteins were eluted in SDS PAGE sample buffer and analyzed by SDS PAGE and immunoblotting. Bound levels of β1-integrin were determined and displayed as the ratio of β1-integrin at 24 h divided by β1-integrin levels at 0 h.

3.2.3 Cell biological methods

3.2.3.1 Culture of HEK293T and HeLa cells

HeLa and HEK293T cells were cultured DMEM containing 25 mM D-glucose, 4mM L-glutamine and phenol red supplemented with 10% (v/v) heat-inactivated fetal bovine serum, 100 U/mL penicillin and 100 µg/mL streptomycin. Cells were not used beyond passage 30 and routinely tested for mycoplasma contamination.

3.2.3.2 Culture of C2C12 cells

C2C12 cells were cultured in cultured DMEM containing 25 mM D-glucose, 4mM L-glutamine and phenol red supplemented with 10% (v/v) heat-inactivated fetal bovine serum, 100 U/mL penicillin and 100 µg/mL streptomycin. Cells were always kept at low confluence (<70%) to avoid the initiation of differentiation. Furthermore, cells were not used beyond passage 30 and routinely tested for mycoplasma contamination. For differentiation into myotubes, either $4x10^4$ cells per well were seeded on 0.1% (w/v) gelatin (Sigma)-coated ibiTreat 8-well chambers (ibidi) or $3x10^5$ cells were seeded on 0.1% (w/v) gelatin coated 6 well plates. This resulted in cells being at 90% confluency the next day. Subsequently, cells were washed three times with PBS to remove residual FBS and incubated in differentiation medium (DMEM containing 25 mM D-glucose, 4mM L-glutamine and phenol red supplemented with 2% (v/v) heat-inactivated horse serum, 100 U/mL penicillin and 100 µg/mL streptomycin) for 6 days. The medium was replaced daily. Differentiation was analyzed by immunoblotting for the early differentiation marker myogenin and the late differentiation marker myosin heavy chain (MHC). Furthermore, immunocytochemistry using myosin heavy chain antibodies and DAPI staining was performed. The nuclear fusion index (indicative of differentiation initiation) was acquired by determining the ratio of nuclei in MHC positive myotubes to the total number

3.2.3.3 Transfection of culture cells

For the transfection with siRNAs, cells were reverse transfected with 50 nM (HEK293T and HeLa cells) or 100 nM (C2C12 cells) siRNA using jetPRIME according to the manufacturer's instructions: for each µl of a 100 µM siRNA stock, four times the volume of jetPRIME and 1/20 of the amount of cell culture medium of jetPRIME buffer (e.g. 100 µl jetPRIME buffer for 2 ml medium in a 6 well plate) was used. All components were mixed and incubated for 10 min at RT and subsequently added to the cells. Transfection was repeated on the following day. Cells were processed after 72 h. For siRNA mediated knock down of Rab7A, cells were reverse transfected with 100 nM siRNA and transfected for a second time after 48h. Cells were processed 48h after the second transfection. For rescue experiments, cells treated with siRNA were transfected 12h prior to the experiment with plasmid DNA using jetPRIME according to the manufacturer's instructions: per µg of plasmid DNA, 2 µl of jetPRIME were used. JetPRIME buffer amount was 1/20 of the volume of medium used. All components were mixed and incubated for 10 min at RT and subsequently added to the cells. For the transfection with DNA, plasmids were transfected with jetPRIME, according to the manufacturer's instructions, for formats up to 6 well plates and with calcium phosphate (CaP) for larger formats. For CaP transfections in 10 cm dishes, 0.1 % TE buffer, 2x HBS and 2 M $CaCl_2$ were brought to RT. Subsequently, 400 µl 0.1 % TE was mixed with 10 µg DNA (5 µg of each construct for co-transfections) and 60 µl 2 M $CaCl_2$. 500 µl 2x HBS were added to a tube, placed on a vortex and the DNA mixture was added dropwise. After 10 min incubation at RT, the mixture was carefully added to the cells. Cells were incubated for at least 12 h (HEK293T and HeLa cells) or 36 h (C2C12 cells) before further processing.
For rescue experiments, siRNA treated cells were transfected with plasmid DNA using jetPRIME 12 h prior to the experiment.

3.2.3.4 Immunofluorescent staining (IF)

For IF, cells were seeded onto Matrigel-coated coverslips. The next day, cells were washed twice in PBS and fixed for 15 min at RT with 4% (w/v) PFA and 4% (w/v) sucrose in PBS. Subsequently, cells were washed 3 times with PBS, permeabilized and blocked for 30 min at RT in blocking buffer (10% (v/v) NGS, 0.05% (w/v) saponin in PBS). Primary and Alexa

Fluor-conjugated secondary antibodies diluted in blocking were incubated at RT for 2 h (or at 4 °C over night) and 1 h, respectively. Cells were washed 3 times with PBS and mounted using DAPI-containing mounting medium.

For IF of HeLa cells endogenously expressing eGFP-PI3KC2β, cells were seeded onto Matrigel-coated coverslips. The next day, cells were washed twice in PBS and pre-permeabilized with 0.05% saponin in PBS for 60 s, followed by a brief washing step in PBS. Subsequently, cells were fixed and stained as described above.

For IF to be analyzed by TIRF microscopy, ibidi 8 well plates were coated with Matrigel and cells were seeded one day prior to the experiment. Cells were washed twice in PBS and fixed for 15 min at RT with 4% (w/v) PFA and 4% (w/v) sucrose in PBS. Subsequently, cells were washed 3 times with PBS and permeabilized and blocked for 30 min at RT in blocking buffer (10% (v/v) NGS, 0.1% (w/v) triton x-100 in PBS). Primary and Alexa Fluor-conjugated secondary antibodies diluted in blocking were incubated at RT for 2 h and 1 h, respectively. Finally, cells were washed 3 times with PBS.

For surface stainings in HeLa cells, cells were seeded onto Matrigel-coated coverslips. The next day, cells were washed twice in ice-cold PBS and incubated with fluorescently labelled antibodies in blocking buffer (10 % NGS in PBS) for 45 min on ice. Cells were washed twice in ice-cold PBS and fixed for 30 min on ice with 4% (w/v) PFA and 4% (w/v) sucrose in PBS. Subsequently, cells were washed 3 times with PBS and mounted using DAPI-containing mounting medium.

For surface stainings in C2C12 cells, cells were seeded onto matrigel-coated coverslips. The next day, cells were washed twice in ice-cold PBS and incubated with primary antibodies in blocking buffer (10 % NGS in PBS) for 45 min on ice. Cells were washed twice in ice-cold PBS and fixed for 30 min on ice with 4% (w/v) PFA and 4% (w/v) sucrose in PBS. After 3 washing steps with PBS, secondary antibodies were diluted in blocking buffer and incubated for 90 min at RT. Subsequently, cells were washed 3 times with PBS and mounted using DAPI-containing mounting medium.

For lipid stainings, HeLa or C2C12 cells were seeded onto Matrigel-coated coverslips. The next day, cells were washed twice in PBS and fixed with 2% (w/v) PFA and 2% (w/v) sucrose in PBS for 20 min at RT. To quench the PFA, cells were washed twice in PBS + 50 mM NH_4Cl and subsequently permeabilized with 20 µM in Buffer A (20 mM PIPES pH 6.8, 137 mM NaCl, 2.7 mM KCl) for 5 min. Cells were washed 3 times in Buffer A and blocked for 30 min in

Buffer A with 5 % NGS. Primary antibody was diluted in Buffer A containing 5 % NGS and added to the cells for 2 h at RT. After 3 washing steps in Buffer A, cells were incubated with secondary antibodies in Buffer A with 5 % NGS, washed 4 times in Buffer A and postfixed for 5 min with PBS with 50mM NH4Cl, permeabilized with 20µM digitonin in Buffer A (20mM PIPES pH 6.8,137mM NaCl, 2.7mM KCl) for 5 min, washed 3 times in Buffer A, blocked 30 min Buffer A with 5% normal goat serum, incubated with the primary antibodies in Buffer A with 5% normal goat serum for 2 hours, washed 3 times 5 min in Buffer A, incubated 1 hour with the secondary antibodies in Buffer A with 5% normal goat serum, washed 4 times 5 min Buffer A, postfixed for 5 min with 2% (w/v) PFA and 2% (w/v) sucrose in PBS. After 3 washing steps with PBS + 50 mM NH_4Cl followed by two washing steps with PBS, coverslips were mounted using DAPI containing mounting medium.

For stainings of eGFP-Raptor HEK293T cells, cells were seeded onto Matrigel-coated coverslips. The next day, cells were washed twice in PBS and fixed with 4% (w/v) PFA and 4% (w/v) sucrose in PBS for 15 min at RT. After 3 washing steps with PBS, cells were permeabilized and blocked in blocking buffer (0.1 % Triton X-100, 10 % Goat serum in PBS). Subsequently, primary antibodies were incubated in blocking buffer at °C o.n. The next day, coverslips were washed 3 times with PBS and incubated with secondary antibodies for 1 h at RT. After 3 additional washing steps, coverslips were mounted using DAPI containing mounting medium.

3.2.3.5 Generating knock-in cell lines using CRISPR/Cas9

To generate knock-in cell lines, the genomic sequence of the target protein was analyzed using the UCSC genome browser. For the design of guide RNAs (gRNA), the genomic sequence around the start codon was extracted from the UCSC genome browser and used for gRNA design by CCTop. Guides were chosen to have minimal off targets and to ideally span over the start codon. If this was impossible, the PAM sequence had to be removed from the donor construct, as additional cleavage even after successful editing was possible. The chosen gRNA was cloned into the PX458 vector as described in the cloning section. PX458 encodes GFP-tagged Cas9 and promotor and framework for the gRNA. For donor vector design, approximately 1000 bp upstream of the start codon and 1000 bp downstream of the start codon were selected as homology arms (avoiding repeat sequences and sequences of a GC content > 65 % at the start or the endo of the homology sequence, respectively). The

homology arms and the tag to be introduced (usually eGFP) were amplified by PCR and assembled into the vector as described in the cloning section. Subsequently, a 10 cm dish of 60-70 % confluent HEK293T was transfected with 5 µg PX458 carrying the gRNA sequence and 10 µg Donor plasmid using jetPRIME. Three days after transfection, single, GFP positive cells were sorted into 20 96 well plates by FACS and incubated until grown to confluency (3-4 weeks). Subsequently, the clones were split into two wells of a 24 well plate, one well was used for screening and one for maintenance. For screening, 200 µl 2x SDS-PAGE sample was added to one well of the 24 well plate and cells were lysed and briefly sonified. Subsequently, 10 µl were analyzed by immunoblotting using GFP and protein specific antibodies. Positive clones were expanded and further characterized.

3.2.3.6 Active β1-integrin uptake assay in HeLa cells

To determine active β1-integrin uptake levels, I made use of an antibody-based assay. Active integrins differ in their conformation from inactive integrins and can be detected by conformation specific antibodies. Using a directly Alexa-647 labelled antibody, cell surface active β1-integrins can be stained and chased after uptake. The amount of internalized active β1-integrins depends on the amount of active β1-intergin available at the plasma membrane. Thus, cell surface levels need to be determined to normalize internalized integrin levels. Furthermore, active β1-integrins are quickly recycled and only a small fraction is targeted for degradation (Moreno-Layseca et al., 2019). Thus, multiple cycles of endocytosis are required to detect differences in endocytosis rates. Therefore, the assay was performed for 60 min. Since the antibody cannot be detached from the cell surface by any means, internalized active β1-integrins cannot be imaged using z-stacks of the entire cell. Thus, only the middle plane of cells was imaged so that no interference of surface localized active β1-integrins occurred. In detail, the experiment was performed as follows:

For integrin uptake assays, HeLa cells were starved for 90 min in serum-free DMEM and subsequently surface stained for active β1-integrin as described above. Two coverslips per condition were prepared. One coverslip was fixed as described to assess surface levels; the other coverslip was incubated in DMEM + 10% FBS for 1 h at 37 °C, 5 % CO2, washed twice in PBS and fixed for 15 min at RT with 4 % (w/v) PFA and 2 % (w/v) sucrose in PBS. Cells were

washed twice with PBS and mounted using DAPI-containing mounting medium. Coverslips were imaged using LSM710 or LSM780 microscopes with 8-bit settings. For analysis of internalized active β1-integrin levels, z-stacks were acquired, and β1-integrin intensity was determined in the middle plane. Internalized levels were normalized to surface levels.

3.2.3.7 Integrin uptake in C2C12 cells

β1-integrin uptake in C2C12 cells was measured using an assay analogous to the assay used in HeLa cells. It is also based on a specific antibody that recognizes the active conformation but requires a secondary antibody as it is not directly labelled.

For active β1-integrin uptake assays, C2C12 cells seeded on Matrigel-coated coverslips were starved for 90 min in serum-free DMEM and subsequently surface stained for active β1-integrin as described above. Cells were washed twice with PBS and incubated in DMEM + 10% FBS for 90 min at 37 °C, 5% CO_2. Subsequently, cells were washed twice in PBS, fixed in 4% PFA for 15 min at room temperature and stained with fluorescently labeled secondary antibodies diluted in blocking buffer (10% (v/v) NGS, 0.1% (w/v) triton X-100 in PBS) for 45 min. After three washing steps in PBS, coverslips were mounted and imaged using LSM710 or LSM780 microscopes with 8-bit settings. For analysis of internalized active β1-integrin levels, z-stacks were acquired, and slices were summed up. After background subtraction (sliding paraboloid, rolling ball radius 10 pixels), images were thresholded (60-max) and the overall active β1-integrin intensity (integrated density) was determined. Next internalized active β1-integrin in typical puncta was measured. Therefore, particles were detected (size 0.1-1.5 μm^2, circularity 0-1) and the integrated density within these particles was measured. Internalized active β1-integrin was determined through the ratio of active β1-integrin in puncta divided by total active β1-integrin intensity.

3.2.3.8 Transferrin uptake assay

Transferrin uptake assays were performed with COS7 cells. Cells treated with siRNAs were seeded on Matrigel-coated coverslips and serum-starved for 1.5 h and were either used for uptake or transferrin receptor surface labelling. For transferrin uptake, cells were incubated

with 25 µg ml^{-1} transferrin–Alexa647 (Molecular Probes, Invitrogen) for 10 min at 37 °C. After two washes with ice-cold PBS cells were acid washed at pH 5.3 (0.2 M sodium acetate, 200 mM sodium chloride) on ice for 2 min to remove surface-bound transferrin, washed 2 times with ice-cold PBS and fixed with 4% paraformaldehyde (PFA) for 15 min at room temperature. For surface labelling, cells were incubated with 25 µg ml−1 transferrin–Alexa647 at 4 °C for 45 min. Cells were washed 3 times with ice-cold PBS for 1 min and fixed with 4% PFA for 15 min at room temperature. Transferrin labelling was analyzed using a Nikon Eclipse Ti microscope operated by open-source ImageJ-based micromanager software. Internalized transferrin per cell was quantified and normalized to the amount of surface-bound transferrin determined in the same experiment as a measure for the efficiency of internalization.

3.2.3.9 Transferrin recycling assay

Transferrin recycling assays were performed in HeLa cells. Cells treated with siRNAs were seeded on Matrigel-coated coverslips and serum-starved for 1.5 h. Cells were loaded with 25 µg ml^{-1} transferrin–Alexa647 (Molecular Probes, Invitrogen) for 30 min at 37 °C. After two washes with ice-cold PBS cells were acid washed at pH 5.3 (0.2 M sodium acetate, 200 mM sodium chloride) on ice for 2 min to remove surface-bound transferrin and washed twice with PBS again. For recycling, cells were transferred to full medium and incubated for 0/10/30 and 60 min at 37 °C. After two washes with ice-cold PBS cells were acid washed at pH 5.3 (0.2 M sodium acetate, 200 mM sodium chloride) on ice for 2 min to remove recycled transferrin and fixed with 4% paraformaldehyde (PFA) for 15 min at room temperature. Internal transferrin was analyzed using a Nikon Eclipse Ti microscope operated by open-source ImageJ-based micromanager software. Internal transferrin per cell at each time point was quantified and normalized to the amount of internal transferrin at t = 0 min.

3.2.3.10 FACS

For FACS analysis, C2C12 cells cultured on 6 well dishes were rinsed twice with PBS and detached using Pronase. Cells were collected in tubes and washed in PBS + 2% FBS. Cells were

resuspended in 5% BSA in PBS, cell numbers were adjusted, and cells incubated with primary antibodies for 60 min at 4 °C. Subsequently, cells were washed 3 times in ice cold PBS and stained with secondary antibodies in PBS + 5% BSA for 45 min at 4 °C. After 3washes in PBS cells were analyzed using a BD LSR Fortessa flow cytometer.

3.2.3.11 CCP dynamics

For the determination of CCP dynamics, COS7 cells stably expressing eGFP-clathrin were treated with siRNAs and seeded into ibidi 8 well dishes. A 180s time-laps series at 0.5 Hz was recorded and analyzed by the FMP imaging facility as described previously (H. Wang et al., 2020).

3.2.3.12 β1-integrin in Lamp2a

To determine the amount of endocytosed β1-integrin trafficked to Lamp2a positive lysosomes, C2C12 cells seeded on Matrigel-coated coverslips were incubated with active β1-integrin antibody (9EG7) diluted in complete DMEM for 45 min on ice. Coverslips were then washed briefly in PBS and subsequently incubated with full DMEM containing 50 µM leupeptin (a protease inhibitor to block lysosomal degradation) for 4 h at 37 °C. Cells were washed 3 times with PBS and fixed for 15 min at RT with 4% (w/v) PFA and 4% (w/v) sucrose in PBS. Coverslips were washed 3 times in PBS and blocked in blocking buffer (10 % NGS, 0.1 % (w/v) saponin in PBS). Primary and Alexa Fluor-conjugated secondary antibodies diluted in the blocking buffer were incubated at RT for 2 h and 1 h, respectively. Subsequently, coverslips were washed extensively and mounted with DAPI containing mounting medium.

3.2.3.13 Microscopy

Immunocytochemistry slides were imaged using a Zeiss Laser Scanning confocal microscope (LSM) 710 or 780 with a 40x or 60x immersion oil (1.3 NA) objective; a 10x air (0.3 NA) objective was used for myotube analysis. A minimum of 10 images per condition (accounting for at least 30 cells) and experiment were acquired. Z-stacks using 0.7 µM spacing were

aquired for all experiments except for myotube analysis, where images from a single plane were generated. For quantification of fluorescent intensity, z-stackes were summed up. Fiji Image J software was used for image processing and analysis. TIRF microscopy was performed using a Nikon Eclipse Ti microscope, equipped with a ×60 TIRF objective (oil-immersion, Nikon), a sCMOS camera (Neo, Andor), a 200 W mercury lamp (Lumen 200, Prior), a triple-colour TIRF setup (laser lines: 488 nm, 568 nm, 647 nm) and operated by open-source ImageJ-based micromanager software.

4 Results

4.1 Proteomic identification of small GTPases that bind to PI3KC2β

To identify small GTPases that interact with PI3KC2β, I made use of GFP-tagged PI3KC2β harboring a mutation that potentially facilitates GTPase binding to the RBD (GFP-PI3KC2β-D1168K). This is based on the analysis of the influence of mutations in PI3Ky on its binding affinity to the small GTPase Ras. Mutation of glutamic acid 919 to lysine in PI3Ky increased its affinity for Ras significantly (Pacold et al., 2000). In PI3KC2β, glutamic acid 919 of PI3Ky corresponds to aspartic acid 1168 (Figure 12a). I therefore speculated that mutating aspartic acid 1168 to lysine might increase the affinity of PI3KC2β to small GTPases. To identify potentially interacting GTPases, GFP-PI3KC2β-D1168K was overexpressed in HEK293T cells and subsequently subjected to immunoprecipitation. Interacting proteins were then identified by mass spectrometry performed by Heike Stephanowitz from the FMP Mass Spectrometry Core Facility. Several small GTPases were identified (Figure 12b). Of these only the interaction of GFP-PI3KC2β with Rab7A could be verified by co-immunoprecipitation using HEK293T cell endogenously expressing eGFP-PI3KC2β (Figure 12 c, Figure 13a).

a

b

Protein	Ion score
RAB5C	91
RAB7A	85
RAB8A	59
RAB5B	51
RAB1B	49
RAB35	38
RAB14	29

c

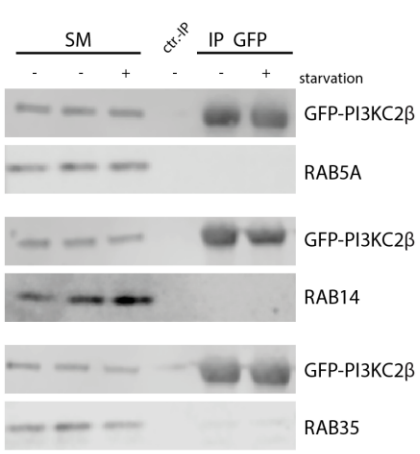

Figure 12: Identification of Rab proteins interacting with PI3KC2β. a) Alignment of PI3KC2β and PI3Kγ. b) Rab proteins interacting with GFP-PI3KC2β-D1168A identified by mass spectrometry. c) Co-immunoprecipitation to verify interactions identified by mass spectrometry. HEK293T cells endogenously expressing eGFP-PI3KC2β were either serum starved or treated with full medium (starvation +/-) and subsequently subjected to immunoprecipitation using GFP trap beads. Potentially interacting Rab proteins were analyzed by immunoblotting.

4.2 PI3KC2β interacts with Rab7A upon serum starvation

Next, I wanted to test whether I could confirm the interaction of PI3KC2β and Rab7A and if this potential interaction is influenced by growth factor starvation. Since PI3KC2β is only recruited to late endosomes and lysosomes under these conditions (Marat et al., 2017). Hence, its interaction with Rab7A should follow the same pattern, if Rab7A is indeed required for the recruitment of PI3KC2β. Indeed, Rab7A co-immunoprecipitated more efficiently with endogenous eGFP-PI3KC2β when the cells were subjected to growth factor starvation prior to the co-immunoprecipitation (Figure 13 a, b).

In line with these findings, endogenously tagged eGFP-PI3KC2β co-localized with endogenous Rab7A in HeLa cells only when cells were growth factor starved (Figure 13 c). This strengthens the hypothesis that Rab7A is in fact required to recruit PI3KC2β to late endosomes or lysosomes.

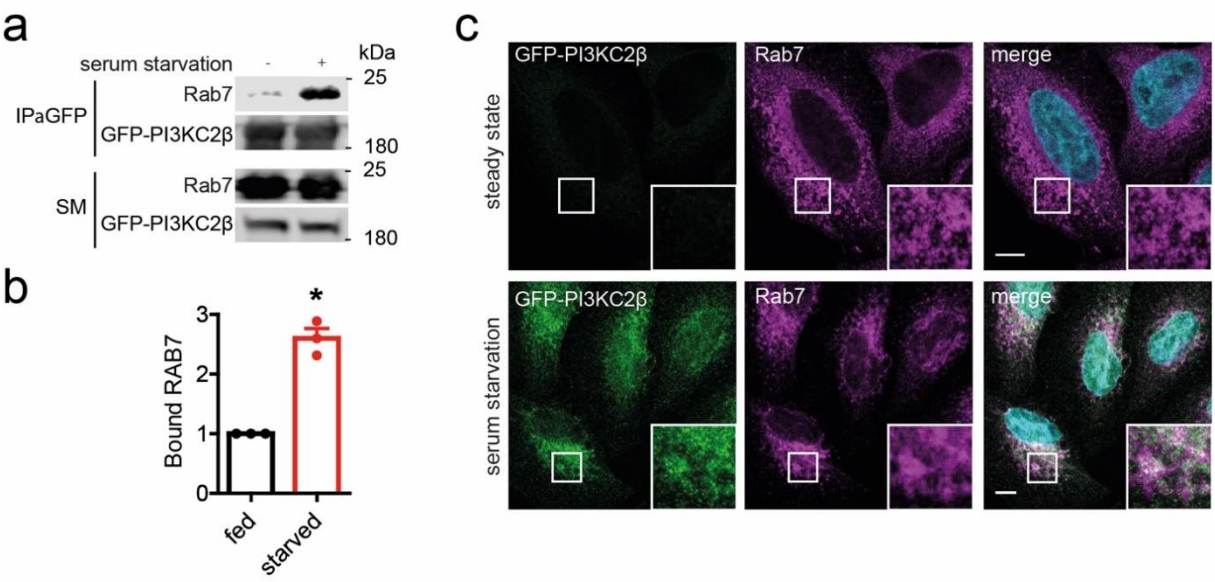

Figure 13: Rab7A interacts with PI3KC2β upon serum starvation. a) HEK293T cells endogenously expressing eGFP-PI3KC2β were either serum starved or treated with full medium (serum starvation +/-) and subsequently subjected to immunoprecipitation using GFP trap beads. Bound Rab7A was analyzed by immunoblotting. b) Quantification of a). The ratio of Rab7A bound to eGFP-PI3KC2β in fed versus starved conditions is shown. Mean +/- s.e.m. (n = 3 independent experiments). A one-sample, two-tailed t-test with a hypothetical mean of 1 was used to assess statistical significance. *P = 0.01. c) HeLa cells endogenously expressing eGFP-PI3KC2β were either serum starved or treated with full medium (serum starvation / steady state) and subsequently stained for eGFP and endogenous Rab7A. Scale bars 10 µm.

4.3 PI3KC2β associates with constitutively active Rab7A

So far, I could show that growth factor starvation facilitates the interaction of PI3KC2β and Rab7A. Since Rab GTPases can adopt two different states, A GDP-bound, inactive state in which they usually can't function to recruit effector proteins to membranes, and a GTP-bound, active state in which they localize to membranes and can recruit their effector proteins (Homma et al., 2021), I aimed to investigate if PI3KC2β binds to the active, GTP bound form of Rab7A. Therefore, I made use of constitutively active Rab7A (Q67L) and constitutively inactive Rab7A (T22N). I transfected HEK293T cells endogenously expressing eGFP-PI3KC2β with mCherry-Rab7A-Q67L or mCherry-Rab7A-T22N, respectively and immunoprecipitated

eGFP-PI3KC2β. Active mCherry-Rab7A-Q67L co-immunoprecipitated with eGFP-PI3KC2β with far greater efficiency compared to inactive mCherry-Rab7A-T22N (Figure 14 a, b).

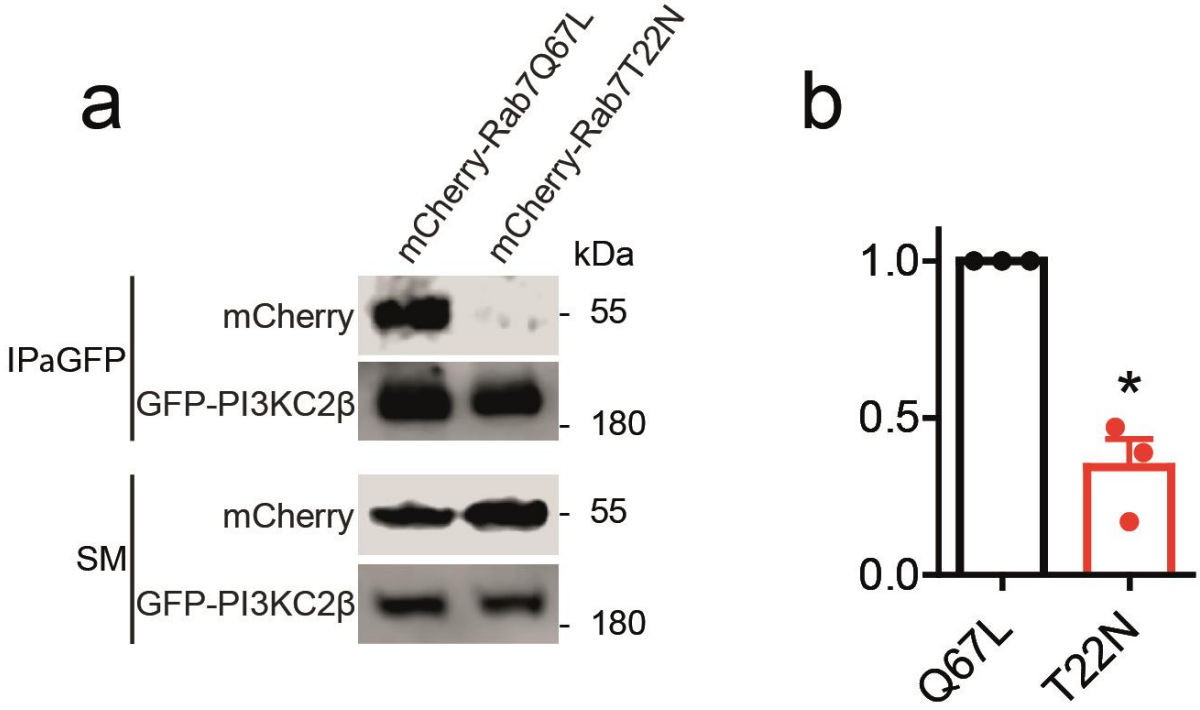

Figure 14: PI3KC2β preferentially binds to constitutively active Rab7A. a) HEK293T cells endogenously expressing eGFP-PI3KC2β were transfected with either constitutively active mCherry-Rab7A (m-Cherry-Rab7Q67L) or inactive mCherry-Rab7A (mCherry-Rab7T22N), serum starved for 2h and subsequently subjected to immunoprecipitation using GFP trap beads. Bound mCherry-Rab7A was analyzed by immunoblotting. b) Quantification of a). The ration of eGFP-PI3KC2β bound inactive mCherry-Rab7A to eGFP-PI3KC2β bound active mCherry-Rab7A is depicted. Mean +/- s.e.m. (n = 3 independent experiments). A one-sample, two-tailed t-test with a hypothetical mean of 1 was used to assess statistical significance. *P = 0.01.

4.4 Rab7A is required for PI3KC2β recruitment to late endosomes and lysosomes and for PI3KC2β function

So far, we established that PI3KC2β can interact with active Rab7A upon growth factor starvation. To test whether this interaction is infact required for proper PI3KC2β function, I depleted HEK293T cells endogenously expressing eGFP-PI3KC2β of Rab7A and monitored the interaction between eGFP-PI3KC2β and the mTORC1 component Raptor under fed and growth factor starved conditions. While growth factor starvation readily triggered the

association of Raptor and eGFP-PI3KC2β in cells treated with control siRNA, the depletion of Rab7A significantly reduced this interaction to around 40% (Figure 15 a, b), indicating that PI3KC2β complex formation with lysosomal Raptor depends on Rab7A.

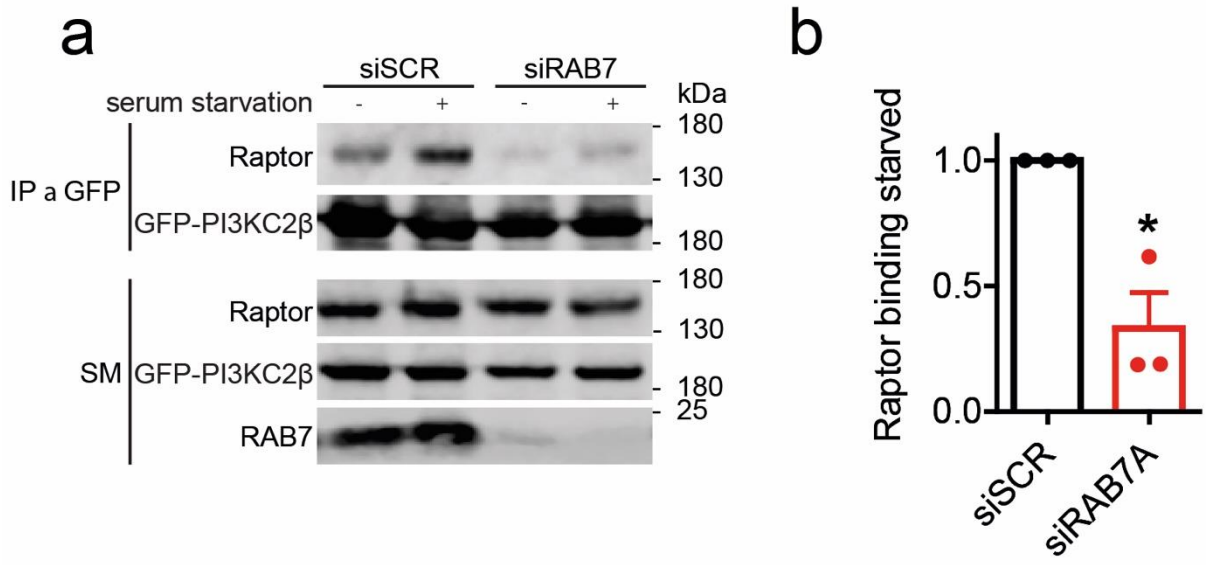

Figure 15: Rab7A is required for the starvation induced association of PI3KC2β with Raptor. a) HEK293T cells endogenously expressing eGFP-PI3KC2β were treated with control (siSCR) or Rab7A (siRAB7) targeting siRNAs and then either serum starved or treated with full medium (serum starvation +/-) and subsequently subjected to immunoprecipitation using GFP trap beads. Bound Raptor was analyzed by immunoblotting. b) Quantification of a). The ratio of Raptor bound to eGFP-PI3KC2β in starved conditions in siSCR versus siRAB7 treated cells is shown. Mean +/- s.e.m. (n = 3 independent experiments). A one-sample, two-tailed t-test with a hypothetical mean of 1 was used to assess statistical significance. *P = 0.04.

I then investigated whether Rab7A is indeed required for the localization of PI3KC2β to late endosomes and lysosomes. To trigger robust activation of PI3KC2β in HeLa cells endogenously expressing eGFP-PI3KC2β, I depleted these cells of PKN2, a kinase that inhibits PI3KC2β recruitment and function (Wallroth et al., 2019) using specific siRNA. Under these conditions eGFP-PI3KC2β co-localized with the late endosomal marker LBPA (Figure 16 c). Co-depleting PKN2 together with Rab7A completely abolished the co-localization of eGFP-PI3KC2β with LBPA, suggesting that Rab7A is required for PI3KC2β recruitment to late endosomes and lysosomes (Figure 16 c).

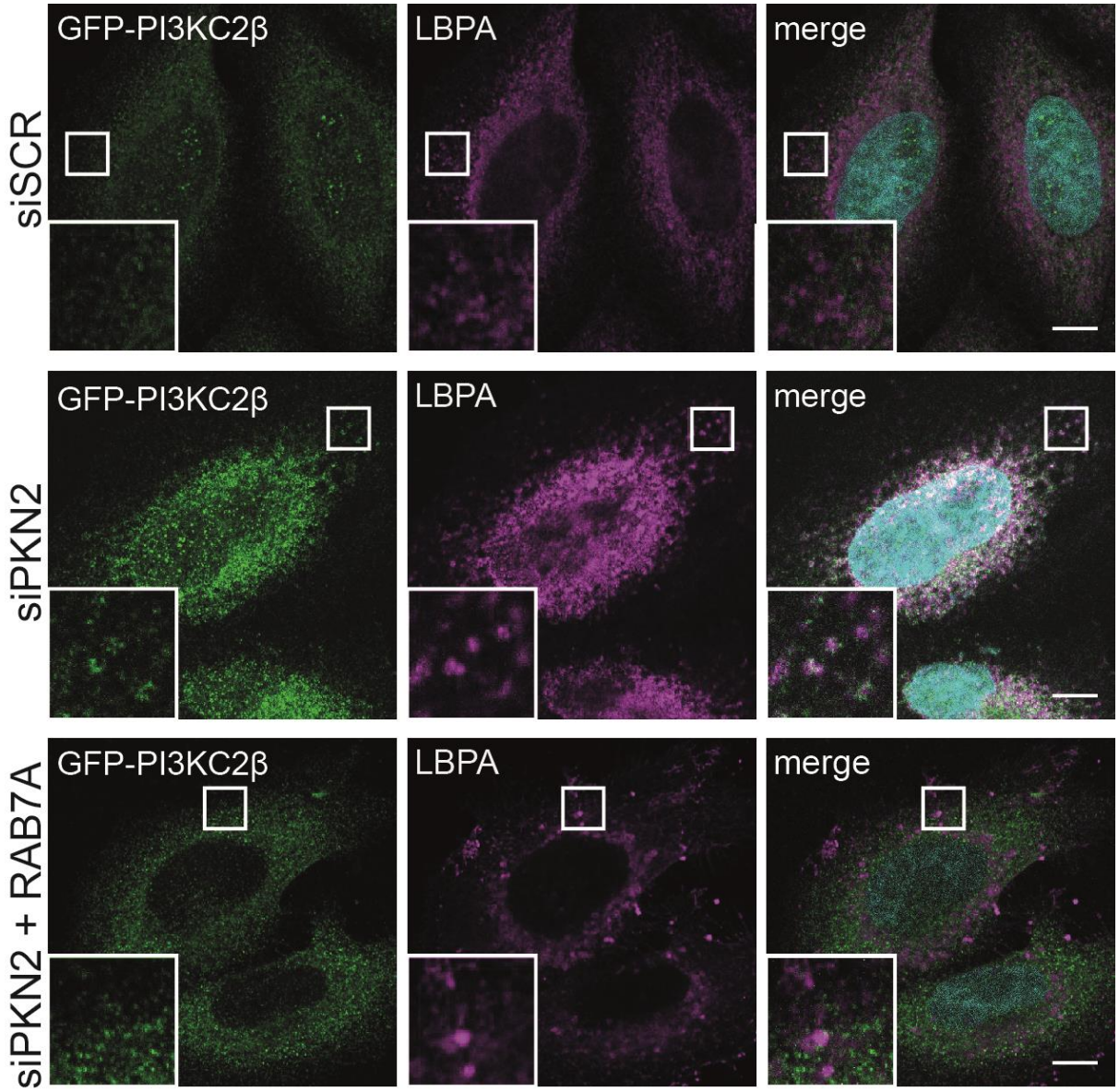

Figure 16: Rab7A is required for PI3KC2β recruitment to late endosomes. HeLa cells endogenously expressing eGFP-PI3KC2β were either treated with control siRNA (siSCR), siRNA targeting PKN2 (siPKN2) or siRNA targeting PKN2 and Rab7A (siPKN2 + RAB7A) and subsequently stained for eGFP and LBPA. Scale bars 10 µm.

Given these results, I speculated that Rab7A is required for proper PI3KC2β function. To put this hypothesis to the test, I depleted HeLa cells of PKN2 or PNK2 and Rab7A and stained the cells for PI(3,4)P_2, the lipid product of PI3KC2β. While the depletion of PKN2 led to a strong increase of vesicular PI(3,4)P2, this effect was abolished by co-depletion of Rab7A (Figure 18 a, b). These data indicate that Rab7A is required for proper PI3KC2β function in HeLa cells. Since late endosomal and lysosomal PI(3,4)P_2 is required for the PI3KC2β mediated

inhibition of mTORC1 (Marat et al., 2017), I tested if Rab7A is indeed required for the PI3KC2β mediated suppression of mTORC1 activity. To this aim, I depleted HEK293T cells of PKN2 to activate PI3KC2β and thereby repress mTORC1 signaling. Indeed, PKN2 depletion significantly reduced mTORC1 activity as measured by p-S6K levels (Figure 17 c, d). In line with the observation that $PI(3,4)P_2$ production by PI3KC2β requires Rab7A, co-depleting Rab7A together with PKN2 completely restored mTORC1 activity as measured by p-S6K levels (Figure 17 c, d).

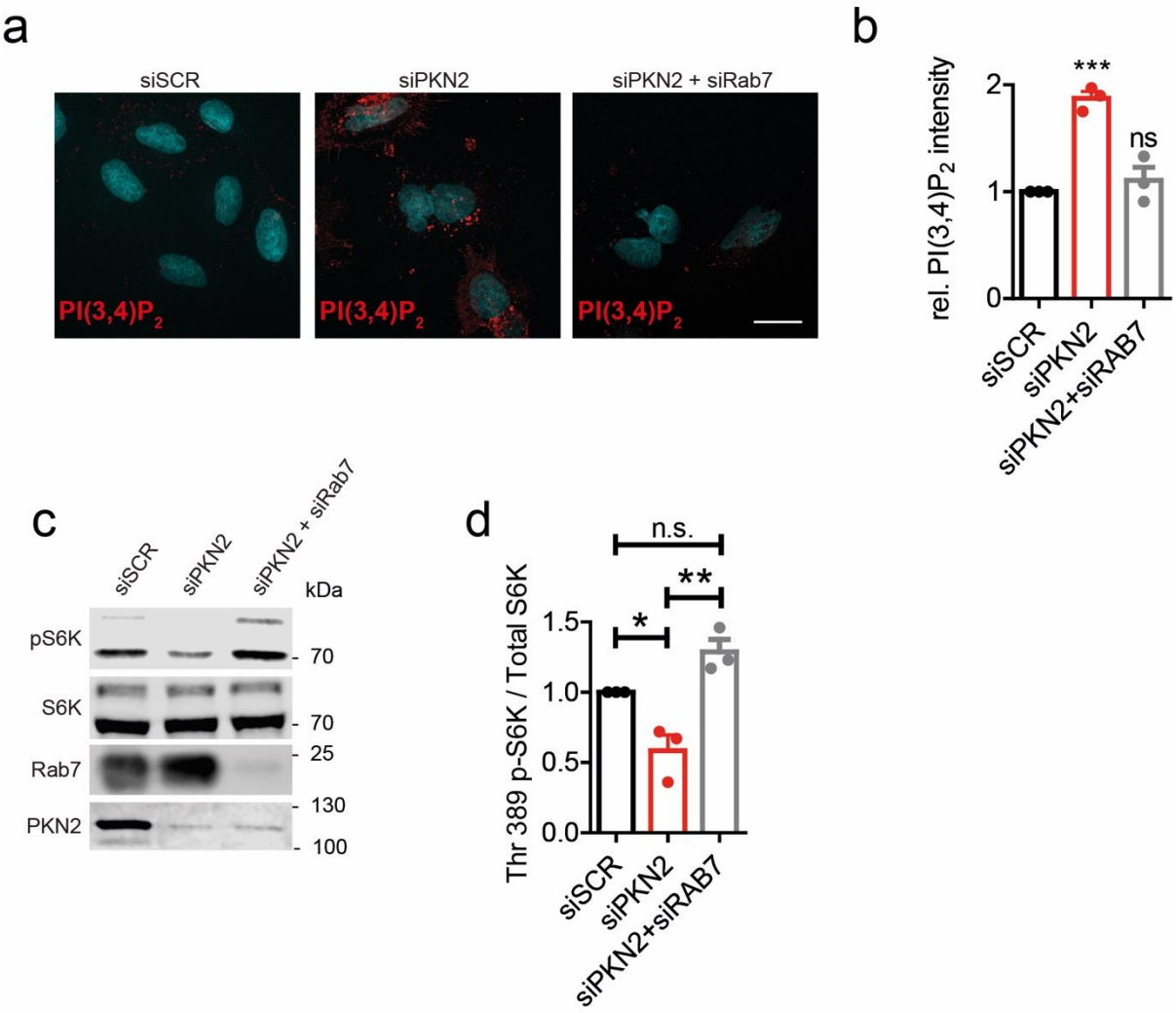

Figure 17: Rab7A is required for PI3KC2β function. Data acquired together with Alexander Wallroth. a) HeLa cells were either treated with control siRNA (siSCR), siRNA targeting PKN2 (siPKN2) or siRNA targeting PKN2 and Rab7A (siPKN2 + RAB7A) and subsequently stained for $PI(3,4)P_2$. Scale bars 20 µm. b) Quantification of a). Mean intensity was determined for all conditions. The ratios of $PI(3,4)P_2$ intensity to siSCR are shown. Mean +/- s.e.m. (n = 3 independent experiments with > 30 cells/condition per experiment). A one-way ANOVA (f = 35.45, total d.f. = 8) and Dunnett's post-test were used. ***P

< 0.001. c) HEK293T cells were either treated with control siRNA (siSCR), siRNA targeting PKN2 (siPKN2) or siRNA targeting PKN2 and Rab7A (siPKN2 + RAB7A), lysates were obtained and analyzed by immunoblotting with the indicated antibodies. d) Quantification of c). The ratio of Thr 389 pS6K to total pS6K normalized to siSCR is depicted. Mean +/- s.e.m. (n = 3 independent experiments). A one-way ANOVA (f = 18.31, total d.f. = 8) and Dunnett's post-test were used. *P < 0.05, **P < 0.01.

Taken together these data together with data obtained by Alexander Wallroth (Wallroth et al., 2019) suggest the following model: Under steady state conditions growth factors activate mTORC2 through receptor tyrosine kinases (RTKs). mTORC2 in turn phosphorylates, and thereby activates the PI3KC2β suppressor PKN2. PKN2 in then phosphorylates PI3KC2β at threonine 279 to facilitate its association with inhibitory 14-3-3 proteins with PI3KC2β. 14-3-3 association triggers the dimerization of PI3KC2β and its sequestration within the cytosol. Upon growth factor starvation, PKN2 is inactivated and PI3KC2β is no longer phosphorylated at threonine 279, thereby enabling PI3KC2β to bind active Rab7A at late endosomes and lysosomes. At these sites PI3KC2β synthesizes PI(3,4)P_2 leading to the association of inhibitory 14-3-3 proteins with the mTORC1 subunit Raptor and, as a consequence to mTORC1 inactivation (Figure 18) (Marat et al., 2017).

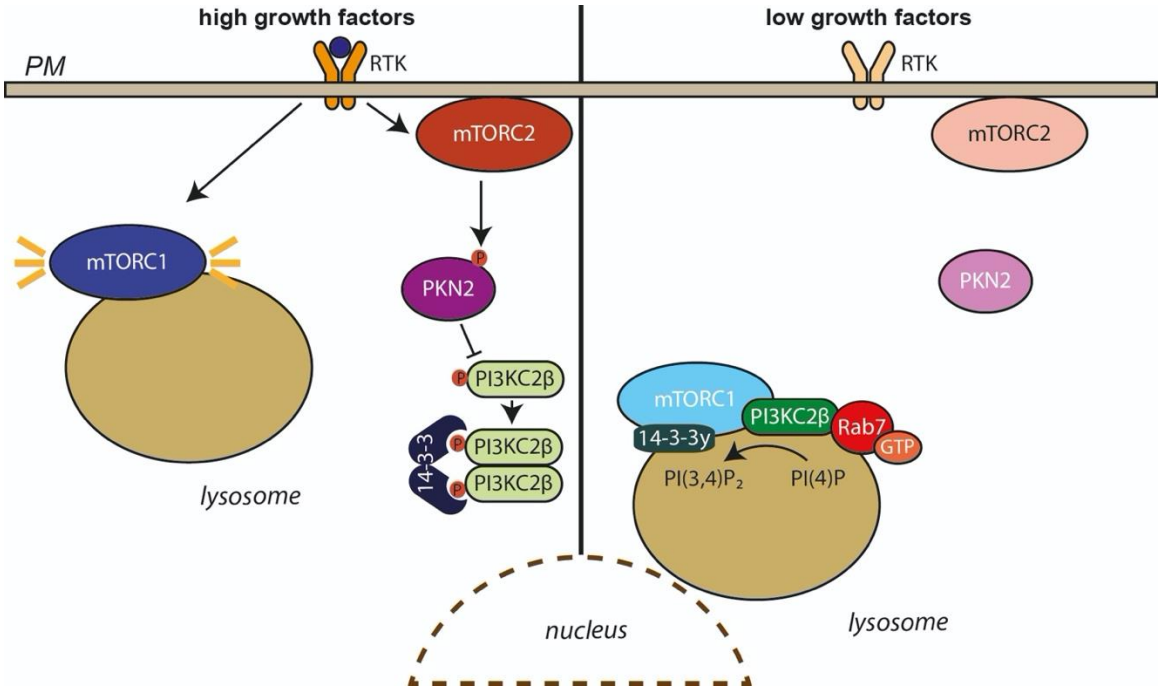

Figure 18: Regulation of PI3KC2β in nutrient signaling. Modified from (Wallroth et al., 2019). Left side: When growth factors are readily available, receptor tyrosine kinases (RTKs) are activated by

growth factors and in turn activate mTORC2. Active mTORC2 phosphorylates and thus activates protein kinase 2 (PKN2) which then phosphorylates PI3KC2β at T279. This phosphorylation leads to the association of 14-3-3 proteins with PI3KC2β and to PI3KC2β dimerization. Dimeric PI3KC2β can no longer associate with late endosomes and lysosomes and therefore cannot inhibit mTORC1 at lysosomes. Right side: Under growth factor starvation, RTKs and thus mTORC2 are inactive. Therefore, PKN2 does not phosphorylate PI3KC2β and PI3KC2β is monomeric. Monomeric PI3KC2β in turn, can bind to GTP bound, active Rab7A which induces the translocation PI3KC2β to late endosomes and lysosomes. There, PI3KC2β associates with the mTORC1 subunit Raptor and produces $PI(3,4)P_2$ from PI(4)P. Lysosomal $PI(3,4)P_2$ facilitates the recruitment of 14-3-3y to Raptor, leading to mTORC1 inhibition.

4.5 PI3KC2β depletion reduces PRAS40 association with mTORC1

The mechanisms how PI3KC2β inhibits mTORC1 at late endosomes and lysosomes remain only partially understood. To address these remaining questions, I aimed to study whether PI3KC2β regulates mTORC1 complex formation and/or composition. An example of such regulatory proteins are the inhibitory factors PRAS40 and DEPTOR, which can assemble with mTORC1 and mTORC2 respectively. To probe possible effects of PI3KC2β on mTORC1 complex formation and/or composition, I generated a HEK293T cell line expressing endogenously tagged eGFP-Raptor using CRISPR/Cas9 technology. This allows for the isolation of the endogenous mTORC1 complex by immunoprecipitating eGFP-Raptor. The cell line generated harbored a heterozygous knock-in as the wild type allele and the modified allele were both detectable (Figure 19 a). In accordance with other studies (Saxton & Sabatini, 2017), eGFP-Raptor nicely colocalized with the lysosomal marker LAMP1 in cells that were first starved and then refed with growth factors and amino acids (Figure 19 b). Next, I aimed to investigate the influence of PI3KC2β loss on mTORC1 composition. To this aim, I treated eGFP-Raptor HEK293T cells with control or PI3KC2β targeting siRNAs and performed immunoprecipitations using GFP-binding beads to isolate the mTORC1 complex. While mTOR kinase readily co-immunoprecipitated with eGFP-Raptor under both conditions, PRAS40 levels were significantly reduced in PI3KC2β depleted cells (Figure 19 c, d, e).

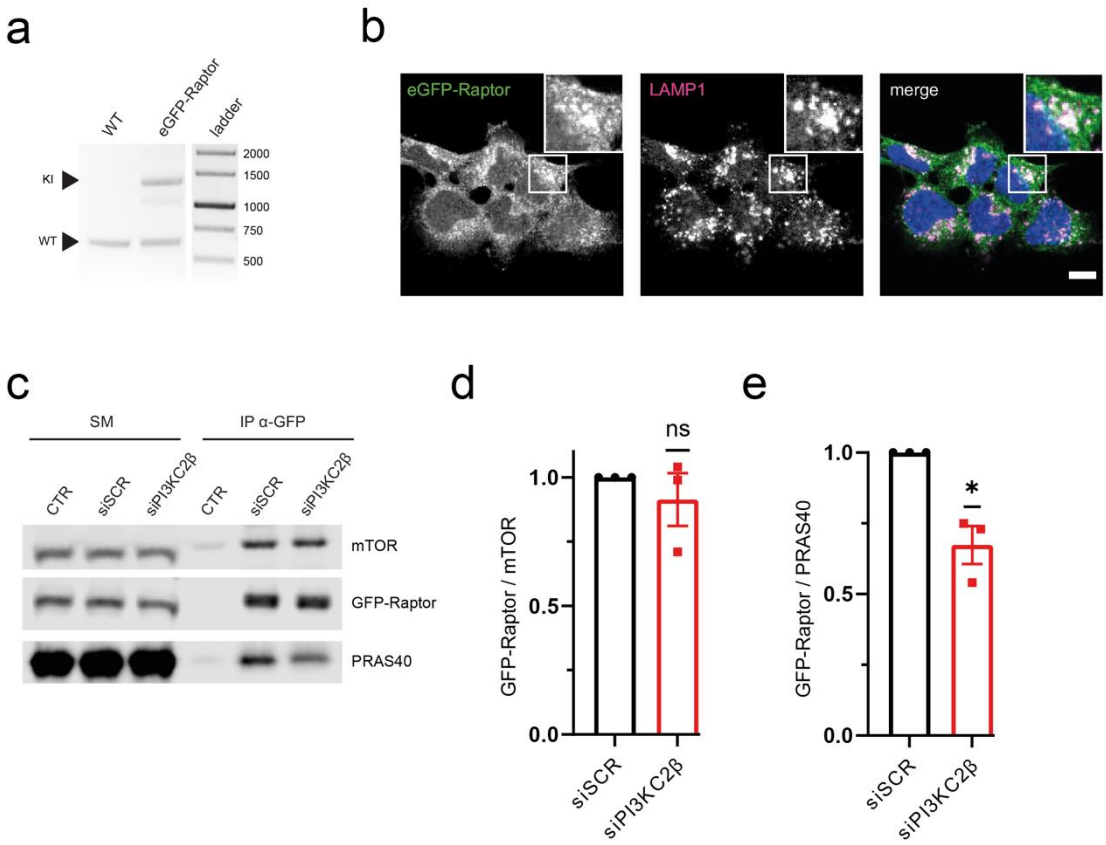

Figure 19: PI3KC2β depletion reduces PRAS40 association with mTORC1. a) PCR of genomic DNA extracted from wild type (WT) or eGFP-Raptor HEK293T cells using primers amplifying a 650 bp fragment around the start codon of the RPTOR gene. A shift to 1400 bp indicates successful integration of eGFP. b) Immunofluorescence staining of eGFP-Raptor HEK293T cells that were starved for 2h in HBSS and refed for 30 min in full medium. The indicated antibodies were used; scale bar 10 µm. c) Co-immunoprecipitation using GFP-trap magnetic agarose beads and lysates from eGFP-Raptor HEK293T cells treated with control (siSCR) or PI3KC2β (siPI3KC2β) targeting siRNAs. Samples were analyzed by immunoblotting using the indicated antibodies. d) Quantification of immunoprecipitated mTOR levels from c) normalized to the levels of eGFP-Raptor. e) Quantification of immunoprecipitated PRAS40 levels from c) normalized to the levels of eGFP-Raptor.

Taken together, these data suggest that PI3KC2β is required for the proper localization of PRAS40 to the mTORC1 complex. How PRAS40 localization depends on PI3KC2β and if PRAS40 is required for the PI3KC2β-mediated inhibition of mTORC1 signaling remains the subject of further studies.

4.6 PI3KC2β regulates levels of active β1 integrin at the cell surface

In addition to its role in nutrient signaling, PI3KC2β has also been linked genetically to X-linked centronuclear myopathy (XLCNM) caused by loss off function of the PI 3-phosphatase MTM1. There is growing evidence that a depletion or inhibition of PI3KC2β in XLCNM models that harbor knock outs of the PI(3)P phosphatase MTM1, can rescue or even revert the disease. XLCNM is characterized by missorted β1 integrins due to dysfunctional recycling, leading to reduced levels of active β1-integrins at the cell surface (Ketel et al., 2016). This likely underlies defects in myotube fusion and may cause developmental defects of skeletal muscle (Schwander et al., 2003).

To investigate the role of PI3KC2β in XLCNM, Paula Samsó used CRISPR/Cas9 to generate C2C12 cell lines in which the genes encoding MTM1, PI3KC2β or both proteins had been genetically inactivated (KOs) (Samsó et al., 2022). These myoblasts were then differentiated into myotubes. While wild type myoblasts readily fused into multinucleated myotubes as indicated by an average of about 5 nuclei per myosin heavy chain (MHC)-positive myotube, MTM1 KO cells failed to do so, averaging 1 nucleus per myotube. This phenotype was rescued in a MTM1/PI3KC2β double KO (double KO#1) cell line and in a PI3KC2β KO cell line depleted of MTM1 ($MTM1^{hypo}$ / PI3KC2β KO) (Figure 20 a, b). In line with these results, the fraction of myotubes with more than 15 nuclei was completely eliminated in all three MTM1 KO cell lines but restored in double KO#1 and $MTM1^{hypo}$ / PI3KC2β KO C2C12 cells. Conversely, there was a profound increase in mononucleated myotubes in MTM1 KO cells (Figure 20 c). More diverse differences were observed in the nuclear fusion index (i.e., the fraction of nuclei localized within MHC positive myotubes) of the MTM1 KO clones. While there was a strong reduction of the nuclear fusion index in MTM1 KO#1, MTM1 KO#2 and MTM1 KO#3 only showed a mild effect. This coincided with a reduced expression of the early differentiation marker myogenin and MHC in clone #1 but not in clone #2 and #3 (Figure 20 d,e). These results indicate that a loss of MTM1 leads to a profound defect in myotube fusion in all MTM1 KO clones. The mild initiation defect observed in MTM1 KO#1 might represent a clonal effect that occurred due to single cell sorting during the CRISPR/Cas9 mediated genome engineering.

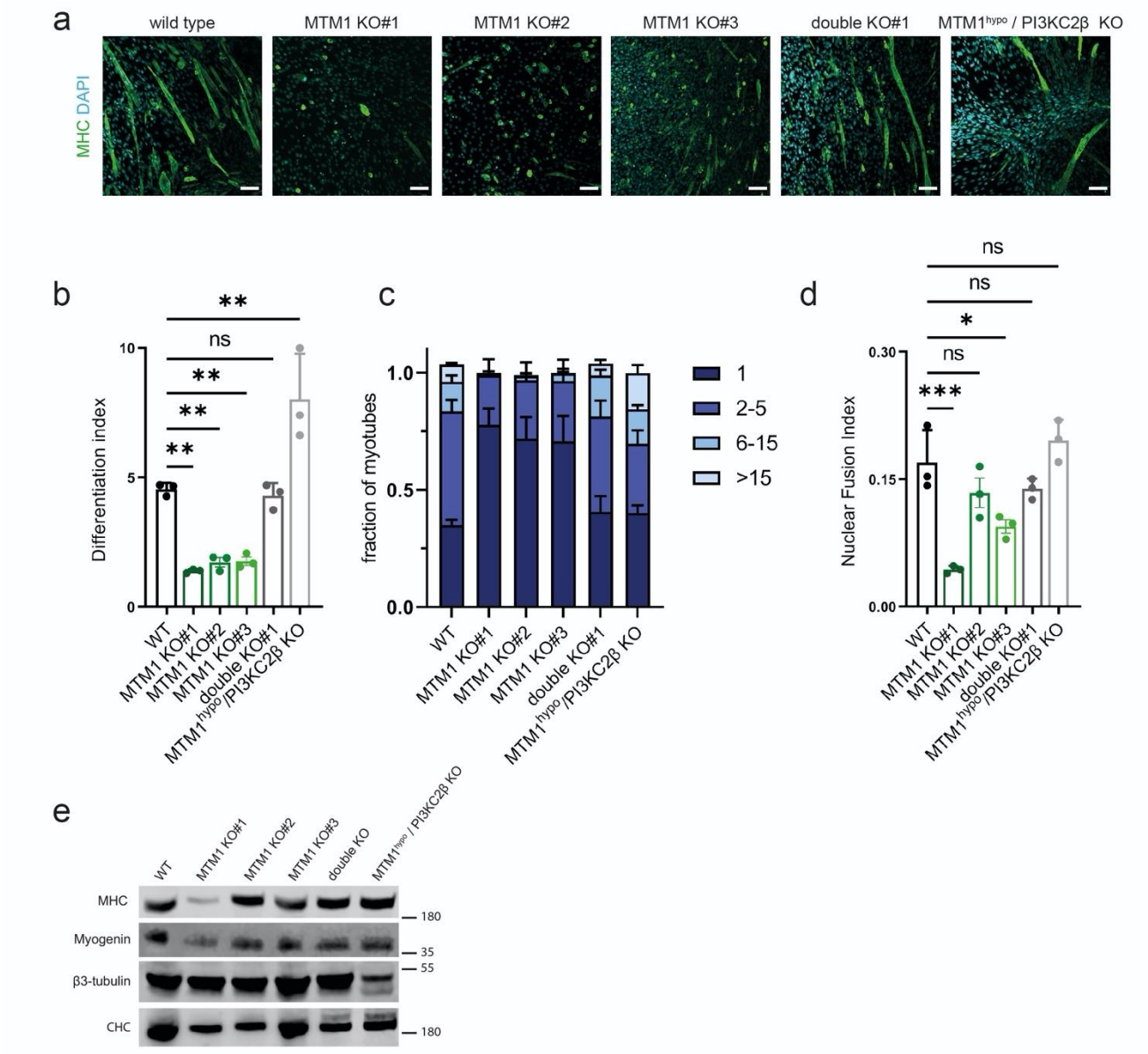

Figure 20: A C2C12 model to study myoblast differentiation upon MTM1 loss. a) Representative images of WT, MTM1 KO#1, MTM1 KO#2, MTM1 KO#3 double KO#1 and MTM1hypo / PI3KC2β KO C2C12 myotubes differentiated for 6 days and immunostained for myosin heavy chain (MHC) as a differentiation marker and DAPI for nuclear staining. Scale bar 100µm. b) Differentiation index (average number of nuclei per MHC positive myotube) of WT, MTM1 KO#1, MTM1 KO#2, MTM1 KO#3, double KO#1 and MTM1hypo / PI3KC2β KO C2C12 myotubes differentiated for 6 days. Mean ± SD from 3 independent experiments compared to WT. For each experiment, 10 images (850 µM x 850 µM) were acquired per condition. One-way analysis of variance (ANOVA; F = 32.71) and Tuckey's multiple-comparison test; ns $p > 0.05$, * $p < 0.05$, **$p < 0.01$, ***$p < 0.001$, ****$p < 0.0001$. WT vs. MTM1 KO#1 p = 0.0032; WT vs. MTM1 KO#2 p = 0.0077; WT vs. MTM1 KO#3 p = 0.0085; WT vs. double KO#1 p = 0.9980; WT vs. MTM1hypo / PI3KC2β KO p = 0.0015. c) Fraction of myotubes containing 1,

2-5, 6-15 or >15 nuclei of wild type (WT), MTM1 KO#1, MTM1 KO#2, MTM1 KO#3, double KO#1 and MTM1hypo / PI3KC2β KO C2C12 cells differentiated for 6 days. Mean ± SD from 3 independent experiments compared to WT. For each experiment, 10 images (850 µM x 850 µM) were acquired per condition. d) Nuclear fusion index (number nuclei in myotubes divided by total number of nuclei) of WT, MTM1 KO#1, MTM1 KO#2, MTM1 KO#3 double KO#1 and MTM1hypo / PI3KC2β KO C2C12 myotubes differentiated for 6 days. Mean ± SD from 3 independent experiments compared to WT. For each experiment, 10 images (850 µM x 850 µM) were acquired per condition. One-way analysis of variance (ANOVA; $F = 15.96$) and Tuckey's multiple-comparison test; ns $p > 0.05$, *$p<0.05$, ***$p < 0.001$. WT vs. MTM1 KO#1 $p = 0.0003$; WT vs. MTM1 KO#2 $p = 0.4675$; WT vs. MTM1 KO#3 $p = 0.0192$ WT vs. double KO#1 $p = 0.6060$; WT vs. MTM1hypo / PI3KC2β KO $p = 0.7549$. e) Immunoblot of cell lysates obtained from WT, MTM1 KO#1, MTM1 KO#2, MTM1 KO#3, double KO and MTM1hypo / PI3KC2β KO C2C12 myotubes differentiated for 6 days. Myosin heavy chain (MHC) was used as a late differentiation marker, myogenin was used as an early differentiation marker and β3-tubulin and clathrin heavy chain (CHC) were used as loading controls.

Myotube fusion requires proper β1 integrin localization. As it is already known that a loss of MTM1 leads to the accumulation of β1 integrins in recycling endosomes, we hypothesized that surface β1 integrin levels might be reduced in MTM1 KO cells, thereby causing the observed defects in myoblast fusion. While we did not observe a reduction in total β1 integrin surface levels (Figure 21 a), we found a significant reduction in active surface β1 integrin (Figure 21 c, d). This was confirmed by FACS analysis (Figure 21 b).

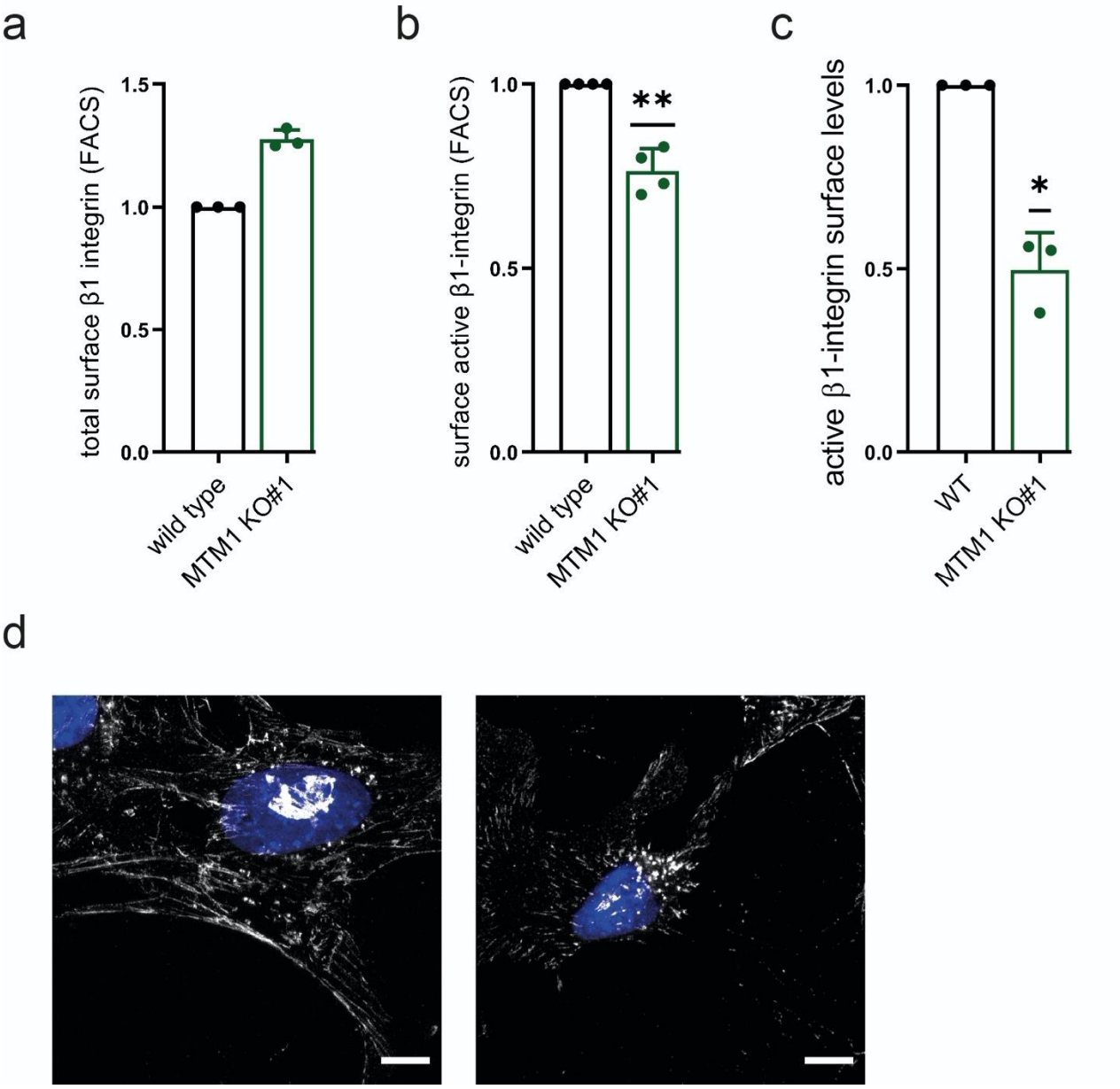

Figure 21: Reduced surface active β1 integrins in a MTM1 knock out C2C12 cells. a) Surface levels of total β1 integrin in wild type and MTM1 KO C2C12 cells measured by flow cytometry. Mean ± SD from 3 independent experiments. Represented as fold changed normalized to the mean of wild type cells. 10,000 cells per condition and experiment were analyzed. b) Surface levels of active β1 integrin in wild type and MTM1 KO C2C12 cells measured by flow cytometry. Mean ± SD from 4 independent experiments. Represented as fold changed normalized to the mean of wild type cells. 10,000 cells per condition and experiment were analyzed. One-sample, two-tailed t test; **p = 0.044. c) Surface levels of active β1 integrin in wild type (WT) and MTM1 KO C2C12 cells measured by fluorescent intensity from immunostainings. Mean ± SD from 3 independent experiments. Represented as fold changed normalized to the mean of wild type cells. One-sample, two-tailed t test; *p = 0.0132. d)

Representative images of wild type (WT) and MTM1 KO C2C12 cells stained for surface active β1 integrins and DAPI. Scale bar 10 µM.

Based on these data we hypothesized that PI3KC2β, a protein known to known to bind clathrin and the endocytic adaptor intersectin-1 (ITSN1), might be involved in the regulation of active β1 integrin surface levels as well. To test this, I depleted HeLa cells of PI3KC2β using specific siRNAs. This led to a profound increase in active β1 integrin levels at the cell surface (Figure 22 a, b).

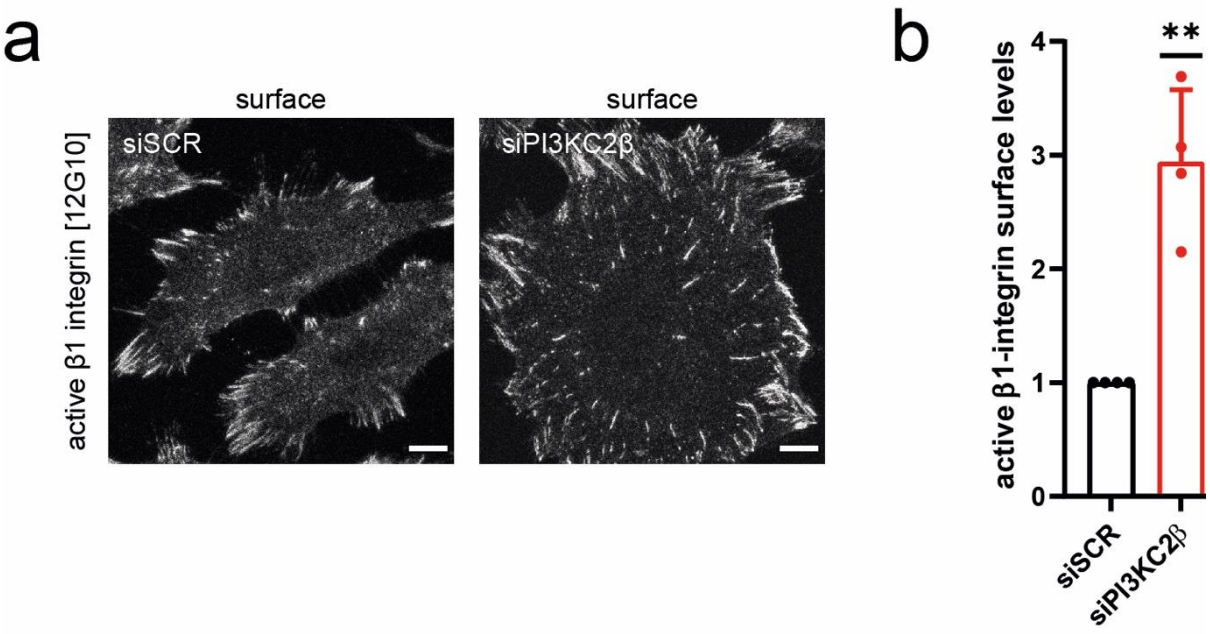

Figure 22: PI3KC2β depletion leads to increased surfaces levels of active β integrin. a) HeLa cells were treated with control (siSCR) or PI3KC2β (siPI3KC2β) targeting siRNAs and subsequently stained for surface active β1 integrin. Scale bars 10 µm. b) Quantification of a). Integrated density was measured and normalized to the mean of siSCR. Mean +/- s.e.m. (n = 4 independent experiments with > 30 cells/condition per experiment). A one sample t-test with a hypothetical mean of 1 was used. **P = 0.0089.

This phenotype was restored by re-expressing WT eGFP-PI3KC2β but not by GFP alone or by kinase inactive eGFP-PI3KC2β. Hence, the regulation of surface active β1 integrin levels depends on PI3KC2β kinase activity (Figure 24 a, b).

PI3KC2β has been reported to synthesize PI(3)P and PI(3,4)P_2 in a cell type and localization-dependent manner (Koch et al., 2021). To investigate which lipid is required for the rescue of active β1 integrin surface levels upon PI3KC2β depletion, I conducted rescue experiments using either the wild type enzyme, or a class III like mutant that is only able to produce PI(3)P but not PI(3,4)P_2 (Gozzelino et al., 2022). PI(4)P binding is mediated by a basic box (KRDR in PI3KC2β) in the activation loop in PI 3-kinases. This is required for the phosphorylation of 4' phosphorylated phosphoinositides and Vps34, which is known to only accept PI but not PI(4)P as a substrate, is missing this basic box (Figure 23)(Koch et al., 2021; Pirola et al., 2001).

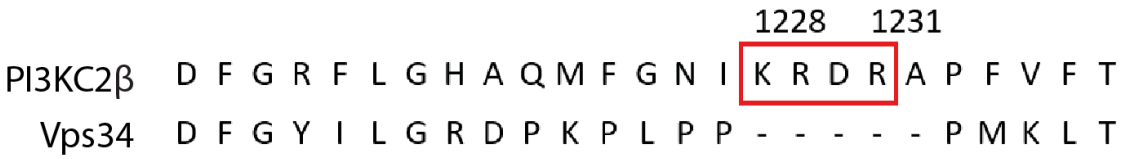

Figure 23: Alignment of the PI3KC2β and Vps34 activation loops.

To generate the class III-like PI3KC2β mutant, Gozzelino et al. changed the KRDR motif to KPLP thereby disrupting the basic box and catalytic activity towards PI(4)P without impairing catalytic activity towards PI (Gozzelino et al., 2022).

Strikingly, only the wild type enzyme was able to restore elevated active β1 integrin surface levels, suggesting that this process depends on PI(3,4)P_2 (Figure 24 c).

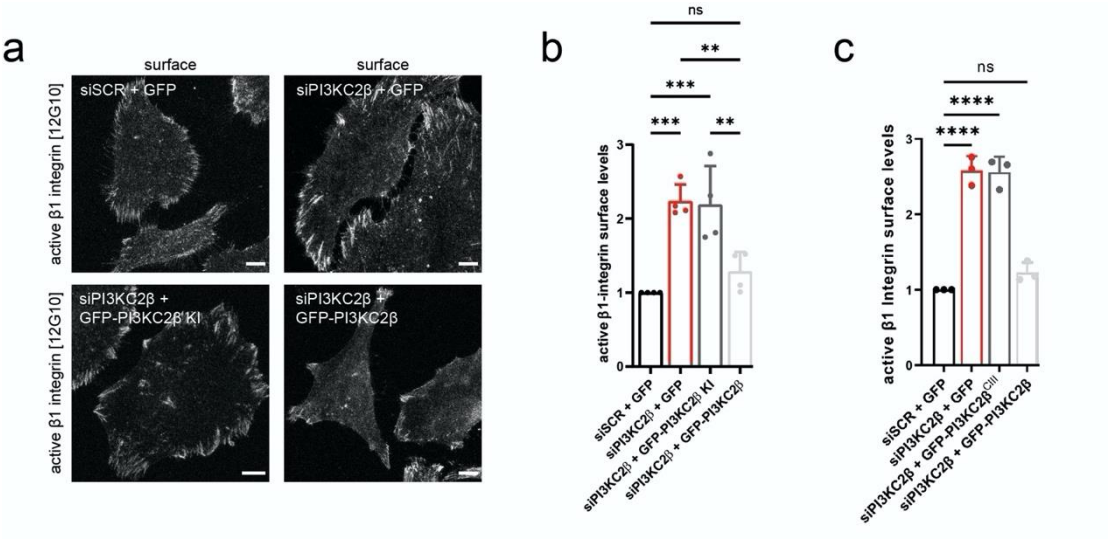

Figure 24: The regulation of surface active β1 integrin levels by PI3KC2β depends on PI3KC2β kinase activity. a) HeLa cells were treated with control (siSCR) or PI3KC2β (siPI3KC2β) targeting siRNAs. The siSCR treated cells were then transfected with eGFP(siSCR+GFP) and the siPI3KC2β treated cells were transfected with eGFP (siPI3KC2β + GFP), eGFP-PI3KC2β (siPI3KC2β + GFP-PI3KC2β), kinase inactive eGFP-PI3KC2β(siPI3KC2β + GFP-PI3KC2β KI) or class III like eGFP-PI3KC2β(siPI3KC2β + GFP-PI3KC2β^{CIII}), respectively. Subsequently, cells were stained for surface active β1 integrin. Scale bars 10 µm. b) Quantification of a). Integrated density was measured and normalized to the mean of siSCR + GFP. Mean +/- s.e.m. (n = 4 independent experiments with > 30 cells/condition per experiment). A one-way ANOVA (f = 15.83, total d.f. = 15) and Tukey's multiple comparison post-test were used. *P < 0.05, **P < 0.01, ***P < 0.001.

4.7 PI3KC2β regulates endocytosis, recycling, and lysosomal degradation

So far, we established that a loss of PI3KC2β leads to increased surface levels of active β1 integrin that can be restored by re-expressing the wild type protein. There are several possibilities how PI3KC2β might regulate active β1 integrin surface levels (Figure 25). First, PI3KC2β might be involved in the endocytosis of active β1 integrins and a depletion of PI3KC2β might therefore lead to lower endocytosis rates and, as a result, higher plasma membrane levels of active β1 integrins. The closely related PI3KC2α is required for the final stages of clathrin-mediated endocytosis (CME) (Posor et al., 2013), hence, a role for PI3KC2β in CME seems plausible.

Second, PI3KC2β might regulate the lysosomal degradation of β1 integrins. In this scenario depletion of PI3KC2β would reduce β1 integrin degradation and, thereby, indirectly to higher active β1 integrin surface levels (e.g. via recycling). PI3KC2β is known to inhibit mTORC1 at lysosomes to promote catabolic functions such as autophagy (Marat et al., 2017), so it seems plausible that PI3KC2β function might be required for proper lysosomal degradation.

Finally, the recycling of β1 integrin might be facilitated by PI3KC2β depletion. XLCNM is caused by the loss of MTM1 function, a phosphatase required for the removal of PI(3)P on recycling endosomes. This is a crucial step in endocytic recycling as recycling endosomes need to acquire PI(4)P in order for exocytosis to occur (Ketel et al., 2016).

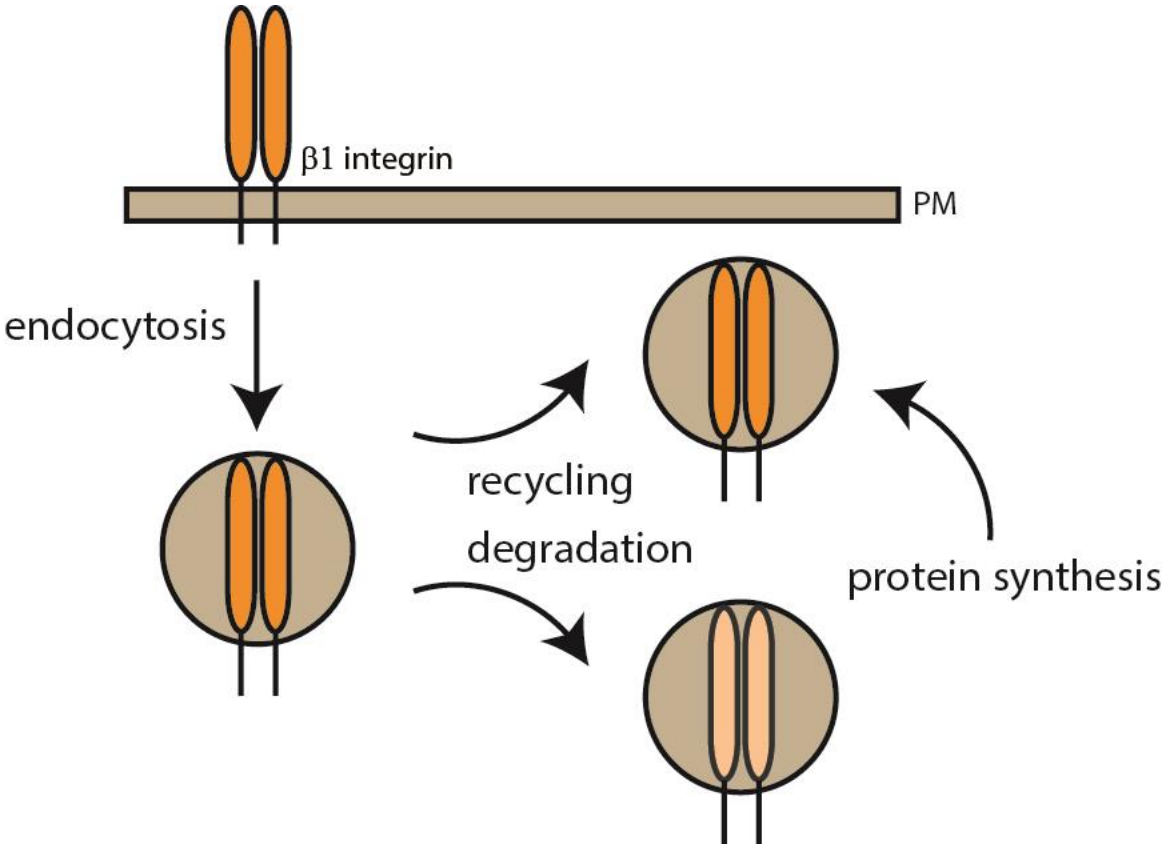

Figure 25: Pathways regulating active β1 integrin surface levels. β1 integrin surface levels are controlled by cycles of endocytosis and recycling. After endocytosis, β1 integrin can either be degraded or recycled back to the plasma membrane. Furthermore, synthesis of new β1 integrin proteins might influence β1 integrin surface levels as well.

To test for these possibilities, I made use of simple assays. First, the influence of PI3KC2β on transferrin endocytosis, a well-established CME cargo, was tested. PI3KC2β

depletion led to a mild, yet significant decrease of transferrin endocytosis to around 75% compared to control cells. Depletion of the related PI3KC2α enzyme reduced transferrin endocytosis to about 40% of controls. Interestingly, double depletion of PI3KC2β and PI3KC2α did not further decrease transferrin endocytosis suggesting that both kinases may fulfill distinct roles in endocytosis (Figure 26 a).

To assess whether PI3KC2β plays a role in endocytic recycling, transferrin recycling was analyzed. Indeed, depletion of PI3KC2β accelerated endocytic recycling of transferrin-Alexa647 (Figure 26 b). After 10 min of recycling, about 40% of internalized transferrin had recycled back to the plasma membrane in cells treated with siRNA targeting PI3KC2β whereas only 20% had been recycled in control cells.

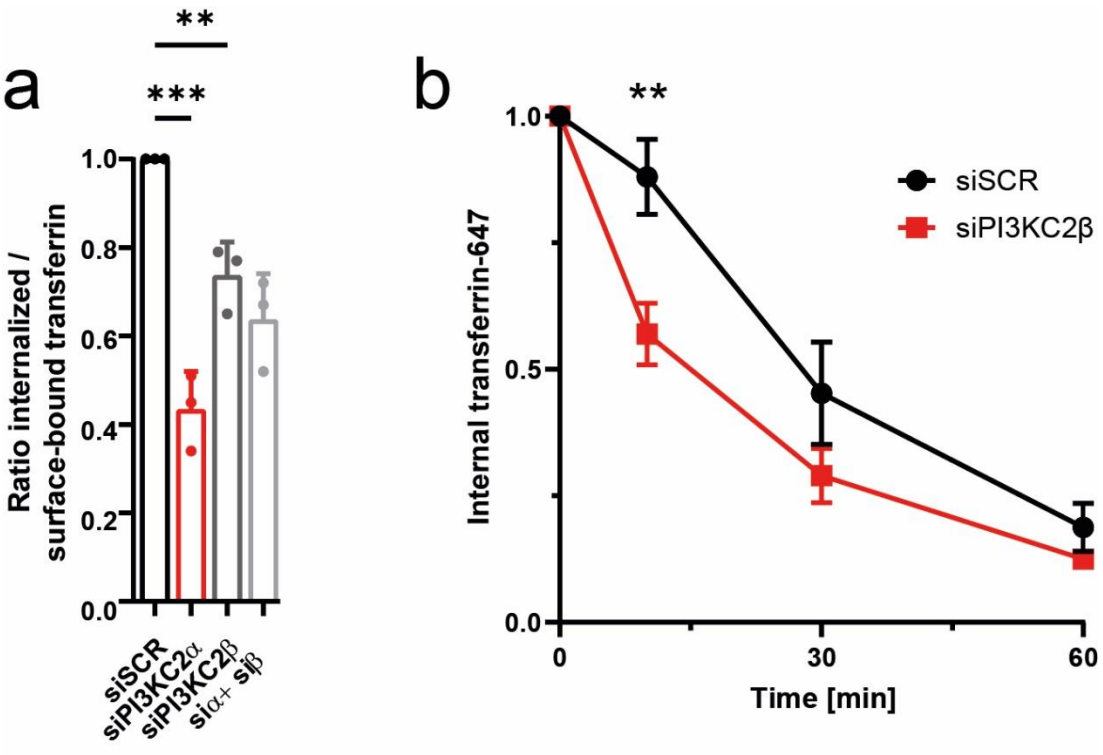

Figure 26: PI3KC2β depletion reduces transferrin endocytosis and accelerates transferrin recycling. a) COS7 were treated with control (siSCR), PI3KC2β (siPI3KC2β), PI3KC2α (siPI3KC2α) or PI3KC2α and PI3KC2β (siα + siβ) targeting siRNAs and transferrin-647 surface and uptake levels were determined. The ratio of internalized to surface-bound transferrin normalized to the mean of the control is depicted. Mean +/- s.e.m. (n = 3 independent experiments with > 30 cells/condition per experiment). A one-way ANOVA (f = 54.96, total d.f. = 8) and Tukey's multiple comparison post-test were used. **P = 0.0067, ***P = 0.001. b) COS7 cells were treated with control (siSCR) or PI3KC2β (siPI3KC2β)

targeting siRNAs and transferrin-647 recycling was determined. Depicted is the percentage of remaining internal transferrin-647 at various time points normalized to the levels at t = 0 min of each condition. Mean +/- s.e.m. (n=3 independent experiments with > 30 cells/condition per experiment). A one-way ANOVA (f = 41.48, total d.f. = 31) and Šídák's multiple comparisons test were used. siSCR 10min vs. siPI3KC2β 10min **p = 0.0019, siSCR 30min vs. siPI3KC2β 30min ns, p = 0.1433, siSCR 60min vs. siPI3KC2β 60min ns, p = 0.8202.

Finally, to address if loss of PI3KC2β impairs the degradation of β1 integrins, HeLa cells were depleted of PI3KC2β, and total β1 integrin levels were determined by immunoblotting. Cells depleted of PI3KC2β displayed elevated total β1 integrin levels compared to control cells (Figure 27 a, b). To measure the turnover of total surface β1 integrins I used a surface biotinylation assay: Control siRNA-treated or siPI3KC2β-treated HeLa cells were subjected to surface biotinylation and subsequently chased for 0h or 24h. Biotinylated proteins were isolated and analyzed by immunoblotting. After 24h, control siRNA-treated cells had turned over essentially all surface β1 integrins, whereas siPI3KC2β treated cells had only turned over about 75 % of all surface β1 integrins (Figure 27 c, d). This likely represents a cumulative effect caused by slower endocytosis, faster recycling, and a higher percentage of recycling instead of degradation of β1 integrins. Of note, total surface β1 integrin levels observed in the starting material of the turnover experiment were not increased upon PI3KC2β depletion (Figure 27 c).

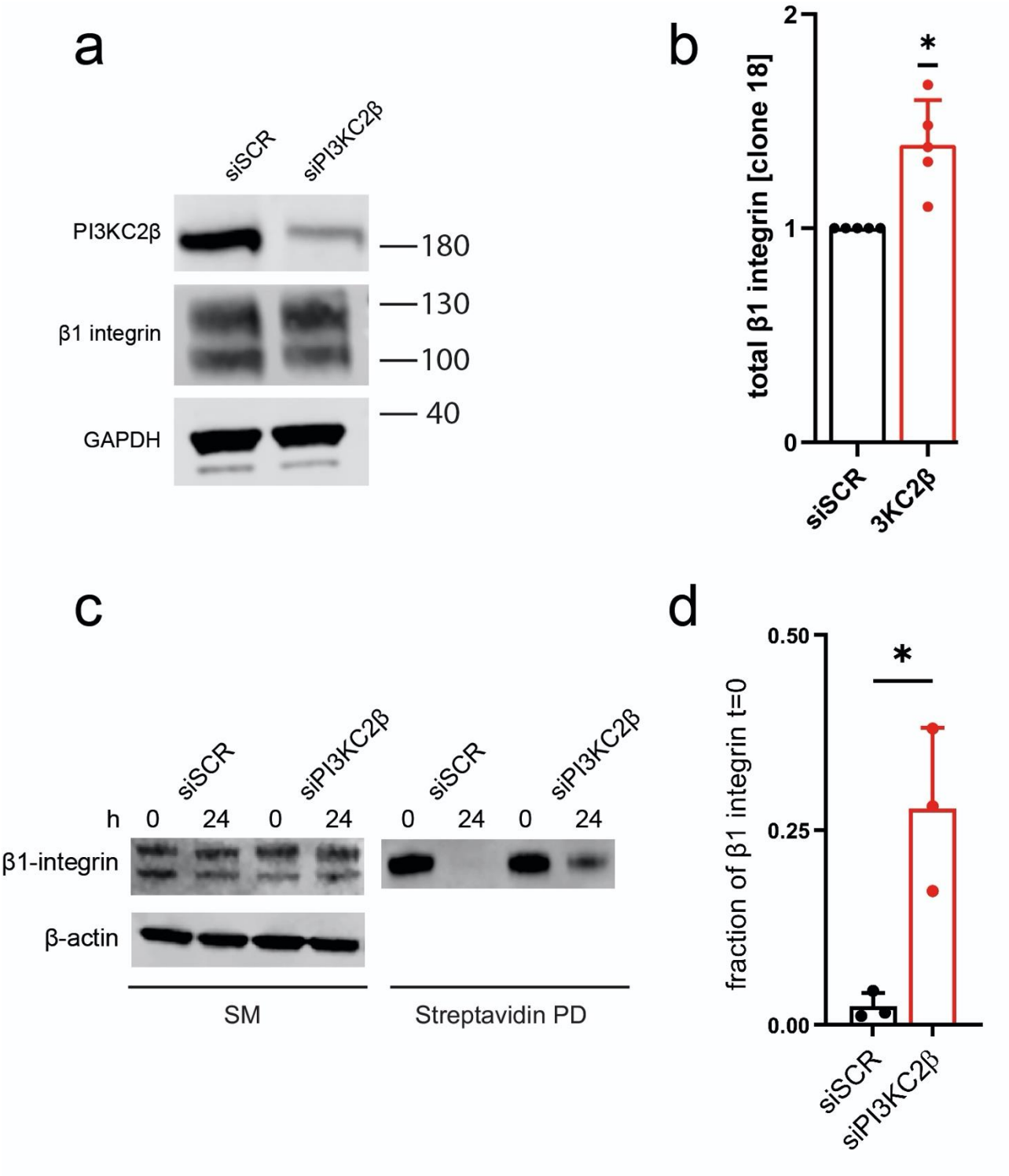

Figure 27: PI3KC2β depletion reduces β1 integrin turnover. a) PI3KC2β and total β1 integrin levels in lysates from HeLa cells treated with either control (siSCR) or PI3KC2β-targeting (siPI3KC2β) siRNAs. Samples were analyzed by immunoblotting using the indicated antibodies. A representative blot is depicted. b) Quantification of a). Total β1-integrin levels normalized to GAPDH are depicted. Mean ± SD from 5 independent experiments. Data was normalized to control (siSCR). One-sample, two-tailed t test; *p = 0.0146. c) Streptavidin pulldown using lysates of surface biotinylated HeLa cells treated

with control (siSCR) or PI3KC2β-targeting (siPI3KC2β) siRNAs. After surface biotinylation, cells were incubated at 37 °C for 0 or 24h, lysed and subjected to streptavidin pulldown. Bound proteins were analyzed by immunoblotting with the indicated antibodies. d) Quantification of c). The ratio of β1 integrin after 24 h and β1 integrin after 0h is depicted. Mean ± SD from 3 independent experiments. Two-tailed t test; *p = 0.0141.

4.8 PI3KC2β is required for active β1 integrin endocytosis

The above data suggest that PI3KC2β may affect the efficacy of endocytosis and endosomal sorting of internalized transferrin. I thus hypothesized that PI3KC2β may affect the plasma membrane levels of active β1-integrins by controlling its endocytic internalization. To test this hypothesis, I first analyzed clathrin-coated pit (CCP) dynamics. Previous work has established that the closely related enzyme potently regulates CCP dynamics and, thereby, CME (Posor et al., 2013). I found that the siRNA-mediated depletion of PI3KC2β in COS7 cells stably expressing CLC-eGFP decreased the fraction of dynamic CCPs to 65% of that seen in control cells (Figure 28 a, b), i.e. an effect that was milder than that observed for PI3KC2α depleted cells (Figure 28 a, b). Thus, a role for PI3KC2β in endocytosis or more specifically in integrin endocytosis seems plausible.

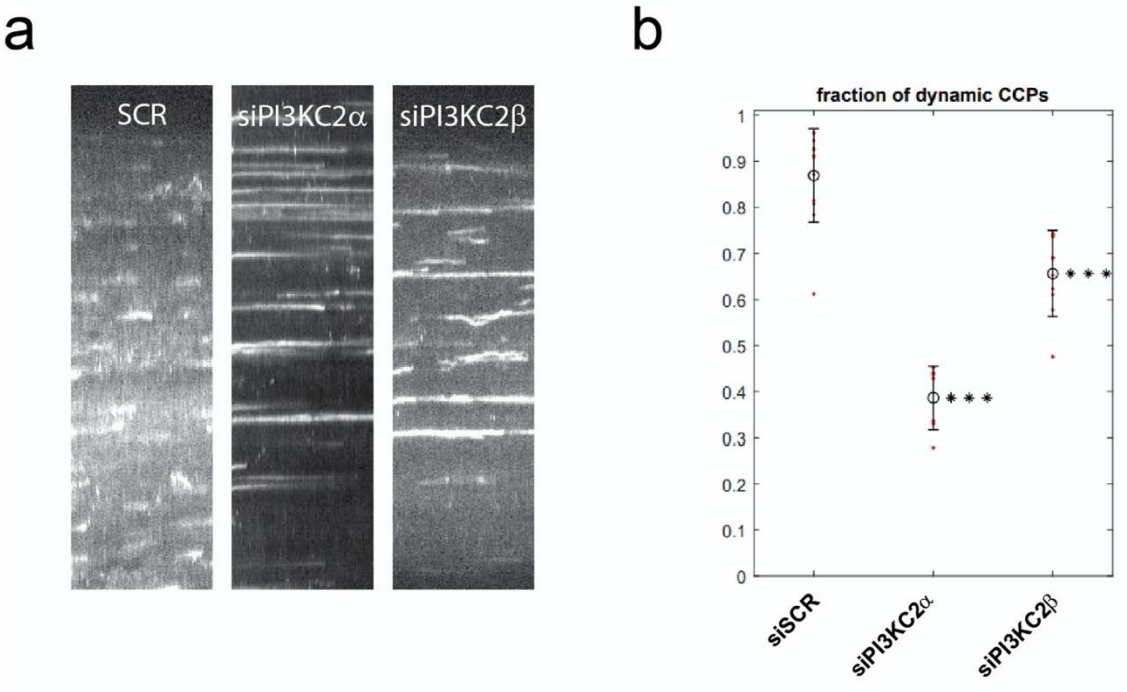

Figure 28: PI3KC2β depletion impairs clathrin coated pit dynamics and increases the number of static CCPs. a) COS7 cells stably expressing eGFP-clathrin were treated with control (siSCR), PI3KC2α

targeting (siPI3KC2α) or PI3KC2β targeting (siPI3KC2β) siRNAs. Kymographs were aquired over 180 s, 0.5 Hz by TIRF imaging. b) Fraction of dynamic CCPs analyzed by quantitative automated 2D tracking. Mean ± SD, *** $p < 0.001$.

To investigate if PI3KC2β depletion in fact impairs active β1 integrin endocytosis, HeLa cells were treated with siRNAs targeting PI3KC2β and active β1 integrin endocytosis was measured. To do so, surface active β1 integrins were labelled with an antibody specific for the active conformation of β1 integrin, and cells were incubated in full medium for 60 min to allow for endocytosis. Subsequently, internalized active β1 integrin levels were quantified and normalized to surface levels. Cells depleted of PI3KC2β indeed showed a reduction of β1 integrin endocytosis to 40% of control cells (Figure 29 a). Defective active integrin endocytosis was completely restored by re-expressing WT eGFP-PI3KC2β but not by re-expressing kinase inactive or a class III like eGFP-PI3KC2β (Figure 29 b, c). Hence, PI3KC2β controls active β1 integrin endocytosis in a kinase and PI(3,4)P_2 dependent manner.

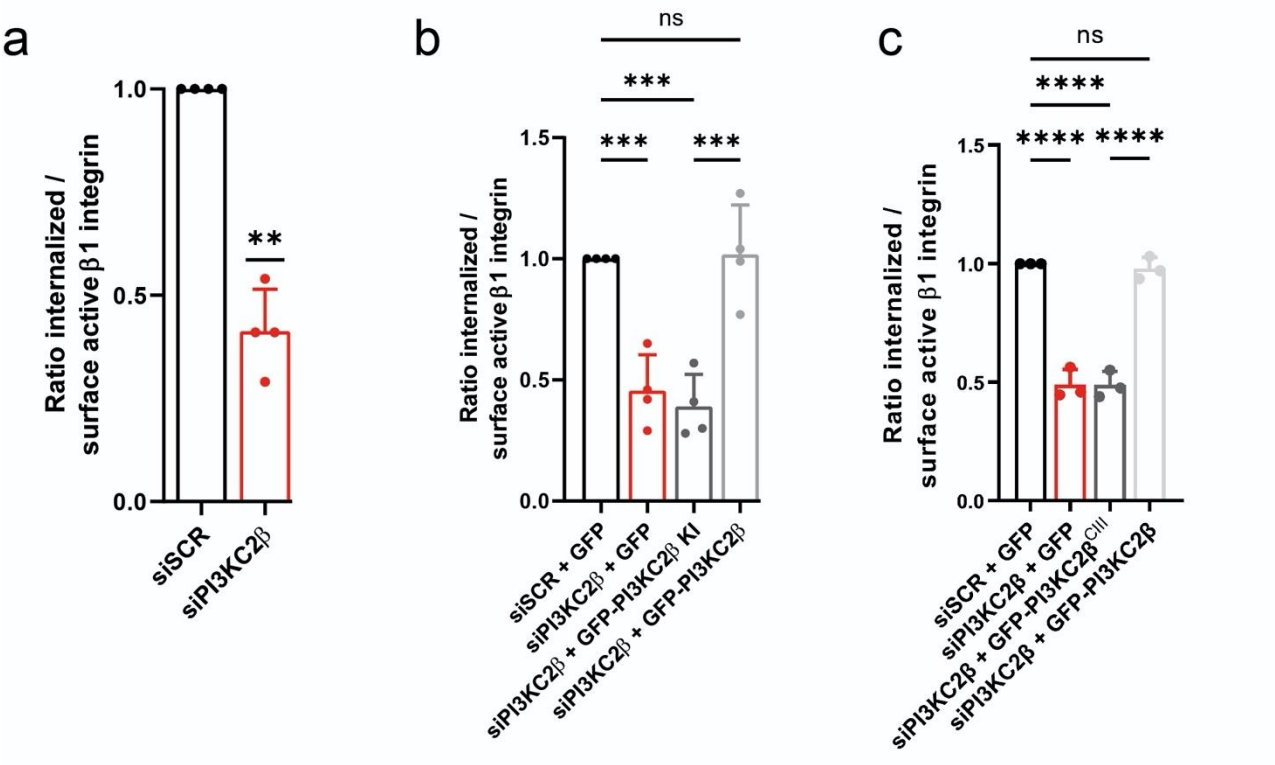

Figure 29: PI3KC2β facilitates active β1 integrin endocytosis in a kinase dependent manner. a) Relative internalized to surface active β1-integrin ratio in HeLa cells treated with control (siSCR) or PI3KC2β-targeting (siPI3KC2β) siRNA. Mean ± SD from 4 independent experiments represented as fold change compared to siSCR with a hypothetical mean of 1. One sample t-test with a hypothetical mean

of 1 was used for analysis **p<0.01. b) Relative internalized to surface active β1-integrin ratio in HeLa cells treated with control (siSCR) or PI3KC2β-targeting (siPI3KC2β) siRNA and transfected with plasmids encoding for eGFP, eGFP-PI3KC2β or kinase inactive eGFP-PI3KC2β (eGFP-PI3KC2β KI). Mean ± SD from 4 independent experiments represented as fold change compared to control (siSCR+GFP) with a hypothetical mean of 1. One-way analysis of variance (ANOVA; F = 22.52) and Tukey's multiple-comparison test; siSCR+GFP vs siPI3KC2β+GFP ***p = 0.0008, siSCR+GFP vs siPI3KC2β+GFP-PI3KC2β KI ***p = 0.0003, siSCR+GFP vs siPI3KC2β+GFP-PI3KC2β n.s. p = 0.9981, siPI3KC2β+GFP vs siPI3KC2β+GFP-PI3KC2β ***p = 0.0006, siPI3KC2β+GFP-PI3KC2β KI vs siPI3KC2β+GFP-PI3KC2β ***p = 0.0002. c) Relative internalized to surface active β1-integrin ratio in HeLa cells treated with control (siSCR) or PI3KC2β-targeting (siPI3KC2β) siRNA and transfected with plasmids encoding for eGFP, eGFP-PI3KC2β or classIII like eGFP-PI3KC2β (eGFP-PI3KC2βCIII). Mean ± SD from 3 independent experiments represented as fold change compared to control (siSCR+GFP) with a hypothetical mean of 1. 10 images per condition and experiment were acquired accounting for 30-60 cells. One-way analysis of variance (ANOVA; F = 104.0) and Tukey's multiple-comparison test; siSCR+GFP vs siPI3KC2β+GFP ****p < 0.0001, siSCR+GFP vs siPI3KC2β+GFP-PI3KC2β ns p = 0.9520, siPI3KC2β+GFP vs siPI3KC2β+GFP-PI3KC2βCIII ns p > 0.9999, siPI3KC2β+GFP vs siPI3KC2β+GFP-PI3KC2β ****p < 0.0001, siPI3KC2β+GFP-PI3KC2β vs siPI3KC2β+GFP-PI3KC2βCIII ****p < 0.0001.

4.9 PI3KC2β interacts with the integrin endocytosis adaptor Dab2

To this end, I could show that PI(3,4)P_2 production by PI3KC2β is required for proper CME of active β1 integrins. How this occurs exactly is unknown. To identify a potential mechanism, I performed co-immunoprecipitation experiments to screen for known endocytic integrin adaptors that might associate with PI3KC2β. Previously, it was found that PI3KC2β interacts with clathrin itself and the endocytic scaffolding protein intersectin-1 (Das et al., 2007; Wheeler & Domin, 2006). Indeed, both proteins co-immunoprecipitated with endogenous eGFP-PI3KC2β (Figure 29 a). Furthermore, the endocytic adaptor Dab2 was identified as a novel interactor of PI3KC2β (Figure 30 a). Dab2 was shown to be required for β1 integrin endocytosis but, akin to PI3KC2β, was largely dispensable for transferrin endocytosis (Teckchandani et al., 2012).

As clathrin and intersectin-1 are known to bind to the unstructured N-terminal domain of PI3KC2β (Das et al., 2007; Wheeler & Domin, 2006) , I hypothesized that Dab2 might also

bind to the same region. To challenge that hypothesis, full length eGFP-PI3KC2β or eGFP-PI3KC2β lacking the N-terminal domain (eGFP-PI3KC2β ΔN) were overexpressed in HEK293T cells and subjected to immunoprecipitation. As expected, clathrin heavy chain and intersectin-1 did only co-immunoprecipitate with full length eGFP-PI3KC2β but not with eGFP-PI3KC2β ΔN (Figure 29 b). Similarly, Dab2 only co-immunoprecipitated with full length eGFP-PI3KC2β but not with eGFP-PI3KC2β ΔN (Figure 30 b). This indicates that Dab2 also binds either directly to the PI3KC2β domain or interacts with PI3KC2β via intersectin-1, a protein that has been shown to directly interact with Dab2 (Teckchandani et al., 2012).

To map the binding sites of these proteins to the unstructured N-terminal domain of PI3KC2β, pull downs using truncated, GST-tagged constructs of the PI3KC2β N-terminal domain were performed. While clathrin heavy chain already interacted with the smallest construct (i.e. amino acids 27-106), intersectin-1 and Dab2 only interacted with constructs that at least contained amino acids 27-184 (Figure 30 c). Notably, intersectin-1 and Dab2 showed identical interaction patterns. I thus consider it likely that Dab2 interacts with PI3KC2β indirectly using intersectin-1 as a bridging factor.

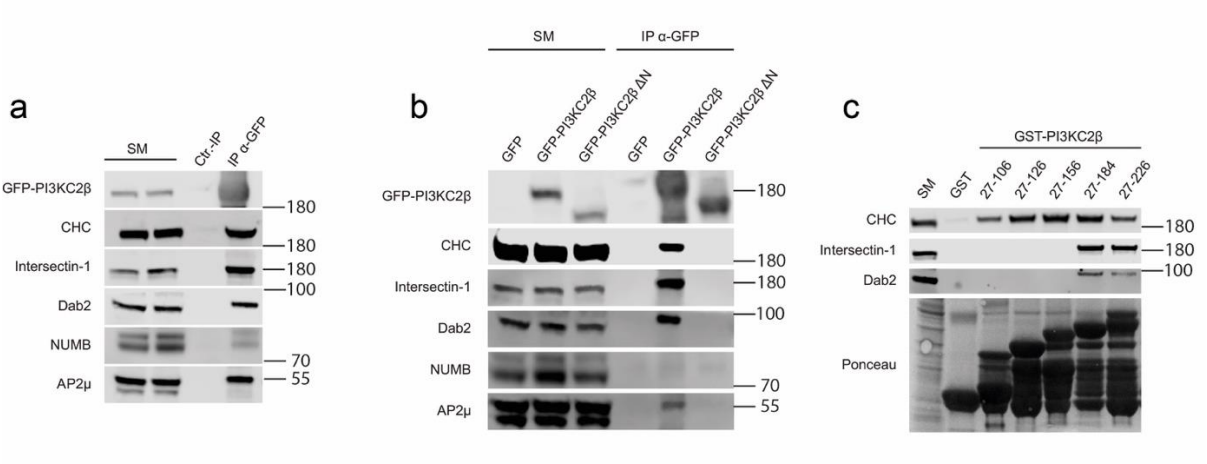

Figure 30: PI3KC2β interacts with endocytic adaptor proteins via its unstructured n-terminal domain. a) HEK293T cells endogenously expressing eGFP-PI3KC2β were subjected to immunoprecipitation using GFP trap beads. Bound proteins were analyzed by immunoblotting using the indicated antibodies. b) eGFP, eGFP-PI3KC2β or eGFP-PI3KC2β ΔN were transiently expressed in HEK293T cells and subjected to immunoprecipitation using GFP trap beads. Bound proteins were analyzed by immunoblotting using the indicated antibodies. c) Pulldown experiment using HEK293T lysate and GST-tagged regions of the n-terminal domain of PI3KC2β or GST as a control. Proteins bound to the GST-tagged constructs were analyzed by immunoblotting using the indicated antibodies.

Next, PI3KC2β localization at the plasma membrane was probed by TIRF microscopy. Endogenously expressed eGFP-PI3KC2β in HeLa cells co-localized with clathrin heavy chain, intersectin-1 and AP-2 (Figure 31 a, b, c). Of interest, PI3KC2β was present at most CCPs but not at all CCPs (Figure 31 a).

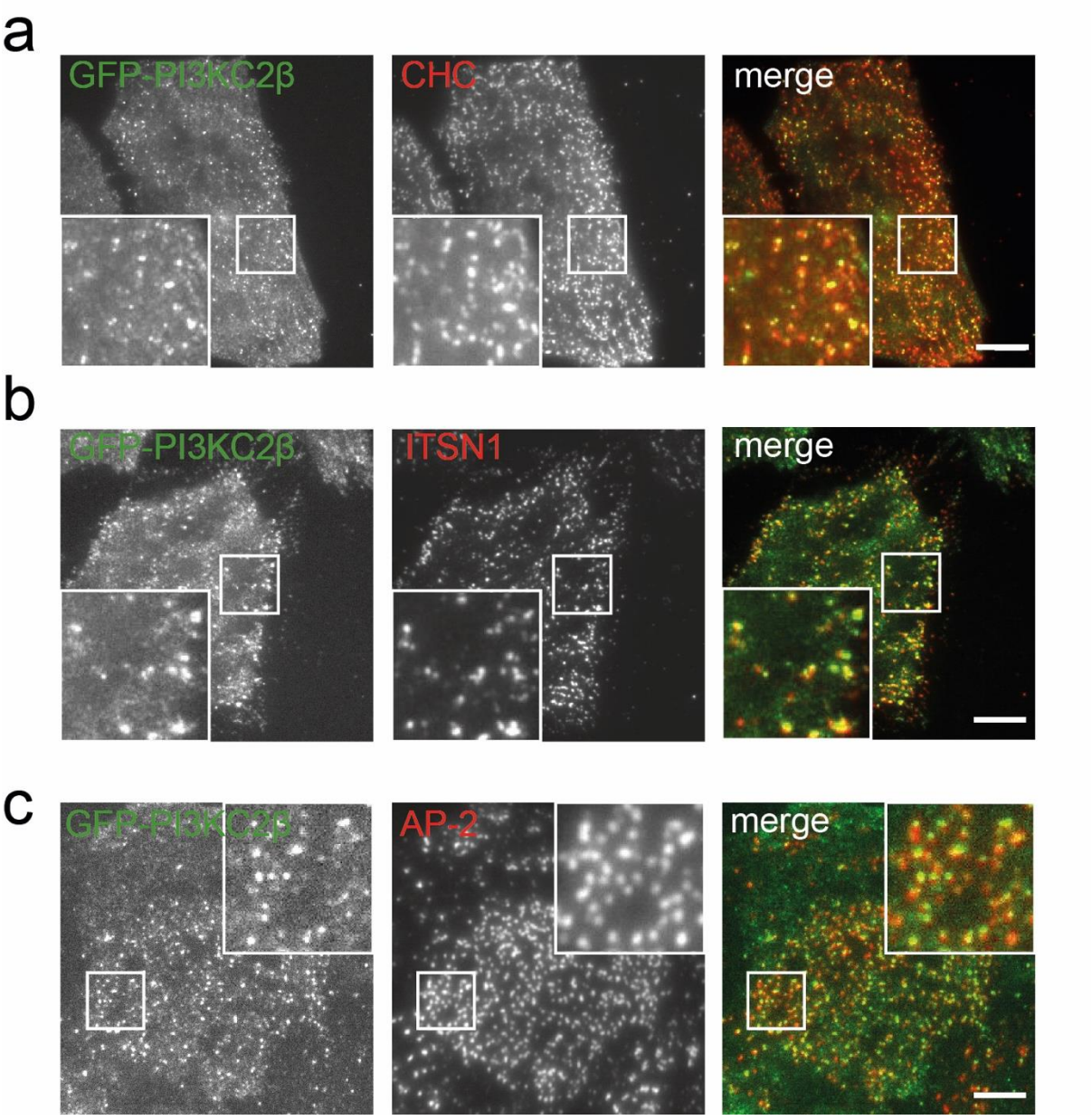

Figure 31: PI3KC2β localizes to clathrin coated pits. Representative TIRF images of HeLa cells endogenously expressing eGFP-PI3KC2β (green) stained for endogenous endocytic proteins (red). Scale bar 10 µM. a) Clathrin heavy chain (CHC), b) Intersectin-1 (ITSN1), c) AP-2.

4.10 Dab2 and intersectin-1 are required for active β1 integrin endocytosis

If PI3KC2β indeed regulates active β1 integrin endocytosis via intersectin-1 and Dab2, the depletion of either of these proteins should recapitulate the effects of PI3KC2β depletion on active β1 integrin surface levels and endocytosis. Indeed, depletion of either intersectin-1 or Dab2 led to the accumulation of active β1 integrin at the cell surface. Notably, this accumulation was not as profound as seen for PI3KC2β depletion (Figure 32 a, b). Interestingly, active β1-integrin endocytosis was reduced more strongly upon intersectin-1 or Dab2 depletion than upon PI3KC2β depletion (Figure 32 c) suggesting that PI3KC2β not only regulates active β1-integrin surface levels via endocytosis but also via inhibiting active β1 integrin recycling.

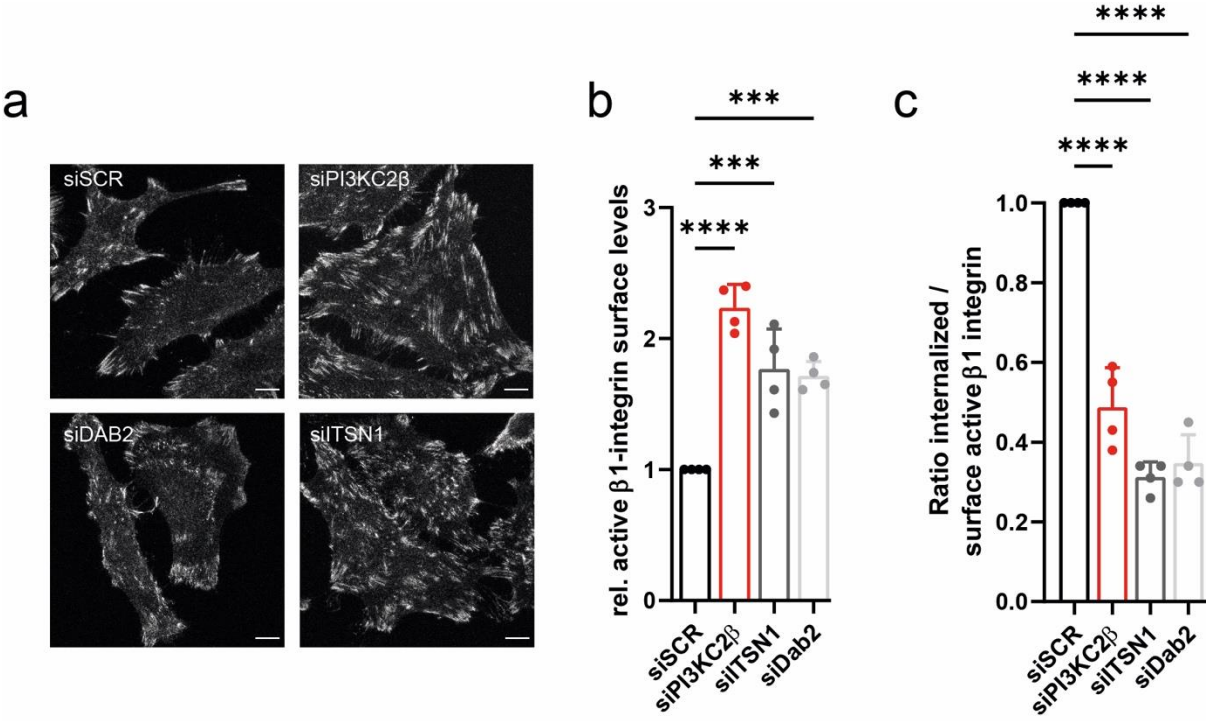

Figure 32: ITSN1 and Dab2 are required for active β1 integrin endocytosis. a) Representative images of HeLa cells treated with control (siSCR), PI3KC2β targeting (siPI3KC2β), Dab2 targeting (siDab2) or Intersectin-1 targeting (siITSN1) siRNAs stained for surface active β1 integrin. Scale bar 10 µM. b) Quantification of a) Mean ± SD from 4 independent experiments represented as fold change compared to siSCR with a hypothetical mean of 1. ANOVA (F = 26.85) and Tukey's multiple comparison test; siSCR vs. siPI3KC2β ****p < 0.0001; siSCR vs. siITSN1 ***p = 0.0001; siSCR vs. siDab2 ***p = 0.0003. c) Relative internalized to surface active β1-integrin ratio in HeLa cells treated with control (siSCR), PI3KC2β- (siPI3KC2β), ITSN1- (siITSN1) or Dab2-targeting (siDab2) siRNA. Mean ± SD from 4

independent experiments represented as fold change compared to control (siSCR) with a hypothetical mean of 1. ANOVA (F = 99.74) and Tukey's multiple comparison test; ****p < 0.0001.

4.11 Inhibition of endocytic recycling restores elevated active β1 integrin surface levels observed upon PI3KC2β depletion

Since PI3KC2β seems to also influence the endosomal recycling of active β1 integrins, I aimed to assess the contribution of endosomal recycling to the elevated surface pool of active β1 integrins upon PI3KC2β depletion. Therefore, I conducted double knockdown experiments targeting MTM1 or the exocyst components Exo70 and Sec3, respectively. Strikingly, these co-depletions nearly restored active β1 integrin surface levels (Figure 33 a, b). This strongly indicates that PI3KC2β and MTM1 antagonistically control active β1 integrin endocytosis and recycling.

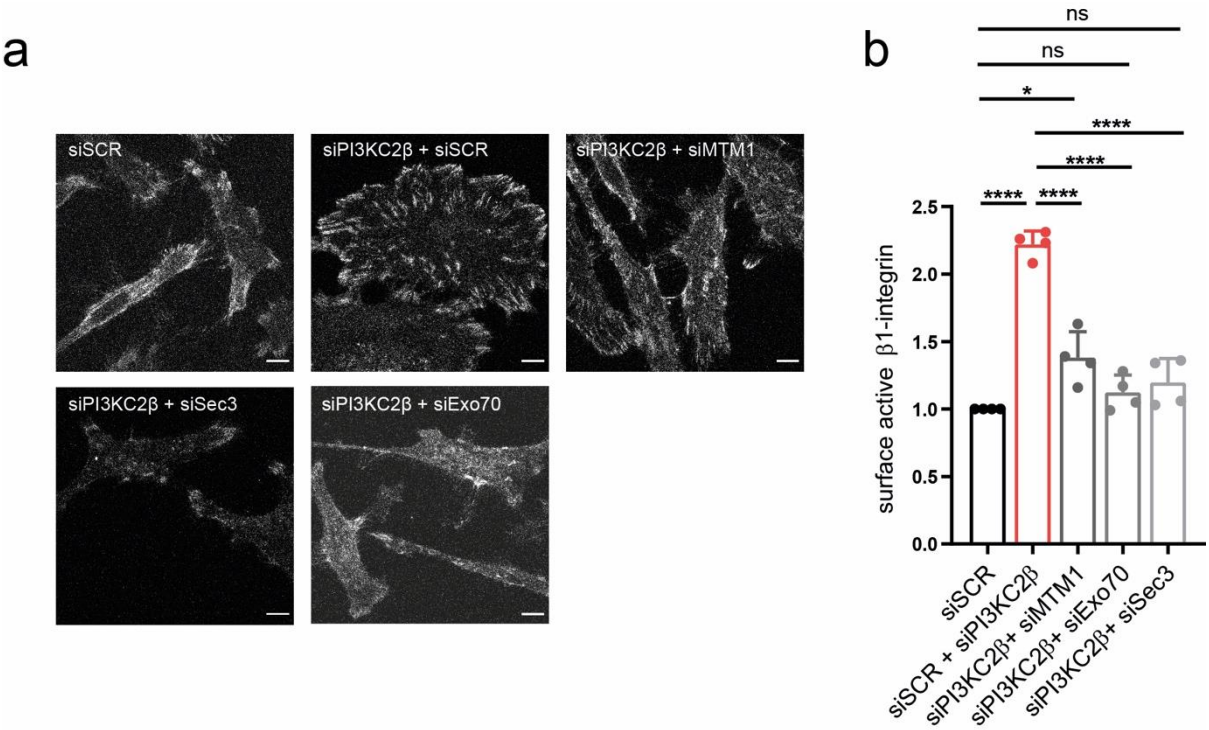

Figure 33: Co-depletion of exocyst components restores surface active β1 integrin levels upon PI3KC2β depletion. a) Representative images of HeLa cells treated with PI3KC2β- (siPI3KC2β), MTM1- (siMTM1), Exo70- (siExo70) or Sec3-targeting (siSec3) siRNA in the indicated combinations surface stained for active β1-integrin. b) Quantification of a). Mean ± SD from 4 independent experiments represented as fold change compared to control (siSCR) with a hypothetical mean of 1. ANOVA

(F = 49.88) and Tukey's multiple-comparison test; siSCR vs siSCR+siPI3KC2β ****p < 0.0001, siSCR vs siPI3KC2β+siMTM1 *p = 0.0107, siSCR vs siPI3KC2β+siExo70 n.s. p = 0.7205, siSCR vs siPI3KC2β+siSec3 n.s. p = 0.3015, siSCR+siPI3KC2β vs siPI3KC2β+siMTM1 ****p < 0.0001, siSCR+siPI3KC2β vs siPI3KC2β+siExo70 ****p < 0.0001, siSCR+siPI3KC2β vs siPI3KC2β+siSec3 ****p < 0.0001.

4.12 Inhibition of endocytosis restores active β1 integrin surface levels in MTM1 KO C2C12

To probe if the results in HeLa cells are applicable to C2C12 myoblasts, I repeated key experiments in these cells. Knock down of either clathrin heavy chain or dynamin 2 in MTM1 KO C2C12 cells restored active β1 integrin surface levels, suggesting that the inhibition of active β1 integrin endocytosis indeed rescues the phenotype (Figure 33 a). Furthermore, PI3KC2β KO cells showed reduced active β1 integrin in LAMP2a positive lysosomes 6h after endocytosis, suggesting impaired degradation of β1 integrins upon PI3KC2β loss in these cells (Figure 34 c, d). Finally, PI3KC2β KO C2C12 cells showed a strongly reduced internalization rate of active β1 integrins. Only 25 % of initial surface active β1 integrins were internalized after 90 min whereas WT C2C12 cells internalized around 50% (Figure 34 e, f).

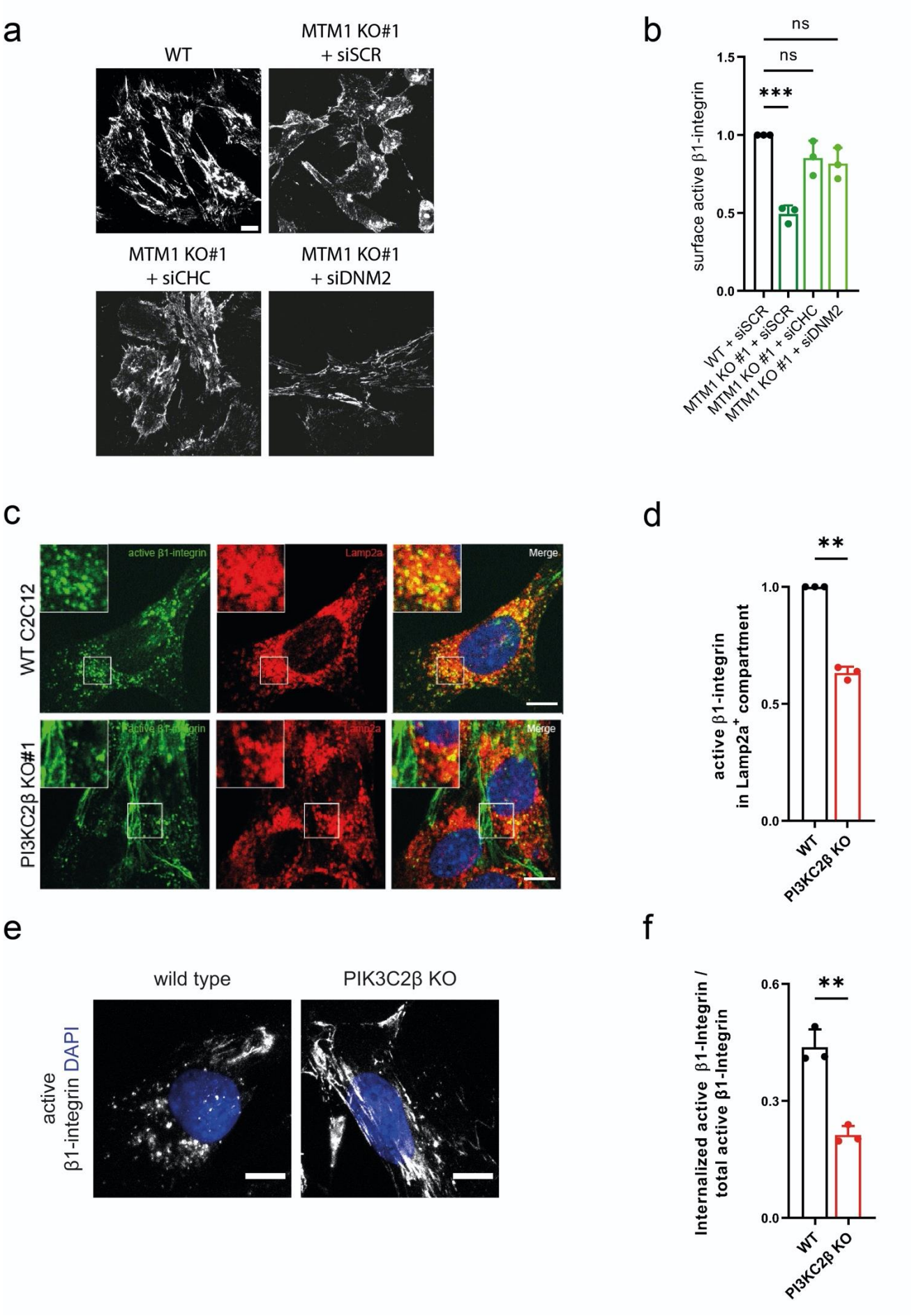
a
WT
MTM1 KO#1
+ siSCR
MTM1 KO#1
+ siCHC
MTM1 KO#1
+ siDNM2
b
ns
ns
***
surface active β1-integrin
1.5
1.0
0.5
0.0
WT + siSCR
MTM1 KO #1 + siSCR
MTM1 KO #1 + siCHC
MTM1 KO #1 + siDNM2
c
WT C2C12
PI3KC2β KO#1
active β1-integrin
Lamp2a
Merge
d
**
active β1-integrin
in Lamp2a+ compartment
1.0
0.5
0.0
WT
PI3KC2β KO
e
wild type
PIK3C2β KO
active
β1-integrin DAPI
f
**
Internalized active β1-Integrin /
total active β1-Integrin
0.6
0.3
0.0
WT
PI3KC2β KO

Figure 34: Inhibition of endocytosis in MTM1 KO C2C12 cells restores active β1 integrin surface levels. a) Representative images of wild type (WT) or MTM1 KO C2C12 cells treated with control (siSCR), clathrin heavy chain targeting (siCHC) or dynamin 2 targeting (siDNM2) siRNAs and stained for active suface β1 integrin. Scale bar 10 µM. b) Quantification of a). Mean ± SD from 3 independent experiments represented as fold change compared to control (WT + siSCR) with a hypothetical mean of 1. ANOVA (F = 18.24) and Tuckey's multiple-comparison test; WT + siSCR vs. MTM1 KO#1 + siSCR ***p = 0.0002; WT + siSCR vs. MTM1 KO#1 + siCHC ns p = 0.2946; WT + siSCR vs. MTM1 KO#1 + siDNM2 ns p = 0.1408; MTM1 KO#1 + siSCR vs. MTM1 KO#1 + siCHC **p = 0.0031; MTM1 KO#1 + siSCR vs. MTM1 KO#1 + siDNM2 **p = 0.0282. c) Representative images of active β1-integrin in late endosomal/lysosomal compartment (LAMP-2a) in wild type (WT) and PI3KC2β KO (PI3KC2β KO#1) C2C12 cells after 4h of active β1-integrin uptake. Scale bar 10 µM. d) Quantification of c). Mean ± SD 3 independent experiments. Represented as fold change compared to WT with a hypothetical mean of 1. One-sample two-tailed t test; **p = 0.0019. e) Representative images of active β1-integrin after 90 min of uptake in wild type (WT) and PI3KC2β KO (PI3KC2β KO#1) C2C12 cells. Scale bar 10 µM. f) Quantification of e). The ratio of internalized to total active β1-integrin was determined and is represented as the fold change compared to WT with a hypothetical mean of 1. Mean ± SD from 3 independent experiments. Unpaired two-tailed t test; **p = 0.0016.

4.13 Inhibition of PI3KC2β but not PI3KC2α leads to elevated active β1 integrin surface levels in HeLa cells

Finally, I aimed to investigate if newly developed PI3KC2α specific (PITCOIN3) and PI3KC2α / PI3KC2β (PITCOIN2) specific inhibitors (Lo, Belabed, et al., 2022; Lo, Zhang, et al., 2022) can induce elevated surface active β1 integrin levels in HeLa cells and thus could potentially rescue the phenotypes observed in MTM1 KO cells. While the PI3KC2α specific PITCOIN3 did not significantly alter surface active β1 integrin levels, the PI3KC2α / PI3KC2β specific PITCOIN2 elevated surface active β1 integrin levels about 2-fold compared to DMSO treated control cells (Figure 35 a, b). This indicated that PI3KC2α might not be relevant for active β1 integrin endocytosis. In line with these findings, GFP-PI3KC2α did not co-immunoprecipitate with intersectin-1 or Dab2 (Figure 35 c).

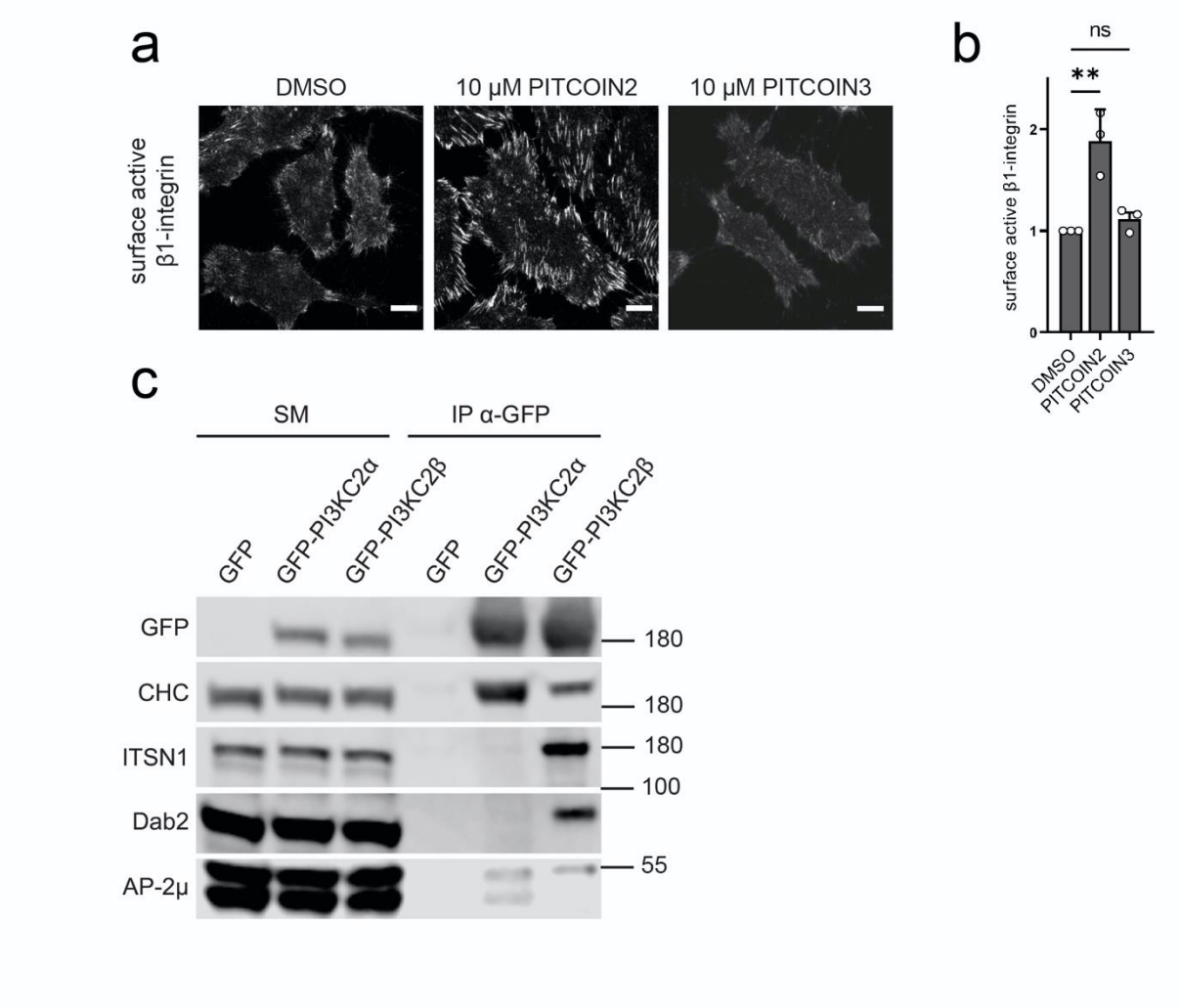

Figure 35: Inhibition of PI3KC2β but not PI3KC2α leads to elevated active β1 integrin surface levels. a) Representative images of HeLa cells surface stained for active β1 integrins after 24h treatment with DMSO, 10 µM PITCOIN2 (PI3KC2α and PI3KC2β targeting) or 10 µM PITCOIN3 (PI3KC2α specific) Scale bars 10 µm. b) Quantification of a). Integrated density was measured and normalized to the mean of DMSO. Mean +/- SD (n = 3 independent experiments with > 30 cells/condition per experiment). A one-way ANOVA (f = 18.37) and Tukey's multiple comparison post-test were used. ** p = 0.0034; ns p = 0.7643. c) Co-IP of eGFP, eGFP-PI3KC2α and eGFP-PI3KC2β over expressed in HEK293T cells using GFP-trap magnetic agarose beads. Samples were analyzed by immunoblotting using the indicated antibodies. 1.25% of total lysate was used as starting material.

5 Discussion

In this study, I investigated the functions of PI3KC2β in two different cellular processes. In the first part, I show that Rab7A is required to recruit PI3KC2β to late endosomes and lysosomes to repress mTORC1 signaling upon growth factor starvation, and in the second part, I identified a role for PI3KC2β in endocytosis of active β1 integrins at the plasma membrane. Furthermore, I provided evidence that active β1 integrin trafficking antagonistically regulated by PI3KC2β and MTM1 underlies the pathology of XLCNM.

5.1 PI3KC2β regulates mTORC1 signaling at late endosomes and lysosomes

In order to adapt to cues such as growth factors and amino acids, mTORC1 signaling is regulated at multiple levels. When growth factor levels are low, mTORC1 signaling is repressed by TSC complex activity that leads to Rheb and hence mTORC1 inactivation (Saxton & Sabatini, 2017). Apart from the TSC complex, PI3KC2β was identified to be activated and recruited to late endosomes and lysosomes under low growth factor conditions to produce $PI(3,4)P_2$, leading to mTORC1 repression (Marat et al., 2017). How PI3KC2β is actively recruited to late endosomes and lysosomes was previously unknown.

5.1.1 Active Rab7A recruits PI3KC2β to late endosomes and lysosomes upon growth factor starvation to promote PI(3,4)P2 production and mTORC1 signaling inhibition

In this study, I show that PI3KC2β is recruited to late endosomes and lysosomes by active, GTP bound Rab7A. GTP bound Rab7A was required for the growth factor starvation induced recruitment of PI3KC2β and subsequent $PI(3,4)P_2$ synthesis, as well as for mTORC1 repression. Rab7A is the hallmark Rab of the endolysosomal system and controls the transport of endocytic cargo to lysosomes for degradation. Lysosome function depends on Rab7A activity as it controls lysosome biogenesis and positioning (Guerra & Bucci, 2016). Similar to PI3KC2β, Rab7A activity is increased upon nutrient starvation and Rab7A accumulates on LBPA positive late endosomes and lysosomes in the perinuclear region and is furthermore required for the maturation of autophagosomes (Gutierrez, Munafo, Beron, &

Colombo, 2004; Jager et al., 2004). Interestingly, overexpression of constitutively active Rab7 Q67L in HEK293T cells was shown to potently inhibit mTORC1 mediated S6 kinase phosphorylation (Li et al., 2010). This is in line with our findings that active Rab7A recruits PI3KC2β to late endosomes and lysosomes upon growth factor starvation to promote mTORC1 inhibition. It seems plausible that the Rab7A mediated inhibition of mTORC1 is dependent on PI3KC2β.

Interestingly, the PI(3,4)P_2 phosphatase INPP4B was recently identified as an Rab7A effector in MCF-7 breast cancer cells (Rodgers et al., 2021). Overexpression of INPP4B promoted the generation of late endosomal PI(3)P pools by the dephosphorylation of late endosomal PI(3,4)P_2. This process might be important to terminate PI3KC2β signaling at late endosomes and reactivate mTORC1, as endosomal PI(3)P is required for proper mTORC1 activation (Hong et al., 2017).

5.1.2 PI(3,4)P_2 mediated inhibition of mTORC1 signaling

How PI3KC2β inhibits mTORC1 activity at late endosomes and lysosomes under growth factor starvation conditions remains elusive. Marat et al., show that inhibitory 14-3-3γ proteins localize to the mTORC1 subunit Raptor in a PI(3,4)P_2 dependent manner (Marat et al., 2017). It seems possible though, that further effectors of PI(3,4)P_2 are required for mTORC1 inhibition. Late endosomal PI(3,4)P_2 produced by PI3KC2β was linked to the export of endocytosed cholesterol from late endosomes to the ER via the cholesterol transporter ORP1L (Dong et al., 2019). PI3KC2β loss resulted in a late endosomal accumulation of cholesterol, a known activator of mTORC1. High late endosomal cholesterol levels activate mTORC1 via SLC38A9(Castellano et al., 2017) and LYCHOS (Shin et al., 2022). It is unclear however, if the accumulation of late endosomal cholesterol upon PI3KC2β loss is sufficient to activate mTORC1. Along these lines, late endosomal cholesterol is required for mTORC1 localization to lysosomes (Lim et al., 2019) but PI3KC2β depletion did not affect mTOCR1 localization. In fact, mTORC1 must be at the lysosome for PI3KC2β to act on it (Marat et al., 2017). Also, ORP1L is only one of many cholesterol transporters at late endosome ER contact sites and the main exporter of late endosomal cholesterol seems to be NPC1 (Lim et al., 2019).

As phosphoinositides often function to recruit proteins to membranes, I speculated that PI3KC2β mediated PI(3,4)P_2 synthesis might promote the association of inhibitory

proteins to lysosomal mTORC1. For mTORC1, PRAS40 is a known inhibitory protein that associates with the Raptor subunit to block Raptor mediated mTORC1 signaling (Sancak et al., 2007; Saxton & Sabatini, 2017).To test for a potential role of PI3KC2β I established a CRISPR/Cas9 genome edited HEK293T cell line endogenously expressing eGFP-Raptor. This allowed for the isolation of endogenous mTORC1. Using this cell line, I could show that PRAS40 interacted with mTORC1 to a lesser extend upon PI3KC2β depletion. Thus, it seems plausible that a part of the inhibitory effect of PI3KC2β on mTORC1 activity is mediated through PRAS40. How PI3KC2β affects PRAS40 binding to mTORC1 remains the subject of further studies. The new cell line can furthermore be used to study mTORC1 biology and PI3KC2β on mTORC1 activity in further detail. So far, most studies that looked at mTORC1 composition relied on overexpression of tagged mTORC1 subunits, or the direct immunoprecipitation using antibodies. Both approaches come with limitations such as overexpression artifacts or unspecific antibody binding that can be overcome using the eGFP-Raptor HEK293T cell line.

5.2 PI3KC2β localizes to late endosomes and the plasma membrane

Apart from its role at late endosomes and lysosomes (Marat et al., 2017; Wallroth et al., 2019), PI3KC2β also localizes to the plasma membrane (Wheeler & Domin, 2001). For the recruitment to late endosomes and lysosomes, growth factor starvation and Rab7A activity are required. How PI3KC2β is recruited to the plasma membrane is not fully understood. Early studies have shown that PI3KC2β is recruited to Grb2 upon EGF stimulation to promote EGF signaling (Wheeler & Domin, 2001). These are the exact conditions where we find PI3KC2β inactive in the cytoplasm. This might be explained by two independent pools of PI3KC2β: one at late endosomes and lysosomes and one at the plasma membrane. Along these lines, I observed that the interaction of PI3KC2β and endocytic adaptors like clathrin or Dab2 was not affected by growth factor starvation or PKN2 inhibition (data not shown) but both, PKN2 inhibition and growth factor starvation led to an enhanced recruitment of PI3KC2β to focal adhesions (Posor et al., 2022). As for cellular signaling, receptors are often endocytosed after ligand binding to terminate the signal. It is thinkable that PI3KC2β is required for the endocytosis of some receptors and might therefore be recruited to plasma membrane

receptors not to transmit the signal but to terminate it instead (Irannejad, Tsvetanova, Lobingier, & von Zastrow, 2015). It can furthermore not be excluded that PI3KC2β fulfills opposing functions depending on the cell type (Koch et al., 2021). Furthermore, it is unlikely that PI3KC2β is recruited to the plasma membrane by Rab7A as Rab7A does not localize there. Therefore, another small GTPase might be involved in this process. My mass spectrometry results provided several other Rab proteins that co-immunoprecipitated with PI3KC2β. I could not confirm these potential interactions by immunoblotting, but I cannot exclude that they do in fact still interact with PI3KC2β, as mass spectrometry is far more sensitive than immunoblotting. Similar to the interaction with Rab7A, potential interactions with other small GTPases might also be enhanced under conditions like nutrient starvation and might therefore have escaped my notice.

5.3 PI3KC2β in centronuclear myopathy, endocytosis, and recycling

5.3.1 PI3KC2β depletion rescues defects caused by MTM1 loss in a cellular XLCNM model

In this study, we show that the depletion of PI3KC2β restores differentiation defects observed upon MTM1 knock out in a C2C12 XLCNM model. Contrary to prior belief (Ribeiro et al., 2011; Sabha et al., 2016), we provide evidence that this rescue is not mediated by lowering elevated endosomal PI(3)P levels observed upon MTM1 loss (Ketel et al., 2016; Sabha et al., 2016), but instead depends on the inhibition of active β1 integrin endocytosis and the promotion of active β1 integrin recycling.

5.3.2 The PI3KC2β mediated rescue of XLCNM does not depend on endosomal PI(3)P levels

Loss of MTM1 lead to a significant increase in PI(3)P levels in MTM1 KO C2C12 cells but this increase could not be restored by PI3KC2β loss (Samsó et al., 2022), even though defective differentiation was readily rescued. This opposes the generally accepted concept, that PI3KC2β loss rescues XLCNM by restoring endosomal PI(3)P levels. This idea stems from work in *drosophila* where MTM1 and the only class II PI 3-kinase isoform in *drosophila*, PI3K68D antagonistically regulate endosomal PI(3)P levels to ensure proper endolysosomal

function and integrin trafficking (Ribeiro et al., 2011; Velichkova et al., 2010). In mammals, there are three isoforms of class II PI 3-kinases: PI3KC2α, PI3KC2β and PI3KC2γ (Koch et al., 2021). While endosomal PI(3)P by PI3KC2α is indeed required for endosomal recycling in mammalian cells (Franco et al., 2014), no such function is known for PI3KC2β (Koch et al., 2021). Furthermore, the unstructured N-terminal domain of PI3KC2α and PI3KC2β is not conserved in *drosophila* PI3K68D. This domain mediates the association of PI3KC2β with the endocytic proteins clathrin, intersectin-1 and Dab2 and hence is required for the regulation of active β1 integrin endocytosis. Therefore, it seems plausible that class II PI 3-kinases have evolved to fulfill isoform specific, specialized functions in mammalian cells.

In line with findings that defects in the endosomal trafficking of β1 integrins underlie the pathology of XLCNM (Gomez-Oca et al., 2021; Ketel et al., 2016; Ribeiro et al., 2011), we show that MTM1 KO C2C12 cells have significantly reduced surface levels of active β1 integrins. This was also rescued by PI3KC2β depletion. We show that PI3KC2β controls active β1 integrin surface levels by promoting active β1 integrin endocytosis and lysosomal degradation and inhibiting endosomal recycling. HeLa cells depleted of PI3KC2β showed a profound decrease of active β1 integrin endocytosis that could only be rescued by re-expressing wild type PI3KC2β but not by the expression of a class III-like mutant that only synthesizes PI(3)P but not PI(3,4)P_2. This observation further argues that the rescue observed does not depend on PI(3)P. Interestingly, reduced active β1 integrin surface levels in MTM1 KO C2C12 cells could not only be rescued by PI3KC2β depletion but also by knock down of clathrin or dynamin 2, two proteins essential for CME of active β1 integrins.

We therefore provide evidence for a model where MTM1 and PI3KC2β antagonistically control active β1 integrin trafficking.

5.3.3 Defective endocytic sorting of active β1 integrins underlies the pathology of XLCNM

The observation that active β1 integrin trafficking is essential for proper muscle function and development transfers perfectly to other genes involved in centronuclear myopathies: Hyperactivating GoF mutations in DNM2, a protein also involved in active β1 integrin endocytosis (Chao & Kunz, 2009; Ezratty et al., 2009; Lee et al., 2014), cause centronuclear myopathy as well (Bitoun et al., 2005). These mutations increase the endocytic

rate and thus are likely to cause reduced active β1 integrin surface levels. In mouse models of DNM2 caused CNM, disease phenotypes can be rescued by reducing DNM2 levels (Buono et al., 2018). Strikingly, this rescue also works in XLCNM models that harbor LoF mutations in MTM1 (Cowling et al., 2014). These data strongly suggest that rescue mechanisms of MTM1 caused XLCNM do not work through restoring endosomal PI(3)P levels, but through the modulation of active β1 integrin trafficking. In line with this, we could also rescue reduced active β1 integrin surface levels in MTM1 KO C2C12 cells by depleting DNM2.

Another gene that is implicated in the pathogenesis of CNM is BIN1 encoding for the Amphiphysin-2 protein. LoF mutations in BIN1 cause CNM as well (Nicot et al., 2007). Amphiphysin-2 is involved in endosomal sorting and endocytosis, too (Prokic, Cowling, & Laporte, 2014). Thus, an involvement in active β1 integrin trafficking is conceivable. In HeLa cells, knock down of BIN1 only mildly affects transferrin endocytosis but leads to an intracellular accumulation of transferrin similar to what has been observed for MTM1 depletion (Ketel et al., 2016; A. J. Muller et al., 2003; Pant et al., 2009; Prokic et al., 2014). In line with this, BIN1 overexpression counteracts defects observed by GoF mutations in DNM2 (Cowling et al., 2017; Lionello et al., 2022). This likely means that increased recycling rates counteract increased endocytosis rates caused by DNM2 hyperactivity. This rescue also works the other way round as BIN1 LoF mutations can be rescued by DNM2 depletion (Silva-Rojas et al., 2022). The discussed causes and treatment options for CNM are summarized in Table 11.

Table 14: Causes and treatment options for CNM

Cause of CNM	(Putative) effect on endosomal trafficking	Potential treatment
LoF mutations in MTM1	Defective endosomal recycling	Reduction of DNM2 levels, Depletion of PI3KC2β
LoF mutations in BIN1	Defective endosomal recycling	Reduction of DNM2 levels
GoF mutations in DNM2	Elevated endocytosis rates	Reduction of DNM2 levels, Overexpression of BIN1

The suggested mechanism also implies that the inhibition or depletion of PI3KC2β might be an effective treatment option for CNM caused by either GoF mutations in DNM2 or LoF mutations in BIN1.

5.3.4 PI3KC2β regulates active β1 integrin endocytosis and degradation

In this study, I show that PI3KC2β is required for proper active β1 integrin endocytosis. The depletion of PI3KC2β in HeLa cells or knock out in C2C12 cells drastically decreased active β1 integrin endocytosis and caused elevated active β1 integrin surface levels. Mechanistically, I show that PI3KC2β co-immunoprecipitates with the β1 integrin endocytosis adaptor Dab2 and the endocytic adaptor protein ITSN1. Interestingly, PI3KC2β only mildly affected transferrin endocytosis. This is in line with prior findings, that Dab2 is not required for transferrin endocytosis but only for β1 integrin endocytosis (Chao & Kunz, 2009; Teckchandani et al., 2012). We further provide evidence that PI3KC2β is also involved in determining the fate of endocytosed active β1 integrins. We show that PI3KC2β depletion in HeLa cells facilitates endocytic recycling and decreases lysosomal degradation. The depletion of PI3KC2β lead to increased β1 integrin levels in HeLa cells and β1 integrin turnover was significantly reduced. Along these lines, elevated active surface β1 integrin levels observed upon PI3KC2β depletion could be restored by blocking endosomal recycling by co-depletion of either MTM1 or Sec3 and Exo70, respectively. An interesting possibility is that PI3KC2β might directly regulate the fate of endocytosed active β1 integrins: PI3KC2β generates PI(3,4)P_2 during endocytosis which must lead to reduced PI(4)P levels. Thus, endocytosed cargo might be more likely targeted for degradation rather than recycling, as recycling requires PI(4)P. Furthermore, a loss of PI3KC2β has been shown to trigger the accumulation of APPL1 positive very early endosomes (Alliouachene et al., 2015) which are crucial for the fast recycling of endocytosed integrins (Broussard et al., 2012; Diggins, Kang, Weaver, & Webb, 2018). PI3KC2β might therefore regulate integrin fate through an APPL1 switch. This will be the subject of further studies.

5.3.5 PI3KC2β is required for focal adhesion disassembly

A recent study shows that PI3KC2β is also required for focal adhesion (FA) disassembly via RhoA inactivation through the PI(3,4)P_2 activated RhoA GAP ARAP3. This leads to the turnover of stress fibers and FA destabilization (Posor et al., 2022). On top of the destabilization, we show that PI3KC2β is also required for the endocytosis of active β1 integrins, an integral component of focal adhesions. The internalization of active β1 integrins was shown to be required for focal adhesion disassembly (Chao & Kunz, 2009; Ezratty et al., 2009). Interestingly, Posor et al. did not observe an effect of PI3KC2β depletion on total β1 integrin endocytosis. This discrepancy can be explained by the fact that about 80 % of surface localized β1 integrins are in the inactive conformation (Arjonen et al., 2012) and Posor et al. only investigated total β1 integrin endocytosis without testing for effects on active β1 integrins. In line with that we did not observe an increase of total β1 integrin surface levels in HeLa cells depleted of PI3KC2β (Figure 26 c) but only an increase in active β1 integrin surface levels (Figure 22 a, b). Since β1 integrins in focal adhesions are in the active conformation, they are also internalized in the active conformation upon focal adhesion disassembly (Arjonen et al., 2012). Thus, PI3KC2β seems to specifically act on the clathrin mediated endocytosis of active total β1 integrins but not on CME of inactive β1 integrins. Taken together, this promotes a model, where PI3KC2β generated PI(3,4)P_2 first leads to FA destabilization followed by internalization of active β1 integrins.

PI3KC2β might further be required for the delivery of matrix metalloproteases (MMPs) from Rab7A positive lysosomes (Chevalier et al., 2016; Frittoli, Palamidessi, Disanza, & Scita, 2011; Poincloux, Lizarraga, & Chavrier, 2009) since PI3KC2β is actively recruited to this compartment (Wallroth et al., 2019). MMPs are required for the initiation of focal adhesion disassembly as the release the integrin receptor from the extracellular matrix (Stehbens et al., 2014).

5.4 Pharmacological inhibition of PI3KC2β as a treatment in centronuclear myopathy

We show that pharmacological inhibition of PI3KC2β leads to elevated surface active β1 integrin levels in HeLa cells (this study) and rescues decreased active b1 integrin surface

levels in undifferentiated MTM1 KO C2C12 cells (Samsó et al., 2022). However, long term treatment of MTM1 KO C2C12 cells lead to cell toxicity and did not rescue myotube formation (data not shown). The used inhibitor only targets PI3KC2β as an off target and is mainly active against PI3KC2α. Thus, high concentrations were required to effectively target PI3KC2β. Novel inhibitors that specifically target PI3KC2β and can be used at lower concentrations, to minimize the risk of cytotoxicity, might be a valuable tool to rescue myotube formation in MTM1 KO C2C12 cells and serve as lead candidates for the development of a PI3KC2β based treatment option for MTM1 caused XLCNM and possibly also BIN1 or DNM2 caused CNM. The compound used in this study serves as a lead compound to develop these PI3KC2β specific inhibitors. With emerging structural information on class II PI3Ks, inhibitor development will be further facilitated (Lo, Zhang, et al., 2022).

6 Outlook

6.1 Recruitment of PI3KC2β to late endosomes, lysosomes, and the plasma membrane

Rab7A regulates a large spectrum of cellular functions and Rab7A activity is tightly regulated by GAPs and GEFs that are specific for a certain cellular process (Guerra & Bucci, 2016; Stroupe, 2018). We did not investigate which GEFs and GAPs are important for PI3KC2β recruitment. Understanding this is important as it is another layer of regulation of PI3KC2β activity. This will remain the focus of future studies.

While I do show that PI3KC2β preferentially co-immunoprecipitates with the active, GTP-locked form of Rab7A (Rab7A-Q67L), I did not assess if PI3KC2β directly binds to Rab7A. Therefore, in vitro binding assays with recombinant Rab7A and recombinant PI3KC2β would be required. Also, the exact binding mechanism would be of great interest as this was not described for any Class II PI3K so far. There is structural information on Class I PI3Ks and Ras binding (Pacold et al., 2000) but given the low conservation of the Class I PI3K ras-binding domain (RBD) and the Class II PI3K RBD the mode of binding is very likely to differ.

Furthermore, the role of the C-terminal PX and C2 domains of PI3KC2β has not been studied yet. As already described for PI3KC2α, these domains might be important regulators of PI3KC2β activity. In PI3KC2α, the PX and C2 domains fold back onto the kinase domain and inhibit the catalytic activity. For activation, PI3KC2α requires the PX and C2 domains to bind to PIP_2 at the plasma membrane and the n-terminus to bind clathrin. This causes a conformational change of the enzyme from a closed, catalytically less active to an open, catalytically active form (H. Wang et al., 2018). Given the overall quite conserved sequence of PI3KC2α and PI3KC2β (Koch et al., 2021), a similar mechanism of regulation seems plausible for PI3KC2β as well. In line with this, $PI(4,5)P_2$ is abundant at the plasma membrane and there also is a smaller pool on lysosomes (Ebner, Koch, & Haucke, 2019; Wallroth & Haucke, 2018). Thus, PI3KC2β could be activated by $PI(4,5)P_2$ at both compartments.

6.2 PI(3,4)P2 mediated inhibition of mTORC1 signaling

In this study I show that PI3KC2β is required for the association of PRAS40 with the mTORC1 subunit of Raptor. How PI3KC2β regulates PRAS40 localization however remains unclear. Further experiments will be needed to determine if PRAS40 is a $PI(3,4)P_2$ effector or if PI3KC2β regulates its regulation via a kinase independent scaffolding mechanism. Scaffolding functions have already been described for the closely related PI3KC2α that is required for the proper localization of TACC3 to the mitotic spindle (Gulluni et al., 2017). This is mediated by the helical bundle domain, a structural element exclusively found in class II PI 3-kinases (Lo, Zhang, et al., 2022).

Furthermore, it is unclear which proteins are influenced by late endosomal and lysosomal $PI(3,4)P_2$ produced by PI3KC2β upon growth factor starvation. Also, it will be interesting to test if processes apart from mTORC1 inhibition are affected by lysosomal $PI(3,4)P_2$. To identify new PI(3,4)P2 effector proteins, the manipulation of PI3KC2β or PKN2 to boost lysosomal $PI(3,4)P_2$ levels combined with proximity biotinylation might be a powerful tool.

6.3 How does PI3KC2β influence mTORC1 signaling?

So far, it is unclear which mTORC1 substrates are affected by PI3KC2β activity. A recently emerging field of study is the precise regulation of mTOR activity. It was long thought that mTORC1 is either active at the lysosomal surface or inactive in the cytoplasm (Napolitano, Di Malta, & Ballabio, 2022; Saxton & Sabatini, 2017). Recently, it was shown that Raptor is not required for the phosphorylation of all mTORC1 substrates but rather only for those containing a TOS motif. The mTORC1 mediated phosphorylation of TFEB for example, was independent of Raptor (and mTORC2 component Rictor) and only depended on the Ragulator complex. Ragulator in turn was only required for TFEB phosphorylation but not for the phosphorylation of classical Raptor dependent targets like P70 S6 kinase (Napolitano et al., 2020). Since PI3KC2β directly interacts with Raptor through its unstructured N-terminal domain and the raptor WD40 domain, it is tempting to speculate that PI3KC2β only affects Raptor dependent mTORC1 targets. Primary evidence for that was already provided by Marat

et al., as they showed that PI3KC2β depletion did lead to increased phospho P70 S6 kinase levels but did not alter the phosphorylation state of raptor independent ULK1 (Marat et al., 2017).

6.4 PI3KC2β regulates active β1 integrin trafficking

In this study, we show that PI3KC2β regulates active β1 integrin endocytosis in a PI(3,4)P_2 dependent manner, but we did not investigate which proteins are affected by PI(3,4)P_2. Further studies will aim to identify the effector of PI(3,4)P_2 required for active β1 integrin endocytosis. Good candidates are SNX9 and FCHDS2 that are known endocytic effectors of PI(3,4)P_2 and act downstream of PI3KC2α (Almeida-Souza et al., 2018; Feng & Yu, 2021; Posor et al., 2013).

We also show evidence that PI3KC2β inhibits endocytic recycling of active β1 integrins and promotes active β1 integrin degradation. How this occurs will be the subject of further studies.

7 References

Alexandrov, K., Horiuchi, H., Steele-Mortimer, O., Seabra, M. C., & Zerial, M. (1994). Rab escort protein-1 is a multifunctional protein that accompanies newly prenylated rab proteins to their target membranes. *The EMBO Journal, 13*(22), 5262-5273. doi:10.1002/j.1460-2075.1994.tb06860.x

Alexandrov, K., Simon, I., Yurchenko, V., Iakovenko, A., Rostkova, E., Scheidig, A. J., & Goody, R. S. (1999). Characterization of the ternary complex between Rab7, REP-1 and Rab geranylgeranyl transferase. *Eur J Biochem, 265*(1), 160-170. doi:10.1046/j.1432-1327.1999.00699.x

Alliouachene, S., Bilanges, B., Chicanne, G., Anderson, K. E., Pearce, W., Ali, K., . . . Vanhaesebroeck, B. (2015). Inactivation of the Class II PI3K-C2beta Potentiates Insulin Signaling and Sensitivity. *Cell Rep, 13*(9), 1881-1894. doi:10.1016/j.celrep.2015.10.052

Almeida-Souza, L., Frank, R. A. W., Garcia-Nafria, J., Colussi, A., Gunawardana, N., Johnson, C. M., . . . McMahon, H. T. (2018). A Flat BAR Protein Promotes Actin Polymerization at the Base of Clathrin-Coated Pits. *Cell, 174*(2), 325-337 e314. doi:10.1016/j.cell.2018.05.020

Amoasii, L., Hnia, K., & Laporte, J. (2012). Myotubularin phosphoinositide phosphatases in human diseases. *Curr Top Microbiol Immunol, 362*, 209-233. doi:10.1007/978-94-007-5025-8_10

Antonny, B., Burd, C., De Camilli, P., Chen, E., Daumke, O., Faelber, K., . . . Schmid, S. (2016). Membrane fission by dynamin: what we know and what we need to know. *EMBO J, 35*(21), 2270-2284. doi:10.15252/embj.201694613

Arcaro, A., Zvelebil, M. J., Wallasch, C., Ullrich, A., Waterfield, M. D., & Domin, J. (2000). Class II phosphoinositide 3-kinases are downstream targets of activated polypeptide growth factor receptors. *Mol Cell Biol, 20*(11), 3817-3830. doi:10.1128/mcb.20.11.3817-3830.2000

Arjonen, A., Alanko, J., Veltel, S., & Ivaska, J. (2012). Distinct recycling of active and inactive beta1 integrins. *Traffic, 13*(4), 610-625. doi:10.1111/j.1600-0854.2012.01327.x

Askari, J. A., Buckley, P. A., Mould, A. P., & Humphries, M. J. (2009). Linking integrin conformation to function. *J Cell Sci, 122*(Pt 2), 165-170. doi:10.1242/jcs.018556

Auger, K. R., Serunian, L. A., Soltoff, S. P., Libby, P., & Cantley, L. C. (1989). PDGF-dependent tyrosine phosphorylation stimulates production of novel polyphosphoinositides in intact cells. *Cell, 57*(1), 167-175. doi:10.1016/0092-8674(89)90182-7

Aung, K. T., Yoshioka, K., Aki, S., Ishimaru, K., Takuwa, N., & Takuwa, Y. (2019). The class II phosphoinositide 3-kinases PI3K-C2alpha and PI3K-C2beta differentially regulate clathrin-dependent pinocytosis in human vascular endothelial cells. *J Physiol Sci, 69*(2), 263-280. doi:10.1007/s12576-018-0644-2

Axe, E. L., Walker, S. A., Manifava, M., Chandra, P., Roderick, H. L., Habermann, A., . . . Ktistakis, N. T. (2008). Autophagosome formation from membrane compartments enriched in phosphatidylinositol 3-phosphate and dynamically connected to the endoplasmic reticulum. *Journal of Cell Biology, 182*(4), 685-701. doi:10.1083/jcb.200803137

Bache, K. G., Brech, A., Mehlum, A., & Stenmark, H. (2003). Hrs regulates multivesicular body formation via ESCRT recruitment to endosomes. *J Cell Biol, 162*(3), 435-442. doi:10.1083/jcb.200302131

Balla, T. (2013). Phosphoinositides: tiny lipids with giant impact on cell regulation. *Physiol Rev, 93*(3), 1019-1137. doi:10.1152/physrev.00028.2012

Bar-Peled, L., Chantranupong, L., Cherniack, A. D., Chen, W. W., Ottina, K. A., Grabiner, B. C., . . . Sabatini, D. M. (2013). A Tumor suppressor complex with GAP activity for the Rag GTPases that signal amino acid sufficiency to mTORC1. *Science, 340*(6136), 1100-1106. doi:10.1126/science.1232044

Barylko, B., Mao, Y. S., Wlodarski, P., Jung, G., Binns, D. D., Sun, H. Q., . . . Albanesi, J. P. (2009). Palmitoylation controls the catalytic activity and subcellular distribution of phosphatidylinositol 4-kinase II{alpha}. *J Biol Chem, 284*(15), 9994-10003. doi:10.1074/jbc.M900724200

Baskaran, S., Carlson, L. A., Stjepanovic, G., Young, L. N., Kim, D. J., Grob, P., . . . Hurley, J. H. (2014). Architecture and dynamics of the autophagic phosphatidylinositol 3-kinase complex. *Elife, 3*. doi:10.7554/eLife.05115

Bi, P., Ramirez-Martinez, A., Li, H., Cannavino, J., McAnally, J. R., Shelton, J. M., . . . Olson, E. N. (2017). Control of muscle formation by the fusogenic micropeptide myomixer. *Science, 356*(6335), 323-327. doi:10.1126/science.aam9361

Biancalana, V., Caron, O., Gallati, S., Baas, F., Kress, W., Novelli, G., . . . Mandel, J. L. (2003). Characterisation of mutations in 77 patients with X-linked myotubular myopathy, including a family with a very mild phenotype. *Hum Genet, 112*(2), 135-142. doi:10.1007/s00439-002-0869-1

Bilanges, B., Posor, Y., & Vanhaesebroeck, B. (2019). PI3K isoforms in cell signalling and vesicle trafficking. *Nat Rev Mol Cell Biol, 20*(9), 515-534. doi:10.1038/s41580-019-0129-z

Bitoun, M., Maugenre, S., Jeannet, P. Y., Lacene, E., Ferrer, X., Laforet, P., . . . Guicheney, P. (2005). Mutations in dynamin 2 cause dominant centronuclear myopathy. *Nat Genet, 37*(11), 1207-1209. doi:10.1038/ng1657

Boller, D., Doepfner, K. T., De Laurentiis, A., Guerreiro, A. S., Marinov, M., Shalaby, T., . . . Arcaro, A. (2012). Targeting PI3KC2beta impairs proliferation and survival in acute leukemia, brain tumours and neuroendocrine tumours. *Anticancer Res, 32*(8), 3015-3027.

Bondeva, T., Pirola, L., Bulgarelli-Leva, G., Rubio, I., Wetzker, R., & Wymann, M. P. (1998). Bifurcation of lipid and protein kinase signals of PI3Kgamma to the protein kinases PKB and MAPK. *Science, 282*(5387), 293-296. doi:10.1126/science.282.5387.293

Bottcher, R. T., Stremmel, C., Meves, A., Meyer, H., Widmaier, M., Tseng, H. Y., & Fassler, R. (2012). Sorting nexin 17 prevents lysosomal degradation of beta1 integrins by binding to the beta1-integrin tail. *Nat Cell Biol, 14*(6), 584-592. doi:10.1038/ncb2501

Boura, E., & Nencka, R. (2015). Phosphatidylinositol 4-kinases: Function, structure, and inhibition. *Exp Cell Res, 337*(2), 136-145. doi:10.1016/j.yexcr.2015.03.028

Braccini, L., Ciraolo, E., Campa, C. C., Perino, A., Longo, D. L., Tibolla, G., . . . Hirsch, E. (2015). PI3K-C2gamma is a Rab5 effector selectively controlling endosomal Akt2 activation downstream of insulin signalling. *Nat Commun, 6*, 7400. doi:10.1038/ncomms8400

Broussard, J. A., Lin, W. H., Majumdar, D., Anderson, B., Eason, B., Brown, C. M., & Webb, D. J. (2012). The endosomal adaptor protein APPL1 impairs the turnover of leading edge adhesions to regulate cell migration. *Mol Biol Cell, 23*(8), 1486-1499. doi:10.1091/mbc.E11-02-0124

Brown, J. R., & Auger, K. R. (2011). Phylogenomics of phosphoinositide lipid kinases: perspectives on the evolution of second messenger signaling and drug discovery. *BMC Evol Biol, 11*, 4. doi:10.1186/1471-2148-11-4

Buckles, T. C., Ziemba, B. P., Masson, G. R., Williams, R. L., & Falke, J. J. (2017). Single-Molecule Study Reveals How Receptor and Ras Synergistically Activate PI3Kalpha and PIP3 Signaling. *Biophys J, 113*(11), 2396-2405. doi:10.1016/j.bpj.2017.09.018

Buono, S., Ross, J. A., Tasfaout, H., Levy, Y., Kretz, C., Tayefeh, L., . . . Cowling, B. S. (2018). Reducing dynamin 2 (DNM2) rescues DNM2-related dominant centronuclear myopathy. *Proc Natl Acad Sci U S A, 115*(43), 11066-11071. doi:10.1073/pnas.1808170115

Burke, J. E. (2018). Structural Basis for Regulation of Phosphoinositide Kinases and Their Involvement in Human Disease. *Mol Cell, 71*(5), 653-673. doi:10.1016/j.molcel.2018.08.005

Burke, J. E., Inglis, A. J., Perisic, O., Masson, G. R., McLaughlin, S. H., Rutaganira, F., . . . Williams, R. L. (2014). Structures of PI4KIIIbeta complexes show simultaneous recruitment of Rab11 and its effectors. *Science, 344*(6187), 1035-1038. doi:10.1126/science.1253397

Cabrera, M., Nordmann, M., Perz, A., Schmedt, D., Gerondopoulos, A., Barr, F., . . . Ungermann, C. (2014). The Mon1-Ccz1 GEF activates the Rab7 GTPase Ypt7 via a longin-fold-Rab interface and association with PI3P-positive membranes. *J Cell Sci, 127*(Pt 5), 1043-1051. doi:10.1242/jcs.140921

Calderwood, D. A., Campbell, I. D., & Critchley, D. R. (2013). Talins and kindlins: partners in integrin-mediated adhesion. *Nat Rev Mol Cell Biol, 14*(8), 503-517. doi:10.1038/nrm3624

Campa, C. C., Margaria, J. P., Derle, A., Del Giudice, M., De Santis, M. C., Gozzelino, L., . . . Hirsch, E. (2018). Rab11 activity and PtdIns(3)P turnover removes recycling cargo from endosomes. *Nat Chem Biol, 14*(8), 801-810. doi:10.1038/s41589-018-0086-4

Castellano, B. M., Thelen, A. M., Moldavski, O., Feltes, M., van der Welle, R. E., Mydock-McGrane, L., . . . Zoncu, R. (2017). Lysosomal cholesterol activates mTORC1 via an SLC38A9-Niemann-Pick C1 signaling complex. *Science, 355*(6331), 1306-1311. doi:10.1126/science.aag1417

Chao, W. T., & Kunz, J. (2009). Focal adhesion disassembly requires clathrin-dependent endocytosis of integrins. *FEBS Lett, 583*(8), 1337-1343. doi:10.1016/j.febslet.2009.03.037

Chen, K. E., Tillu, V. A., Chandra, M., & Collins, B. M. (2018). Molecular Basis for Membrane Recruitment by the PX and C2 Domains of Class II Phosphoinositide 3-Kinase-C2alpha. *Structure, 26*(12), 1612-1625 e1614. doi:10.1016/j.str.2018.08.010

Cherfils, J., & Zeghouf, M. (2013). Regulation of small GTPases by GEFs, GAPs, and GDIs. *Physiol Rev, 93*(1), 269-309. doi:10.1152/physrev.00003.2012

Chevalier, C., Collin, G., Descamps, S., Touaitahuata, H., Simon, V., Reymond, N., . . . Benistant, C. (2016). TOM1L1 drives membrane delivery of MT1-MMP to promote ERBB2-induced breast cancer cell invasion. *Nat Commun, 7*, 10765. doi:10.1038/ncomms10765

Chikh, A., Ferro, R., Abbott, J. J., Pineiro, R., Buus, R., Iezzi, M., . . . Falasca, M. (2016). Class II phosphoinositide 3-kinase C2beta regulates a novel signaling pathway involved in breast cancer progression. *Oncotarget, 7*(14), 18325-18345. doi:10.18632/oncotarget.7761

Chinthalapudi, K., Rangarajan, E. S., & Izard, T. (2018). The interaction of talin with the cell membrane is essential for integrin activation and focal adhesion formation. *Proc Natl Acad Sci U S A, 115*(41), 10339-10344. doi:10.1073/pnas.1806275115

Christoforidis, S., Miaczynska, M., Ashman, K., Wilm, M., Zhao, L., Yip, S. C., . . . Zerial, M. (1999). Phosphatidylinositol-3-OH kinases are Rab5 effectors. *Nat Cell Biol, 1*(4), 249-252. doi:10.1038/12075

Cowling, B. S., Chevremont, T., Prokic, I., Kretz, C., Ferry, A., Coirault, C., . . . Laporte, J. (2014). Reducing dynamin 2 expression rescues X-linked centronuclear myopathy. *J Clin Invest, 124*(3), 1350-1363. doi:10.1172/JCI71206

Cowling, B. S., Prokic, I., Tasfaout, H., Rabai, A., Humbert, F., Rinaldi, B., . . . Laporte, J. (2017). Amphiphysin (BIN1) negatively regulates dynamin 2 for normal muscle maturation. *J Clin Invest, 127*(12), 4477-4487. doi:10.1172/JCI90542

Cullen, P. J. (2008). Endosomal sorting and signalling: an emerging role for sorting nexins. *Nat Rev Mol Cell Biol, 9*(7), 574-582. doi:10.1038/nrm2427

Cullen, P. J., & Steinberg, F. (2018). To degrade or not to degrade: mechanisms and significance of endocytic recycling. *Nat Rev Mol Cell Biol, 19*(11), 679-696. doi:10.1038/s41580-018-0053-7

D'Souza, R. S., Lim, J. Y., Turgut, A., Servage, K., Zhang, J., Orth, K., . . . Casanova, J. E. (2020). Calcium-stimulated disassembly of focal adhesions mediated by an ORP3/IQSec1 complex. *Elife, 9*. doi:10.7554/eLife.54113

Das, M., Scappini, E., Martin, N. P., Wong, K. A., Dunn, S., Chen, Y. J., . . . O'Bryan, J. P. (2007). Regulation of neuron survival through an intersectin-phosphoinositide 3'-kinase C2beta-AKT pathway. *Mol Cell Biol, 27*(22), 7906-7917. doi:10.1128/MCB.01369-07

Devereaux, K., Dall'Armi, C., Alcazar-Roman, A., Ogasawara, Y., Zhou, X., Wang, F., . . . Di Paolo, G. (2013). Regulation of mammalian autophagy by class II and III PI 3-kinases through PI3P synthesis. *PLoS One, 8*(10), e76405. doi:10.1371/journal.pone.0076405

Diggins, N. L., Kang, H., Weaver, A., & Webb, D. J. (2018). alpha5beta1 integrin trafficking and Rac activation are regulated by APPL1 in a Rab5-dependent manner to inhibit cell migration. *J Cell Sci, 131*(5). doi:10.1242/jcs.207019

Domin, J., Harper, L., Aubyn, D., Wheeler, M., Florey, O., Haskard, D., . . . Zicha, D. (2005). The class II phosphoinositide 3-kinase PI3K-C2beta regulates cell migration by a PtdIns3P dependent mechanism. *J Cell Physiol, 205*(3), 452-462. doi:10.1002/jcp.20478

Dong, J., Du, X., Wang, H., Wang, J., Lu, C., Chen, X., . . . Wu, J. W. (2019). Allosteric enhancement of ORP1-mediated cholesterol transport by PI(4,5)P2/PI(3,4)P2. *Nat Commun, 10*(1), 829. doi:10.1038/s41467-019-08791-0

Dowling, J. J., Vreede, A. P., Low, S. E., Gibbs, E. M., Kuwada, J. Y., Bonnemann, C. G., & Feldman, E. L. (2009). Loss of myotubularin function results in T-tubule disorganization in zebrafish and human myotubular myopathy. *PLoS Genet, 5*(2), e1000372. doi:10.1371/journal.pgen.1000372

Ebner, M., Koch, P. A., & Haucke, V. (2019). Phosphoinositides in the control of lysosome function and homeostasis. *Biochem Soc Trans, 47*(4), 1173-1185. doi:10.1042/BST20190158

Elkin, S. R., Lakoduk, A. M., & Schmid, S. L. (2016). Endocytic pathways and endosomal trafficking: a primer. *Wien Med Wochenschr, 166*(7-8), 196-204. doi:10.1007/s10354-016-0432-7

Erdmann, K. S., Mao, Y., McCrea, H. J., Zoncu, R., Lee, S., Paradise, S., . . . De Camilli, P. (2007). A role of the Lowe syndrome protein OCRL in early steps of the endocytic pathway. *Dev Cell, 13*(3), 377-390. doi:10.1016/j.devcel.2007.08.004

Ezratty, E. J., Bertaux, C., Marcantonio, E. E., & Gundersen, G. G. (2009). Clathrin mediates integrin endocytosis for focal adhesion disassembly in migrating cells. *J Cell Biol, 187*(5), 733-747. doi:10.1083/jcb.200904054

Falkenburger, B. H., Jensen, J. B., Dickson, E. J., Suh, B. C., & Hille, B. (2010). Phosphoinositides: lipid regulators of membrane proteins. *J Physiol, 588*(Pt 17), 3179-3185. doi:10.1113/jphysiol.2010.192153

Feng, Z., & Yu, C. H. (2021). PI(3,4)P2-mediated membrane tubulation promotes integrin trafficking and invasive cell migration. *Proc Natl Acad Sci U S A, 118*(19). doi:10.1073/pnas.2017645118

Ferguson, S. M., & De Camilli, P. (2012). Dynamin, a membrane-remodelling GTPase. *Nat Rev Mol Cell Biol, 13*(2), 75-88. doi:10.1038/nrm3266

Flynn, P., Mellor, H., Casamassima, A., & Parker, P. J. (2000). Rho GTPase control of protein kinase C-related protein kinase activation by 3-phosphoinositide-dependent protein kinase. *J Biol Chem, 275*(15), 11064-11070. doi:10.1074/jbc.275.15.11064

Franco, I., Gulluni, F., Campa, C. C., Costa, C., Margaria, J. P., Ciraolo, E., . . . Hirsch, E. (2014). PI3K class II alpha controls spatially restricted endosomal PtdIns3P and Rab11 activation to promote primary cilium function. *Dev Cell, 28*(6), 647-658. doi:10.1016/j.devcel.2014.01.022

Franco, I., Margaria, J. P., De Santis, M. C., Ranghino, A., Monteyne, D., Chiaravalli, M., . . . Hirsch, E. (2016). Phosphoinositide 3-Kinase-C2alpha Regulates Polycystin-2 Ciliary Entry and Protects against Kidney Cyst Formation. *J Am Soc Nephrol, 27*(4), 1135-1144. doi:10.1681/ASN.2014100967

Frittoli, E., Palamidessi, A., Disanza, A., & Scita, G. (2011). Secretory and endo/exocytic trafficking in invadopodia formation: the MT1-MMP paradigm. *Eur J Cell Biol, 90*(2-3), 108-114. doi:10.1016/j.ejcb.2010.04.007

Gaidarov, I., Smith, M. E. K., Domin, J., & Keen, J. H. (2001). The Class II Phosphoinositide 3-Kinase C2α Is Activated by Clathrin and Regulates Clathrin-Mediated Membrane Trafficking. *Molecular Cell, 7*(2), 443-449. doi:10.1016/s1097-2765(01)00191-5

Garami, A., Zwartkruis, F. J. T., Nobukuni, T., Joaquin, M., Roccio, M., Stocker, H., . . . Thomas, G. (2003). Insulin Activation of Rheb, a Mediator of mTOR/S6K/4E-BP Signaling, Is Inhibited by TSC1 and 2. *Molecular Cell, 11*(6), 1457-1466. doi:10.1016/s1097-2765(03)00220-x

Girardi, F., Taleb, A., Ebrahimi, M., Datye, A., Gamage, D. G., Peccate, C., . . . Le Grand, F. (2021). TGFbeta signaling curbs cell fusion and muscle regeneration. *Nat Commun, 12*(1), 750. doi:10.1038/s41467-020-20289-8

Gomez-Oca, R., Cowling, B. S., & Laporte, J. (2021). Common Pathogenic Mechanisms in Centronuclear and Myotubular Myopathies and Latest Treatment Advances. *Int J Mol Sci, 22*(21). doi:10.3390/ijms222111377

Goody, R. S., Rak, A., & Alexandrov, K. (2005). The structural and mechanistic basis for recycling of Rab proteins between membrane compartments. *Cell Mol Life Sci, 62*(15), 1657-1670. doi:10.1007/s00018-005-4486-8

Gozzelino, L., Kochlamazashvili, G., Baldassari, S., Mackintosh, A. I., Licchetta, L., Iovino, E., . . . Pippucci, T. (2022). Defective lipid signalling caused by mutations in PIK3C2B underlies focal epilepsy. *Brain, 145*(7), 2313-2331. doi:10.1093/brain/awac082

Grant, B. D., & Donaldson, J. G. (2009). Pathways and mechanisms of endocytic recycling. *Nat Rev Mol Cell Biol, 10*(9), 597-608. doi:10.1038/nrm2755

Griffin, C. A., Kafadar, K. A., & Pavlath, G. K. (2009). MOR23 promotes muscle regeneration and regulates cell adhesion and migration. *Dev Cell, 17*(5), 649-661. doi:10.1016/j.devcel.2009.09.004

Grimmel, M., Backhaus, C., & Proikas-Cezanne, T. (2015). WIPI-Mediated Autophagy and Longevity. *Cells, 4*(2), 202-217. doi:10.3390/cells4020202

Guerra, F., & Bucci, C. (2016). Multiple Roles of the Small GTPase Rab7. *Cells, 5*(3). doi:10.3390/cells5030034

Gulluni, F., Martini, M., De Santis, M. C., Campa, C. C., Ghigo, A., Margaria, J. P., . . . Hirsch, E. (2017). Mitotic Spindle Assembly and Genomic Stability in Breast Cancer Require PI3K-C2alpha Scaffolding Function. *Cancer Cell, 32*(4), 444-459 e447. doi:10.1016/j.ccell.2017.09.002

Gutierrez, M. G., Munafo, D. B., Beron, W., & Colombo, M. I. (2004). Rab7 is required for the normal progression of the autophagic pathway in mammalian cells. *J Cell Sci, 117*(Pt 13), 2687-2697. doi:10.1242/jcs.01114

Hasegawa, J., Strunk, B. S., & Weisman, L. S. (2017). PI5P and PI(3,5)P2: Minor, but Essential Phosphoinositides. *Cell Struct Funct, 42*(1), 49-60. doi:10.1247/csf.17003

Hnia, K., Vaccari, I., Bolino, A., & Laporte, J. (2012). Myotubularin phosphoinositide phosphatases: cellular functions and disease pathophysiology. *Trends Mol Med, 18*(6), 317-327. doi:10.1016/j.molmed.2012.04.004

Homma, Y., Hiragi, S., & Fukuda, M. (2021). Rab family of small GTPases: an updated view on their regulation and functions. *FEBS J, 288*(1), 36-55. doi:10.1111/febs.15453

Hong, Z., Pedersen, N. M., Wang, L., Torgersen, M. L., Stenmark, H., & Raiborg, C. (2017). PtdIns3P controls mTORC1 signaling through lysosomal positioning. *J Cell Biol, 216*(12), 4217-4233. doi:10.1083/jcb.201611073

Hurley, J. H. (2015). ESCRTs are everywhere. *EMBO J, 34*(19), 2398-2407. doi:10.15252/embj.201592484

Huttenlocher, A., & Horwitz, A. R. (2011). Integrins in cell migration. *Cold Spring Harb Perspect Biol, 3*(9), a005074. doi:10.1101/cshperspect.a005074

Hwang, Y., Kim, L. C., Song, W., Edwards, D. N., Cook, R. S., & Chen, J. (2019). Disruption of the Scaffolding Function of mLST8 Selectively Inhibits mTORC2 Assembly and Function and Suppresses mTORC2-Dependent Tumor Growth In Vivo. *Cancer Res, 79*(13), 3178-3184. doi:10.1158/0008-5472.CAN-18-3658

Inoki, K., Li, Y., Xu, T., & Guan, K. L. (2003). Rheb GTPase is a direct target of TSC2 GAP activity and regulates mTOR signaling. *Genes Dev, 17*(15), 1829-1834. doi:10.1101/gad.1110003

Irannejad, R., Tsvetanova, N. G., Lobingier, B. T., & von Zastrow, M. (2015). Effects of endocytosis on receptor-mediated signaling. *Curr Opin Cell Biol, 35*, 137-143. doi:10.1016/j.ceb.2015.05.005

Jaber, N., Dou, Z., Chen, J. S., Catanzaro, J., Jiang, Y. P., Ballou, L. M., . . . Zong, W. X. (2012). Class III PI3K Vps34 plays an essential role in autophagy and in heart and liver function. *Proc Natl Acad Sci U S A, 109*(6), 2003-2008. doi:10.1073/pnas.1112848109

Jager, S., Bucci, C., Tanida, I., Ueno, T., Kominami, E., Saftig, P., & Eskelinen, E. L. (2004). Role for Rab7 in maturation of late autophagic vacuoles. *J Cell Sci, 117*(Pt 20), 4837-4848. doi:10.1242/jcs.01370

Kadlecova, Z., Spielman, S. J., Loerke, D., Mohanakrishnan, A., Reed, D. K., & Schmid, S. L. (2017). Regulation of clathrin-mediated endocytosis by hierarchical allosteric activation of AP2. *J Cell Biol, 216*(1), 167-179. doi:10.1083/jcb.201608071

Kaksonen, M., & Roux, A. (2018). Mechanisms of clathrin-mediated endocytosis. *Nat Rev Mol Cell Biol, 19*(5), 313-326. doi:10.1038/nrm.2017.132

Katso, R. M., Pardo, O. E., Palamidessi, A., Franz, C. M., Marinov, M., De Laurentiis, A., . . . Arcaro, A. (2006). Phosphoinositide 3-Kinase C2beta regulates cytoskeletal organization and cell migration via Rac-dependent mechanisms. *Mol Biol Cell, 17*(9), 3729-3744. doi:10.1091/mbc.e05-11-1083

Kaufmann, U., Kirsch, J., Irintchev, A., Wernig, A., & Starzinski-Powitz, A. (1999). The M-cadherin catenin complex interacts with microtubules in skeletal muscle cells: implications for the fusion of myoblasts. *J Cell Sci, 112 (Pt 1)*, 55-68. doi:10.1242/jcs.112.1.55

Ketel, K., Krauss, M., Nicot, A. S., Puchkov, D., Wieffer, M., Muller, R., . . . Haucke, V. (2016). A phosphoinositide conversion mechanism for exit from endosomes. *Nature, 529*(7586), 408-412. doi:10.1038/nature16516

Kim, E., Goraksha-Hicks, P., Li, L., Neufeld, T. P., & Guan, K. L. (2008). Regulation of TORC1 by Rag GTPases in nutrient response. *Nat Cell Biol, 10*(8), 935-945. doi:10.1038/ncb1753

Kitatani, K., Usui, T., Sriraman, S. K., Toyoshima, M., Ishibashi, M., Shigeta, S., . . . Yaegashi, N. (2016). Ceramide limits phosphatidylinositol-3-kinase C2beta-controlled cell motility in ovarian cancer: potential of ceramide as a metastasis-suppressor lipid. *Oncogene, 35*(21), 2801-2812. doi:10.1038/onc.2015.330

Klima, M., Toth, D. J., Hexnerova, R., Baumlova, A., Chalupska, D., Tykvart, J., . . . Boura, E. (2016). Structural insights and in vitro reconstitution of membrane targeting and activation of human PI4KB by the ACBD3 protein. *Sci Rep, 6*, 23641. doi:10.1038/srep23641

Koch, P. A., Dornan, G. L., Hessenberger, M., & Haucke, V. (2021). The molecular mechanisms mediating class II PI 3-kinase function in cell physiology. *FEBS J, 288*(24), 7025-7042. doi:10.1111/febs.15692

Laporte, J., Hu, L. J., Kretz, C., Mandel, J. L., Kioschis, P., Coy, J. F., . . . Dahl, N. (1996). A gene mutated in X-linked myotubular myopathy defines a new putative tyrosine phosphatase family conserved in yeast. *Nat Genet, 13*(2), 175-182. doi:10.1038/ng0696-175

Lawlor, M. W., & Dowling, J. J. (2021). X-linked myotubular myopathy. *Neuromuscul Disord, 31*(10), 1004-1012. doi:10.1016/j.nmd.2021.08.003

Lee, M. Y., Skoura, A., Park, E. J., Landskroner-Eiger, S., Jozsef, L., Luciano, A. K., . . . Sessa, W. C. (2014). Dynamin 2 regulation of integrin endocytosis, but not VEGF signaling, is crucial for developmental angiogenesis. *Development, 141*(7), 1465-1472. doi:10.1242/dev.104539

Lehka, L., & Redowicz, M. J. (2020). Mechanisms regulating myoblast fusion: A multilevel interplay. *Semin Cell Dev Biol, 104*, 81-92. doi:10.1016/j.semcdb.2020.02.004

Li, L., Kim, E., Yuan, H., Inoki, K., Goraksha-Hicks, P., Schiesher, R. L., . . . Guan, K. L. (2010). Regulation of mTORC1 by the Rab and Arf GTPases. *J Biol Chem, 285*(26), 19705-19709. doi:10.1074/jbc.C110.102483

Lim, C. Y., Davis, O. B., Shin, H. R., Zhang, J., Berdan, C. A., Jiang, X., . . . Zoncu, R. (2019). ER-lysosome contacts enable cholesterol sensing by mTORC1 and drive aberrant growth signalling in Niemann-Pick type C. *Nat Cell Biol, 21*(10), 1206-1218. doi:10.1038/s41556-019-0391-5

Lionello, V. M., Kretz, C., Edelweiss, E., Crucifix, C., Gomez-Oca, R., Messaddeq, N., . . . Laporte, J. (2022). BIN1 modulation in vivo rescues dynamin-related myopathy. *Proc Natl Acad Sci U S A, 119*(9). doi:10.1073/pnas.2109576119

Liu, G. Y., & Sabatini, D. M. (2020). mTOR at the nexus of nutrition, growth, ageing and disease. *Nat Rev Mol Cell Biol, 21*(4), 183-203. doi:10.1038/s41580-019-0199-y

Liu, L., Song, X., He, D., Komma, C., Kita, A., Virbasius, J. V., . . . Zhou, G. W. (2006). Crystal structure of the C2 domain of class II phosphatidylinositide 3-kinase C2alpha. *J Biol Chem, 281*(7), 4254-4260. doi:10.1074/jbc.M510791200

Lo, W. T., Belabed, H., Kucukdisli, M., Metag, J., Roske, Y., Prokofeva, P., . . . Haucke, V. (2022). Development of selective inhibitors of phosphatidylinositol 3-kinase C2alpha. *Nat Chem Biol*. doi:10.1038/s41589-022-01118-z

Lo, W. T., Zhang, Y., Vadas, O., Roske, Y., Gulluni, F., De Santis, M. C., . . . Haucke, V. (2022). Structural basis of phosphatidylinositol 3-kinase C2alpha function. *Nat Struct Mol Biol, 29*(3), 218-228. doi:10.1038/s41594-022-00730-w

Long, X., Lin, Y., Ortiz-Vega, S., Yonezawa, K., & Avruch, J. (2005). Rheb binds and regulates the mTOR kinase. *Curr Biol, 15*(8), 702-713. doi:10.1016/j.cub.2005.02.053

Ma, L., Chen, Z., Erdjument-Bromage, H., Tempst, P., & Pandolfi, P. P. (2005). Phosphorylation and functional inactivation of TSC2 by Erk implications for tuberous sclerosis and cancer pathogenesis. *Cell, 121*(2), 179-193. doi:10.1016/j.cell.2005.02.031

Mandal, K. (2020). Review of PIP2 in Cellular Signaling, Functions and Diseases. *Int J Mol Sci, 21*(21). doi:10.3390/ijms21218342

Manning, B. D., Tee, A. R., Logsdon, M. N., Blenis, J., & Cantley, L. C. (2002). Identification of the Tuberous Sclerosis Complex-2 Tumor Suppressor Gene Product Tuberin as a Target of the Phosphoinositide 3-Kinase/Akt Pathway. *Molecular Cell, 10*(1), 151-162. doi:10.1016/s1097-2765(02)00568-3

Marat, A. L., Wallroth, A., Lo, W. T., Muller, R., Norata, G. D., Falasca, M., . . . Haucke, V. (2017). mTORC1 activity repression by late endosomal phosphatidylinositol 3,4-bisphosphate. *Science, 356*(6341), 968-972. doi:10.1126/science.aaf8310

Mavrommati, I., Cisse, O., Falasca, M., & Maffucci, T. (2016). Novel roles for class II Phosphoinositide 3-Kinase C2beta in signalling pathways involved in prostate cancer cell invasion. *Sci Rep, 6*, 23277. doi:10.1038/srep23277

McMahon, H. T., & Boucrot, E. (2011). Molecular mechanism and physiological functions of clathrin-mediated endocytosis. *Nat Rev Mol Cell Biol, 12*(8), 517-533. doi:10.1038/nrm3151

Mettlen, M., Chen, P. H., Srinivasan, S., Danuser, G., & Schmid, S. L. (2018). Regulation of Clathrin-Mediated Endocytosis. *Annu Rev Biochem, 87*, 871-896. doi:10.1146/annurev-biochem-062917-012644

Millay, D. P., O'Rourke, J. R., Sutherland, L. B., Bezprozvannaya, S., Shelton, J. M., Bassel-Duby, R., & Olson, E. N. (2013). Myomaker is a membrane activator of myoblast fusion and muscle formation. *Nature, 499*(7458), 301-305. doi:10.1038/nature12343

Miller, M. S., Schmidt-Kittler, O., Bolduc, D. M., Brower, E. T., Chaves-Moreira, D., Allaire, M., . . . Gabelli, S. B. (2014). Structural basis of nSH2 regulation and lipid binding in PI3Kalpha. *Oncotarget, 5*(14), 5198-5208. doi:10.18632/oncotarget.2263

Mishra, Y. G., & Manavathi, B. (2021). Focal adhesion dynamics in cellular function and disease. *Cell Signal, 85*, 110046. doi:10.1016/j.cellsig.2021.110046

Mizuno-Yamasaki, E., Medkova, M., Coleman, J., & Novick, P. (2010). Phosphatidylinositol 4-phosphate controls both membrane recruitment and a regulatory switch of the Rab GEF Sec2p. *Dev Cell, 18*(5), 828-840. doi:10.1016/j.devcel.2010.03.016

Moreno-Layseca, P., Icha, J., Hamidi, H., & Ivaska, J. (2019). Integrin trafficking in cells and tissues. *Nat Cell Biol, 21*(2), 122-132. doi:10.1038/s41556-018-0223-z

Mukund, K., & Subramaniam, S. (2020). Skeletal muscle: A review of molecular structure and function, in health and disease. *Wiley Interdiscip Rev Syst Biol Med, 12*(1), e1462. doi:10.1002/wsbm.1462

Muller, A. J., Baker, J. F., DuHadaway, J. B., Ge, K., Farmer, G., Donover, P. S., . . . Prendergast, G. C. (2003). Targeted disruption of the murine Bin1/Amphiphysin II gene does not disable endocytosis but results in embryonic cardiomyopathy with aberrant myofibril formation. *Mol Cell Biol, 23*(12), 4295-4306. doi:10.1128/MCB.23.12.4295-4306.2003

Muller, M. P., & Goody, R. S. (2018). Molecular control of Rab activity by GEFs, GAPs and GDI. *Small GTPases, 9*(1-2), 5-21. doi:10.1080/21541248.2016.1276999

Murray, J. T., Panaretou, C., Stenmark, H., Miaczynska, M., & Backer, J. M. (2002). Role of Rab5 in the recruitment of hVps34/p150 to the early endosome. *Traffic, 3*(6), 416-427. doi:10.1034/j.1600-0854.2002.30605.x

Nader, G. P., Ezratty, E. J., & Gundersen, G. G. (2016). FAK, talin and PIPKIgamma regulate endocytosed integrin activation to polarize focal adhesion assembly. *Nat Cell Biol, 18*(5), 491-503. doi:10.1038/ncb3333

Nakatsu, F., Perera, R. M., Lucast, L., Zoncu, R., Domin, J., Gertler, F. B., . . . De Camilli, P. (2010). The inositol 5-phosphatase SHIP2 regulates endocytic clathrin-coated pit dynamics. *J Cell Biol, 190*(3), 307-315. doi:10.1083/jcb.201005018

Napolitano, G., Di Malta, C., & Ballabio, A. (2022). Non-canonical mTORC1 signaling at the lysosome. *Trends Cell Biol*. doi:10.1016/j.tcb.2022.04.012

Napolitano, G., Di Malta, C., Esposito, A., de Araujo, M. E. G., Pece, S., Bertalot, G., . . . Ballabio, A. (2020). A substrate-specific mTORC1 pathway underlies Birt-Hogg-Dube syndrome. *Nature, 585*(7826), 597-602. doi:10.1038/s41586-020-2444-0

Nicot, A. S., Toussaint, A., Tosch, V., Kretz, C., Wallgren-Pettersson, C., Iwarsson, E., . . . Laporte, J. (2007). Mutations in amphiphysin 2 (BIN1) disrupt interaction with dynamin 2 and cause autosomal recessive centronuclear myopathy. *Nat Genet, 39*(9), 1134-1139. doi:10.1038/ng2086

Nojima, H., Tokunaga, C., Eguchi, S., Oshiro, N., Hidayat, S., Yoshino, K., . . . Yonezawa, K. (2003). The mammalian target of rapamycin (mTOR) partner, raptor, binds the mTOR substrates p70 S6 kinase and 4E-BP1 through their TOR signaling (TOS) motif. *J Biol Chem, 278*(18), 15461-15464. doi:10.1074/jbc.C200665200

Ohashi, Y. (2021). Activation Mechanisms of the VPS34 Complexes. *Cells, 10*(11). doi:10.3390/cells10113124

Pacold, M. E., Suire, S., Perisic, O., Lara-Gonzalez, S., Davis, C. T., Walker, E. H., . . . Williams, R. L. (2000). Crystal Structure and Functional Analysis of Ras Binding to Its Effector Phosphoinositide 3-Kinase γ. *Cell, 103*(6), 931-944. doi:10.1016/s0092-8674(00)00196-3

Pant, S., Sharma, M., Patel, K., Caplan, S., Carr, C. M., & Grant, B. D. (2009). AMPH-1/Amphiphysin/Bin1 functions with RME-1/Ehd1 in endocytic recycling. *Nat Cell Biol, 11*(12), 1399-1410. doi:10.1038/ncb1986

Park, H. H. (2013). Structural basis of membrane trafficking by Rab family small G protein. *Int J Mol Sci, 14*(5), 8912-8923. doi:10.3390/ijms14058912

Paul, N. R., Jacquemet, G., & Caswell, P. T. (2015). Endocytic Trafficking of Integrins in Cell Migration. *Curr Biol, 25*(22), R1092-1105. doi:10.1016/j.cub.2015.09.049

Peterson, T. R., Laplante, M., Thoreen, C. C., Sancak, Y., Kang, S. A., Kuehl, W. M., . . . Sabatini, D. M. (2009). DEPTOR is an mTOR inhibitor frequently overexpressed in multiple myeloma cells and required for their survival. *Cell, 137*(5), 873-886. doi:10.1016/j.cell.2009.03.046

Pfeffer, S. R. (2005). Structural clues to Rab GTPase functional diversity. *J Biol Chem, 280*(16), 15485-15488. doi:10.1074/jbc.R500003200

Pirola, L., Zvelebil, M. J., Bulgarelli-Leva, G., Van Obberghen, E., Waterfield, M. D., & Wymann, M. P. (2001). Activation loop sequences confer substrate specificity to phosphoinositide 3-kinase alpha (PI3Kalpha). Functions of lipid kinase-deficient PI3Kalpha in signaling. *J Biol Chem, 276*(24), 21544-21554. doi:10.1074/jbc.M011330200

Poincloux, R., Lizarraga, F., & Chavrier, P. (2009). Matrix invasion by tumour cells: a focus on MT1-MMP trafficking to invadopodia. *J Cell Sci, 122*(Pt 17), 3015-3024. doi:10.1242/jcs.034561

Posor, Y., Eichhorn-Gruenig, M., Puchkov, D., Schoneberg, J., Ullrich, A., Lampe, A., . . . Haucke, V. (2013). Spatiotemporal control of endocytosis by phosphatidylinositol-3,4-bisphosphate. *Nature, 499*(7457), 233-237. doi:10.1038/nature12360

Posor, Y., Kampyli, C., Bilanges, B., Ganguli, S., Koch, P. A., Wallroth, A., . . . Vanhaesebroeck, B. (2022). Local synthesis of the phosphatidylinositol-3,4-bisphosphate lipid drives focal adhesion turnover. *Dev Cell, 57*(14), 1694-1711 e1697. doi:10.1016/j.devcel.2022.06.011

Powelka, A. M., Sun, J., Li, J., Gao, M., Shaw, L. M., Sonnenberg, A., & Hsu, V. W. (2004). Stimulation-dependent recycling of integrin beta1 regulated by ARF6 and Rab11. *Traffic, 5*(1), 20-36. doi:10.1111/j.1600-0854.2004.00150.x

Prokic, I., Cowling, B. S., & Laporte, J. (2014). Amphiphysin 2 (BIN1) in physiology and diseases. *J Mol Med (Berl), 92*(5), 453-463. doi:10.1007/s00109-014-1138-1

Raiborg, C., & Stenmark, H. (2009). The ESCRT machinery in endosomal sorting of ubiquitylated membrane proteins. *Nature, 458*(7237), 445-452. doi:10.1038/nature07961

Rathinaswamy, M. K., & Burke, J. E. (2020). Class I phosphoinositide 3-kinase (PI3K) regulatory subunits and their roles in signaling and disease. *Adv Biol Regul, 75*, 100657. doi:10.1016/j.jbior.2019.100657

Ribeiro, I., Yuan, L., Tanentzapf, G., Dowling, J. J., & Kiger, A. (2011). Phosphoinositide regulation of integrin trafficking required for muscle attachment and maintenance. *PLoS Genet, 7*(2), e1001295. doi:10.1371/journal.pgen.1001295

Rodgers, S. J., Ooms, L. M., Oorschot, V. M. J., Schittenhelm, R. B., Nguyen, E. V., Hamila, S. A., . . . Mitchell, C. A. (2021). INPP4B promotes PI3Kalpha-dependent late endosome

formation and Wnt/beta-catenin signaling in breast cancer. *Nat Commun, 12*(1), 3140. doi:10.1038/s41467-021-23241-6

Russell, R. C., Tian, Y., Yuan, H., Park, H. W., Chang, Y. Y., Kim, J., . . . Guan, K. L. (2013). ULK1 induces autophagy by phosphorylating Beclin-1 and activating VPS34 lipid kinase. *Nat Cell Biol, 15*(7), 741-750. doi:10.1038/ncb2757

Sabha, N., Volpatti, J. R., Gonorazky, H., Reifler, A., Davidson, A. E., Li, X., . . . Dowling, J. J. (2016). PIK3C2B inhibition improves function and prolongs survival in myotubular myopathy animal models. *J Clin Invest, 126*(9), 3613-3625. doi:10.1172/JCI86841

Samsó, P., Koch, P. A., Posor, Y., Lo, W.-T., Belabed, H., Nazare, M., . . . Haucke, V. (2022). Antagonistic control of active surface integrins by myotubularin and phosphatidylinositol 3-kinase C2β in a myotubular myopathy model. *Proceedings of the National Academy of Sciences, 119*(40). doi:10.1073/pnas.2202236119

Sancak, Y., Bar-Peled, L., Zoncu, R., Markhard, A. L., Nada, S., & Sabatini, D. M. (2010). Ragulator-Rag complex targets mTORC1 to the lysosomal surface and is necessary for its activation by amino acids. *Cell, 141*(2), 290-303. doi:10.1016/j.cell.2010.02.024

Sancak, Y., Peterson, T. R., Shaul, Y. D., Lindquist, R. A., Thoreen, C. C., Bar-Peled, L., & Sabatini, D. M. (2008). The Rag GTPases bind raptor and mediate amino acid signaling to mTORC1. *Science, 320*(5882), 1496-1501. doi:10.1126/science.1157535

Sancak, Y., Thoreen, C. C., Peterson, T. R., Lindquist, R. A., Kang, S. A., Spooner, E., . . . Sabatini, D. M. (2007). PRAS40 is an insulin-regulated inhibitor of the mTORC1 protein kinase. *Mol Cell, 25*(6), 903-915. doi:10.1016/j.molcel.2007.03.003

Sandvig, K., Kavaliauskiene, S., & Skotland, T. (2018). Clathrin-independent endocytosis: an increasing degree of complexity. *Histochem Cell Biol, 150*(2), 107-118. doi:10.1007/s00418-018-1678-5

Sasaki, J., Ishikawa, K., Arita, M., & Taniguchi, K. (2012). ACBD3-mediated recruitment of PI4KB to picornavirus RNA replication sites. *EMBO J, 31*(3), 754-766. doi:10.1038/emboj.2011.429

Saxton, R. A., & Sabatini, D. M. (2017). mTOR Signaling in Growth, Metabolism, and Disease. *Cell, 168*(6), 960-976. doi:10.1016/j.cell.2017.02.004

Schmidt, A., Durgan, J., Magalhaes, A., & Hall, A. (2007). Rho GTPases regulate PRK2/PKN2 to control entry into mitosis and exit from cytokinesis. *EMBO J, 26*(6), 1624-1636. doi:10.1038/sj.emboj.7601637

Schumacher, S., Vazquez Nunez, R., Biertumpfel, C., & Mizuno, N. (2022). Bottom-up reconstitution of focal adhesion complexes. *FEBS J, 289*(12), 3360-3373. doi:10.1111/febs.16023

Schuske, K. R., Richmond, J. E., Matthies, D. S., Davis, W. S., Runz, S., Rube, D. A., . . . Jorgensen, E. M. (2003). Endophilin Is Required for Synaptic Vesicle Endocytosis by Localizing Synaptojanin. *Neuron, 40*(4), 749-762. doi:10.1016/s0896-6273(03)00667-6

Schwander, M., Leu, M., Stumm, M., Dorchies, O. M., Ruegg, U. T., Schittny, J., & Müller, U. (2003). β1 Integrins Regulate Myoblast Fusion and Sarcomere Assembly. *Developmental Cell, 4*(5), 673-685. doi:10.1016/s1534-5807(03)00118-7

Shin, H. R., Citron, Y. R., Wang, L., Tribouillard, L., Goul, C. S., Stipp, R., . . . Zoncu, R. (2022). Lysosomal GPCR-like protein LYCHOS signals cholesterol sufficiency to mTORC1. *Science*, eabg6621. doi:10.1126/science.abg6621

Siempelkamp, B. D., Rathinaswamy, M. K., Jenkins, M. L., & Burke, J. E. (2017). Molecular mechanism of activation of class IA phosphoinositide 3-kinases (PI3Ks) by membrane-localized HRas. *J Biol Chem, 292*(29), 12256-12266. doi:10.1074/jbc.M117.789263

Silva-Rojas, R., Nattarayan, V., Jaque-Fernandez, F., Gomez-Oca, R., Menuet, A., Reiss, D., . . . Laporte, J. (2022). Mice with muscle-specific deletion of Bin1 recapitulate centronuclear myopathy and acute downregulation of dynamin 2 improves their phenotypes. *Mol Ther, 30*(2), 868-880. doi:10.1016/j.ymthe.2021.08.006

Sonnichsen, B., De Renzis, S., Nielsen, E., Rietdorf, J., & Zerial, M. (2000). Distinct membrane domains on endosomes in the recycling pathway visualized by multicolor imaging of Rab4, Rab5, and Rab11. *J Cell Biol, 149*(4), 901-914. doi:10.1083/jcb.149.4.901

Stahelin, R. V., Karathanassis, D., Bruzik, K. S., Waterfield, M. D., Bravo, J., Williams, R. L., & Cho, W. (2006). Structural and membrane binding analysis of the Phox homology domain of phosphoinositide 3-kinase-C2alpha. *J Biol Chem, 281*(51), 39396-39406. doi:10.1074/jbc.M607079200

Stehbens, S. J., Paszek, M., Pemble, H., Ettinger, A., Gierke, S., & Wittmann, T. (2014). CLASPs link focal-adhesion-associated microtubule capture to localized exocytosis and adhesion site turnover. *Nat Cell Biol, 16*(6), 561-573. doi:10.1038/ncb2975

Stenmark, H. (2009). Rab GTPases as coordinators of vesicle traffic. *Nat Rev Mol Cell Biol, 10*(8), 513-525. doi:10.1038/nrm2728

Stephens, L., Hawkins, P. T., & Downes, C. P. (1989). Metabolic and structural evidence for the existence of a third species of polyphosphoinositide in cells: D-phosphatidyl-myo-inositol 3-phosphate. *Biochem J, 259*(1), 267-276. doi:10.1042/bj2590267

Stroupe, C. (2018). This Is the End: Regulation of Rab7 Nucleotide Binding in Endolysosomal Trafficking and Autophagy. *Front Cell Dev Biol, 6*, 129. doi:10.3389/fcell.2018.00129

Tasfaout, H., Cowling, B. S., & Laporte, J. (2018). Centronuclear myopathies under attack: A plethora of therapeutic targets. *J Neuromuscul Dis, 5*(4), 387-406. doi:10.3233/JND-180309

Teckchandani, A., Mulkearns, E. E., Randolph, T. W., Toida, N., & Cooper, J. A. (2012). The clathrin adaptor Dab2 recruits EH domain scaffold proteins to regulate integrin beta1 endocytosis. *Mol Biol Cell, 23*(15), 2905-2916. doi:10.1091/mbc.E11-12-1007

Trochet, D., Prudhon, B., Beuvin, M., Peccate, C., Lorain, S., Julien, L., . . . Bitoun, M. (2018). Allele-specific silencing therapy for Dynamin 2-related dominant centronuclear myopathy. *EMBO Mol Med, 10*(2), 239-253. doi:10.15252/emmm.201707988

Tu, Y., Zhao, L., Billadeau, D. D., & Jia, D. (2020). Endosome-to-TGN Trafficking: Organelle-Vesicle and Organelle-Organelle Interactions. *Front Cell Dev Biol, 8*, 163. doi:10.3389/fcell.2020.00163

Velichkova, M., Juan, J., Kadandale, P., Jean, S., Ribeiro, I., Raman, V., . . . Kiger, A. A. (2010). Drosophila Mtm and class II PI3K coregulate a PI(3)P pool with cortical and endolysosomal functions. *J Cell Biol, 190*(3), 407-425. doi:10.1083/jcb.200911020

Walker, E. H., Perisic, O., Ried, C., Stephens, L., & Williams, R. L. (1999). Structural insights into phosphoinositide 3-kinase catalysis and signalling. *Nature, 402*(6759), 313-320. doi:10.1038/46319

Wallroth, A., & Haucke, V. (2018). Phosphoinositide conversion in endocytosis and the endolysosomal system. *J Biol Chem, 293*(5), 1526-1535. doi:10.1074/jbc.R117.000629

Wallroth, A., Koch, P. A., Marat, A. L., Krause, E., & Haucke, V. (2019). Protein kinase N controls a lysosomal lipid switch to facilitate nutrient signalling via mTORC1. *Nat Cell Biol, 21*(9), 1093-1101. doi:10.1038/s41556-019-0377-3

Wang, D. G., Paddock, M. N., Lundquist, M. R., Sun, J. Y., Mashadova, O., Amadiume, S., . . . Cantley, L. C. (2019). PIP4Ks Suppress Insulin Signaling through a Catalytic-Independent Mechanism. *Cell Rep, 27*(7), 1991-2001 e1995. doi:10.1016/j.celrep.2019.04.070

Wang, H., Lo, W. T., Vujicic Zagar, A., Gulluni, F., Lehmann, M., Scapozza, L., . . . Vadas, O. (2018). Autoregulation of Class II Alpha PI3K Activity by Its Lipid-Binding PX-C2 Domain Module. *Mol Cell, 71*(2), 343-351 e344. doi:10.1016/j.molcel.2018.06.042

Wang, H., Loerke, D., Bruns, C., Muller, R., Koch, P. A., Puchkov, D., . . . Haucke, V. (2020). Phosphatidylinositol 3,4-bisphosphate synthesis and turnover are spatially segregated in the endocytic pathway. *J Biol Chem, 295*(4), 1091-1104. doi:10.1074/jbc.RA119.011774

Wang, Y., Cao, H., Chen, J., & McNiven, M. A. (2011). A direct interaction between the large GTPase dynamin-2 and FAK regulates focal adhesion dynamics in response to active Src. *Mol Biol Cell, 22*(9), 1529-1538. doi:10.1091/mbc.E10-09-0785

Wheeler, M., & Domin, J. (2001). Recruitment of the class II phosphoinositide 3-kinase C2beta to the epidermal growth factor receptor: role of Grb2. *Mol Cell Biol, 21*(19), 6660-6667. doi:10.1128/mcb.21.19.6660-6667.2001

Wheeler, M., & Domin, J. (2006). The N-terminus of phosphoinositide 3-kinase-C2beta regulates lipid kinase activity and binding to clathrin. *J Cell Physiol, 206*(3), 586-593. doi:10.1002/jcp.20507

Wu, C. (2007). Focal adhesion: a focal point in current cell biology and molecular medicine. *Cell Adh Migr, 1*(1), 13-18. doi:10.4161/cam.1.1.4081

Wu, Y. W., Tan, K. T., Waldmann, H., Goody, R. S., & Alexandrov, K. (2007). Interaction analysis of prenylated Rab GTPase with Rab escort protein and GDP dissociation inhibitor explains the need for both regulators. *Proc Natl Acad Sci U S A, 104*(30), 12294-12299. doi:10.1073/pnas.0701817104

Ye, X., McLean, M. A., & Sligar, S. G. (2016). Conformational equilibrium of talin is regulated by anionic lipids. *Biochim Biophys Acta, 1858*(8), 1833-1840. doi:10.1016/j.bbamem.2016.05.005

Yip, C. K., Murata, K., Walz, T., Sabatini, D. M., & Kang, S. A. (2010). Structure of the human mTOR complex I and its implications for rapamycin inhibition. *Mol Cell, 38*(5), 768-774. doi:10.1016/j.molcel.2010.05.017

7 Appendix

7.1 Abbreviations

Table 15: Abbreviations

ADP	Adenosine diphosphate
Akt	RAC-alpha serine/threonine-protein kinase
AP	Autophagosome
AP-2	Adaptor protein 2
APPL1	Adaptor protein, phosphotyrosine interacting with PH domain and leucine zippern1
APS	Ammonium persulfate
ARAP3	Arf-GAP with Rho-GAP domain, ANK repeat and PH domain-containing protein 3
ATF4	Activating transcription factor 4
ATP	Adenosine triphosphate
BAR	Bin/Amphiphysin/RVS
BIN1	Bridging integrator 1
BSA	Bovine serum albumin
CCP	Clathrin coated pit
CHC	Clathrin heavy chain
CLC	Clathrin light chain
CME	Clathrin mediated endocytosis
CNM	Centronuclear myopathy
Dab2	Disabled-2
DAPI	4’,6-diamidino-2-phenylindole
DEPTOR	DEP domain-containing mTOR-interacting protein
DMEM	Dulbecco’s modified eagle medium
DNA	Deoxyribonucleic acid
DNM2	Dynamin-2

EAP	Endocytic accessory protein
ECM	Extracellular matrix
EDTA	Ethylene diamine tetraacetic acid
EE	Early endosome
EEA1	Early endosome antigen 1
EGF	Epidermal growth factor
eGFP	Enhanced green fluorecent protein
EGTA	Triethylene glycol diamine tetraacetic acid
Eps15	Epidermal growth factor receptor pathway substrate 15
ER	Endoplasmatic reticulum
ESCRT	Endosomal sorting complex required for transport
Exo70	Exocyst complex component 70
FA	Focal adhesion
FACS	Fluorescence-activated cell sorting
FCHo 1/2	Fer/Cip4 homology domain-only
GAP	GTPase activating protein
GAPDH	Glyceraldehyde 3-phosphate dehydrogenase
GATOR	GAP activity towards Rags
GDI	GDP-dissociation inhibitor
GDP	Guanosine diphosphate
GEF	Guanine nucleotide exchange factors
GoF	Gain of function
Grb2	Growth factor receptor-bound protein 2
GST	Glutathione S-transferase
GTP	Guanosine triphosphate
HBD	Helix bundle domain
HEK	Human embryonic kidney cells
HeLa	Henrietta Lacks
Hrs	Hepatocyte growth factor-regulated
IP	Immunoprecipitation
IPTG	Isopropyl β-D-1-thiogalactopyranoside

ITSN1	Intersectin-1
KI	Knock-in
KO	Knock-out
LAMP1	Lysosomal-associated membrane protein 1
LB	Lysogeny broth
LBPA	Lysobisphosphatidic acid
LeLys	Late endosome / Lysosome
LoF	Loss of function
LSM	Laser scanning microscope
MAPK	Mitogen-activated protein kinase
MHC	Myosin heavy chain
mLST8	Mammalian lethal with SEC13 protein 8
MOPS	3-morpholinopropane-1-sulfonic acid
MTM	Myotubularin
mTORC1	Mammalian target of rapamycin complex 1
MVB	Multivesicular body
NPC1	Niemann-Pick disease, type C1
NUMB	Protein numb homolog
OCRL	Lowe oculocerebrorenal syndrome protein
ORP1L	Oxysterol-binding protein-related protein 1L
PAGE	Polyacrylamide gel electrophoresis
PAM	Protospacer adjacent motif
PBS	Phosphate-buffered saline
PD	Pulldown
PDK1	Phosphoinositide-dependent kinase 1
PFA	Paraformaldehyde
PI	Phosphoinositide
PI(3,4,5)P3	Phosphatidylinositol-3,4,5-trisphosphate
PI(3,4)P2	Phosphatidylinositol-3,4-bisphosphate
PI(3,5)P2	Phosphatidylinositol-3,5-bisphosphate
PI(3)P	Phosphatidylinositol-3-phosphate

PI(4,5)P2	Phosphatidylinositol-4,5-bisphosphate
PI(4)P	Phosphatidylinositol-4-phosphate
PI(5)P	Phosphatidylinositol-5-phosphate
PI3K	Phosphoinositide-3-kinase
PI4K	Phosphoinositide-4-kinase
PKN2	Serine/threonine protein kinase N2
PM	Plasma membrane
PRAS40	Proline-rich AKT substrate of 40 kDa
PTEN	Phosphatase and tensin homologue deleted on chromosome 10
PX	Phox homology
Raptor	Regulatory-associated protein of mTOR
Rab	Ras-related in brain
Rag	Ras-related small GTP-binding protein
Ras	Rat sarcoma virus
RBD	Ras binding domain
RE	Recycling endosome
REP	Rab escort protein
Rheb	Ras homolog enriched in brain
RhoA	Ras homolog family member A
RIPA	Radioimmunoprecipitation assay buffer
RTK	Receptor tyrosine kinase
S6K	S6 kinase
SD	Standard deviation
SDS	Sodium dodecyl sulfate
SEM	Standard error of the mean
SF	Surface
SHIP2	SH2-containing 5’-inositol phosphatase 2
siRNA	Small interfering RNA
SNX	Sorting nexin
SREBP	Sterol regulatory element-binding protein
TACC3	Transforming acidic coiled-coil-containing protein 3

TBE	Tris/Borate/EDTA
TBS	Tris-buffered saline
TFEB	Transcription factor EB
TGN	Trans golgi network
TOS	Tor signaling motif
TRIS	Tris(hydroxymethyl)aminoethane
TSC	Tuberous sclerosis
ULK1	Unc-51 like autophagy activating kinase
UVRAG	UV radiation resistance-associated gene
VPS	Vacuolar protein sorting
WIPI	WD-repeat protein interacting with phosphoinositides
WT	Wild type
XLCNM	X-linked centronuclear myopathy

7.2 List of Figures

7.3 List of Tables

7.4 Publications

Wallroth, A., **Koch, PA.**, Marat, A., Krause, E., Haucke, V. (2019). Protein kinase N controls a lysosomal lipid switch to facilitate nutrient signalling via mTORC1. *Nat Cell Biol* **9**, 1093-1101.

Samsó, P.*, **Koch, PA.***, Posor, Y., Lo, WT., Belabed, H., Nazare, M., Laporte, J., Haucke, V. (2022). Antagonistic control of active surface integrins by myotubularin and phosphatidylinositol 3-kinase C2β in a myotubular myopathy model. *PNAS* **40,** e2202236119.

* Authors contributed equally

7.5 Other publications

Ebner, M.*, **Koch, PA.***, Haucke, V. (2019). Phosphoinositides in the control of lysosome function and homeostasis. *Biochem Soc T* **4**, 1173-1185.

Wang, H., Loerke, D., Bruns, C., Müller, R., **Koch, PA.**, Puchkov, D., Schultz, C., Haucke, V. (2020). Phosphatidylinositol 3,4-bisphosphate synthesis and turnover are spatially segregated in the endocytic pathway. *J Biol Chem* **4**, 1091-1104.

Koch, PA.*, Dornan, GL.*, Hessenberger, M., Haucke, V. (2021). The Molecular Mechanisms Mediating Class II PI 3-Kinase Function in Cell Physiology. *FEBS J* **24**, 7025-7042.

Posor, Y., Kampyli, C., Bilanges, B., Ganguli, S., **Koch, PA.**, Wallroth, A., Morelli, D., Jenkins, M., Alliouachene, S., Deltcheva, E., Baum, B., Haucke, V., Vanhaesebroeck, B. (2022). Local synthesis of the phosphatidylinositol-3,3-biphosphate lipid drives focal adhesion turnover. *Dev Cell* **14**, 1694-1711.

* Authors contributed equally